Nuclear Science
NEA/NSC/DOC(2003)16

ISBN 92-64-02139-6

Benchmark on Deterministic Transport Calculations Without Spatial Homogenisation

A 2-D/3-D MOX Fuel Assembly Benchmark

NUCLEAR ENERGY AGENCY
ORGANISATION FOR ECONOMIC CO-OPERATION AND DEVELOPMENT

ORGANISATION FOR ECONOMIC CO-OPERATION AND DEVELOPMENT

Pursuant to Article 1 of the Convention signed in Paris on 14th December 1960, and which came into force on 30th September 1961, the Organisation for Economic Co-operation and Development (OECD) shall promote policies designed:

- to achieve the highest sustainable economic growth and employment and a rising standard of living in Member countries, while maintaining financial stability, and thus to contribute to the development of the world economy;
- to contribute to sound economic expansion in Member as well as non-member countries in the process of economic development; and
- to contribute to the expansion of world trade on a multilateral, non-discriminatory basis in accordance with international obligations.

The original Member countries of the OECD are Austria, Belgium, Canada, Denmark, France, Germany, Greece, Iceland, Ireland, Italy, Luxembourg, the Netherlands, Norway, Portugal, Spain, Sweden, Switzerland, Turkey, the United Kingdom and the United States. The following countries became Members subsequently through accession at the dates indicated hereafter: Japan (28th April 1964), Finland (28th January 1969), Australia (7th June 1971), New Zealand (29th May 1973), Mexico (18th May 1994), the Czech Republic (21st December 1995), Hungary (7th May 1996), Poland (22nd November 1996), Korea (12th December 1996) and the Slovak Republic (14 December 2000). The Commission of the European Communities takes part in the work of the OECD (Article 13 of the OECD Convention).

NUCLEAR ENERGY AGENCY

The OECD Nuclear Energy Agency (NEA) was established on 1st February 1958 under the name of the OEEC European Nuclear Energy Agency. It received its present designation on 20th April 1972, when Japan became its first non-European full Member. NEA membership today consists of 28 OECD Member countries: Australia, Austria, Belgium, Canada, Czech Republic, Denmark, Finland, France, Germany, Greece, Hungary, Iceland, Ireland, Italy, Japan, Luxembourg, Mexico, the Netherlands, Norway, Portugal, Republic of Korea, Slovak Republic, Spain, Sweden, Switzerland, Turkey, the United Kingdom and the United States. The Commission of the European Communities also takes part in the work of the Agency.

The mission of the NEA is:

- to assist its Member countries in maintaining and further developing, through international co-operation, the scientific, technological and legal bases required for a safe, environmentally friendly and economical use of nuclear energy for peaceful purposes, as well as
- to provide authoritative assessments and to forge common understandings on key issues, as input to government decisions on nuclear energy policy and to broader OECD policy analyses in areas such as energy and sustainable development.

Specific areas of competence of the NEA include safety and regulation of nuclear activities, radioactive waste management, radiological protection, nuclear science, economic and technical analyses of the nuclear fuel cycle, nuclear law and liability, and public information. The NEA Data Bank provides nuclear data and computer program services for participating countries.

In these and related tasks, the NEA works in close collaboration with the International Atomic Energy Agency in Vienna, with which it has a Co-operation Agreement, as well as with other international organisations in the nuclear field.

FOREWORD

In the framework of the OECD/NEA Expert Group on 3-D Radiation Transport Benchmarks, an international benchmark for testing the ability of modern deterministic transport methods and codes to treat reactor problems without spatial homogenisation was proposed in March 2001.

Twenty solutions were submitted for the two-dimensional configuration and eleven solutions were submitted for the three-dimensional configuration. All of the participants' solutions were compared to a reference Monte Carlo solution. The analysis of the results demonstrates that modern deterministic transport codes and methods can calculate flux distribution reasonably well without relying upon spatial homogenisation techniques.

As a follow-up to the current benchmark, an extension of the 3-D calculations is proposed to provide a more challenging test of the ability of present-day, three-dimensional methods to correctly represent spatial heterogeneities.

TABLE OF CONTENTS

List of tables

List of figures

EXECUTIVE SUMMARY

One of the important issues of deterministic transport methods for whole-core calculations concerns the accuracy of homogenisation techniques. A direct calculation for whole-core heterogeneous geometries was not feasible in the past due to the limited capability of computers. One had to rely upon homogenisation techniques to collapse the spatial heterogeneities into a tractable homogenous description. These homogenisation techniques can introduce substantial error into the flux distribution and consequently, reaction rates in the homogenised zones can be significantly in error. With modern computational abilities, direct whole-core heterogeneous calculations are becoming ever-increasingly feasible. Given the trend in computational ability observed thus far, it is not unreasonable to assume that with time, whole-core calculations will eventually become commonplace.

In this context, an OECD/NEA benchmark problem was proposed to test the ability of modern deterministic transport methods and codes to treat such reactor core problems without spatial homogenisation. For this benchmark both two-dimensional and three-dimensional configurations were developed, and very accurate Monte Carlo reference solutions were obtained for both configurations. Seventeen participants submitted solutions for the two-dimensional configuration and eleven participants contributed solutions for the three-dimensional configuration. All of the participant solutions were compared to the reference Monte Carlo solution. This reference Monte Carlo solution was performed such that very precise estimates of the pin powers were obtained.

Overall, all the results submitted by the participants agreed well with the reference solution. A majority of the participants obtained solutions that were more than acceptable for typical reactor calculations and the remaining errors in the participant solutions can be attributed to the high-order space-angle approximation necessary to solve this particular benchmark problem. It is important to note that the high-order space-angle approximation needed for this benchmark is not necessarily typical for all such whole-core problems. In fact, the high-order space-angle approximation was sought as an attempt to reduce the burden of accuracy placed upon the Monte Carlo solution (time required to obtain the Monte Carlo solution). Thus, this benchmark cannot be taken as a representative calculation for all heterogeneous problems.

As a follow-up to the current benchmark, an extension of the three-dimensional calculations is proposed to provide a more thorough test of present-day three-dimensional methods' abilities to handle spatial heterogeneities while still allowing participants to investigate sensitivities to space-angle approximations implemented in their codes.

Chapter 1

INTRODUCTION

The NEA Expert Group on 3-D Radiation Transport Benchmarks was formed to deal with scientific issues in the field of deterministic and stochastic methods and computer codes relative to three-dimensional radiation transport. The main objectives of the Expert Group are to develop benchmarks and comparison exercises for 3-D radiation transport computer codes, to carry out validation of methods and identify their strengths, limitations, and accuracy, and to suggest needs for method development.

A recent benchmark, *3-D Radiation Transport Benchmarks for Simple Geometries with Void Regions*, considered geometries composed of highly-absorbing medium with voided streaming paths. The analysis of the participant results was completed in 2000 and it was published as an OECD/NEA report [1]. Moreover, the detailed participant results can be found in a special issue of *Progress of Nuclear Energy* [2].

A second important issue of deterministic transport methods for whole-core calculations concerns the accuracy of homogenisation techniques. A direct calculation for whole-core heterogeneous geometries was not feasible in the past due to the limited capability of computers. One had to rely upon homogenisation techniques to collapse the spatial heterogeneities into a tractable homogenous description. These homogenisation techniques can introduce substantial error in the flux distribution and thereby inaccurately predict the reaction rates in the homogenised zones. Modern computational abilities have rendered direct whole-core heterogeneous calculations more feasible, although still very computationally expensive. It is not unreasonable to assume that with time, however, such calculations will eventually become commonplace with the advent of massively parallel computing platforms and vast memory and disk space capabilities.

In this context, an OECD/NEA benchmark problem was proposed to test the ability of modern deterministic transport methods and codes to treat such reactor core problems without spatial homogenisation. For this benchmark both two-dimensional and three-dimensional configurations were developed and very accurate Monte Carlo reference solutions were obtained for both configurations. Seventeen participants submitted a total of twenty results for the two-dimensional configuration and eleven participants each submitted a result for the three-dimensional configuration. This report provides an analysis of all of the participant results compared to the reference Monte Carlo solutions.

Chapter 2

DESCRIPTION OF THE BENCHMARK

The benchmark geometry chosen is the sixteen assembly (quarter core symmetry) C5 MOX fuel assembly problem specified by Cavarec, *et al*. in Ref. [3]. The two-dimensional and three-dimensional configurations are shown in Figure 1. As indicated, for the two-dimensional domain, vacuum boundary conditions are applied to the right and to the bottom of the geometry while reflected boundary conditions are applied to the top and left of the geometry. The overall dimensions of the two-dimensional configuration as shown are 64.26×64.26 cm, while each assembly is 21.42×21.42 cm. For the three-dimensional configuration, the fuel assemblies are 192.78 cm in the z direction (as shown) and an additional 21.42 cm water reflector is added axially. The z boundary conditions are reflected below and vacuum above as indicated in Figure 1. Again referring to Figure 1, the overall dimensions for the three-dimensional configuration are $64.26 \times 64.26 \times 214.20$ cm, while each assembly is $21.42 \times 21.42 \times 192.78$ cm.

Each fuel assembly is made up of a 17×17 lattice of square pin cells, one of which is shown in Figure 2. The side length of each pin cell is 1.26 cm and all of the fuel pins and guide tubes have a 0.54 cm radius. As indicated by Figure 2, there are two compositions for every pin cell. For this benchmark problem a single moderator composition is provided for use in all of the pin cells and for use in the water moderator (reflector) surrounding the assemblies. The composition layout for all four assemblies is provided in Figure 3.

To describe the geometry, a seven-group set of cross-sections was obtained. The number densities and the dimensions of the fuel, cladding and assemblies specified by S. Cathalau, *et al*. in Ref. [4] were input into the collision probability code DRAGON (G. Marleau, *et al*.) which made use of the WIMS-AECL 69-group library [5]. The seven-group, transport-corrected, isotropic scattering cross-sections for UO_2, the three enrichments of MOX, the guide tubes and fission chambers and the moderator described in the problem specification are provided in Appendix A. The participants are meant to use all of the provided cross-sections as specified, but substitute the transport-corrected total cross-section for the total cross-section in their solutions.

In DRAGON, each fuel type was represented as a single pin cell in an infinite-lattice fine-mesh collision probability calculation. A full anisotropic collision probability calculation was performed and standard flux weighting was used to collapse to seven energy groups and to homogenise fuel, gap and cladding materials into homogenised fuel compositions. Although other group structures were tested, (2-group and 12-group), the seven-group set of cross-sections proved the most difficult to solve and thus was chosen to enhance the transport difficulties of heterogeneous problems. The seven-group moderator, homogenised guide tube and fission chamber cross-sections were obtained using a UO_2 fuel spectrum. It is very important to note that all of the pin cells in Figure 3 have the geometry shown in Figure 2, where for the fission chamber and guide tube, the “Fuel-Clad Mix” in Figure 2 is to be replaced with fission chamber or guide tube compositions as necessary.

It is acknowledged that the individual pin-cell lattice representation, the spatial homogenisation, the group collapse and the use of a single set of water cross-sections introduced error into the multi-group solution compared to a continuous energy solution of the same problem. However, the object of this benchmark is not to examine the validity of the multi-group approximation with respect to the continuous energy approach, but instead to provide a reasonable set of multi-group cross-sections in which there is no fuel-coolant homogenisation. In an attempt to assess the errors incurred by the multi-group cross-section methodology, some of the participants went a step further and solved the continuous-energy specification of the benchmark as supplementary contributions. However, these additional continuous-energy solutions were not taken into account in the analysis of results for the consistency of result comparison against the multi-group reference solutions.

With the errors in cross-sections neglected, the geometry defined by Figures 1-3 combined with the seven-group cross-sections of Appendix A provide an adequate basis for determining the accuracy of deterministic transport codes. For both the two-dimensional and three-dimensional problems a reference multi-group Monte Carlo solution was obtained using the MCNP code [6]. These reference solutions provided very precise eigenvalue solutions in addition to pin power predictions for all of the fuel pin cells in Figure 3. For additional comparisons, auxiliary multi-group Monte Carlo reference solutions were obtained by some of the participants using KENO, VIM and MCNP. A comparison of the reference solutions obtained by the participants will be made in Chapter 5 of this report.

Figure 1. Core configuration for the C5 benchmark problem

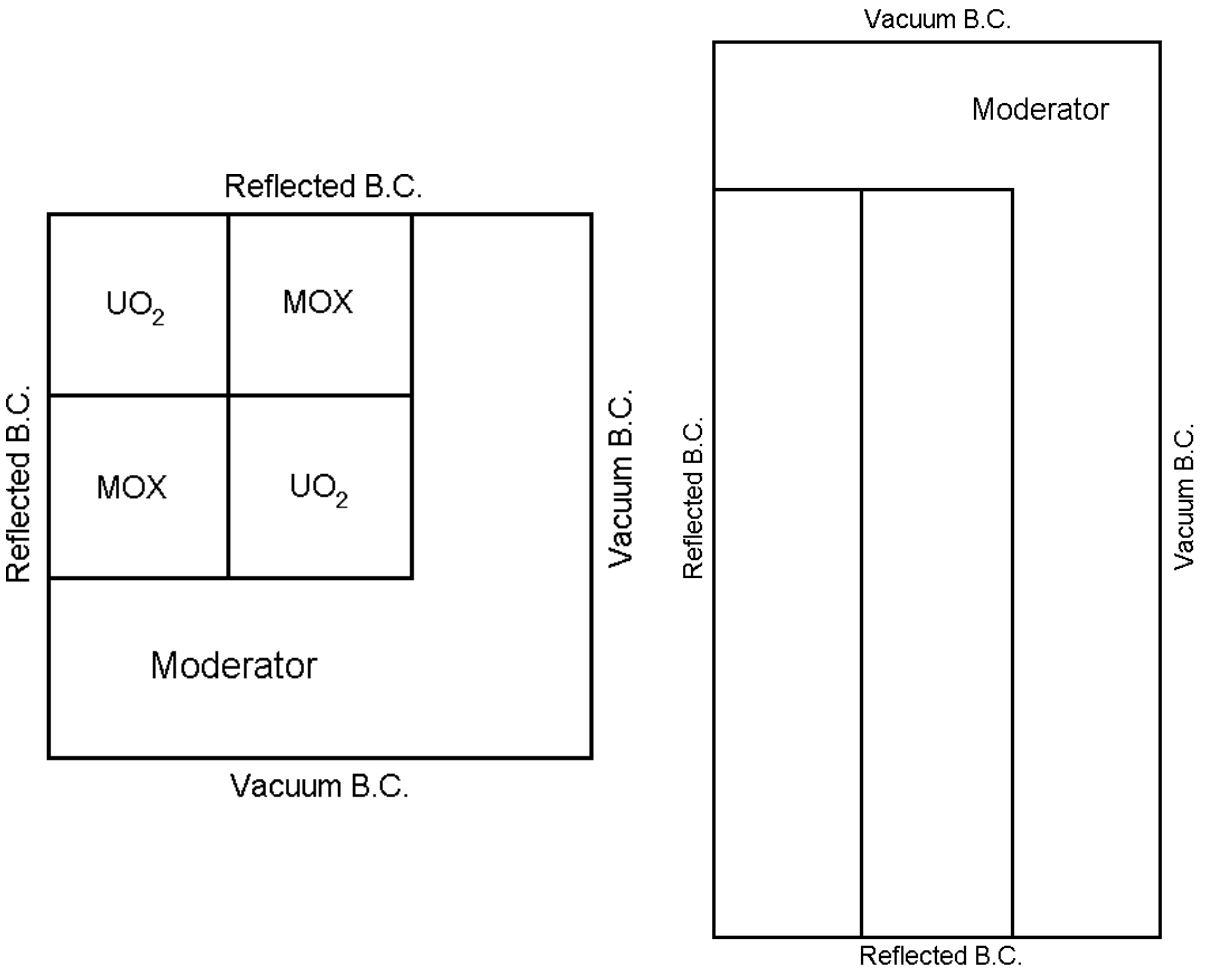

Figure 2. Pin cell geometry

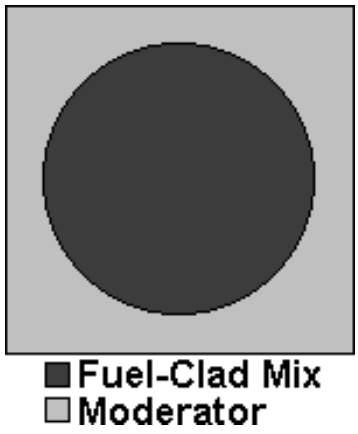

Figure 3. Benchmark pin cell compositions and numbering scheme

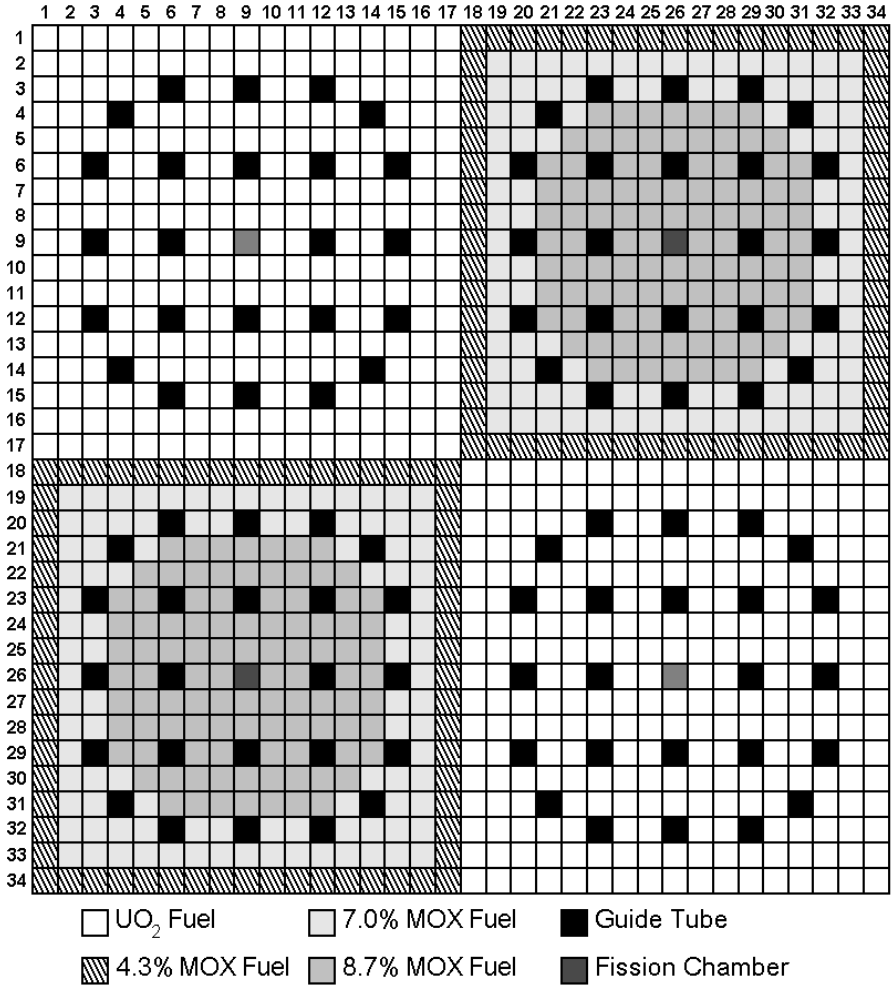

Chapter 3

PARTICIPANTS AND CODES USED

Apart from the Monte Carlo multi-group reference solution (ANL solution) used for the final comparison of contributed results, a few additional Monte Carlo reference solutions were provided by participants and a comparison of those reference solutions obtained by the participants is made in Chapter 5. The following describes those contributors who provided the additional reference solutions.

1. ***Argonne National Laboratory (ANL), USA***
   Participants: M.A. Smith, N. Tsoulfanidis, R.N. Blomquist, E.E. Lewis
   Code used: MCNP and VIM (2-D only)

2. ***Los Alamos National Laboratory (LANL), USA***
   Participant: K. Parsons
   Code used: MCNP

3. ***Oak Ridge National Laboratory (ORNL), USA***
   Participants: Y. Azmy, J. Gehin, R. Orsi (ENEA-Italy)
   Code used: KENO

A total of 17 participants contributed results for the two-dimensional configuration, providing 20 solutions, and 11 participants contributed results for the three-dimensional configuration. A complete list of participants is presented below. Calculation details provided by participants can be found in Appendix B.

1. ***Commissariat à l'Energie Atomique (CEA), France***
   Participants: F. Moreau, S. Santandrea, R. Sanchez
   Code used: APOLLO2 (method of characteristics), CRONOS2 (diffusion and S_N transport)
   Solutions provided: 2-D and 3-D

2. ***Gesellschaft fuer Reaktorsicherheit (GRS), Germany***
   Participants: A. Pautz, S. Langenbuch, W. Zwermann, K. Velkov
   Code used: DORT and TORT (S_N)
   Solutions provided: 2-D and 3-D

3. ***Hanyang University (HU), Korea***
   Participants: J.K. Kim, C.Y. Han
   Code used: TWODANT and THREEDANT (S_N)
   Solutions provided: 2-D and 3-D

4. ***Korea Atomic Energy Research Institute (KAERI), Korea***
   Participants: H.G. Joo, J.Y. Cho, K.S. Kim, S.Q. Zee
   Code used: DeCART (method of characteristics 2-D/diffusion 1-D)
   Solutions provided: 2-D and 3-D

5. ***Korea Advanced Institute of Science and Technology (KAIST), Korea***
   Participants: N.Z. Cho, G.S. Lee, C.J. Park
   Code used: CRX (method of characteristics 2-D/S_N 1-D)
   Solutions provided: 2-D and 3-D

6. ***Institute of Physics and Power Engineering (IPPE), Russian Federation***
   Participant: I.R. Suslov
   Code used: MCCG3D (method of characteristics)
   Solutions provided: 2-D and 3-D

7. ***Russian Research Centre Kurchatov Institue (RRC KI), Russian Federation***
   Participants: V.D. Davidenko, V.F. Tsibulsky
   Code used: UNKGRO (method of characteristics with stochastic rays)
   Solutions provided: 2-D and 3-D

8. ***Argonne National Laboratory (ANL), USA***
   Participants: M.A. Smith, N. Tsoulfanidis, E.E. Lewis, G. Palmiotti, T. Taiwo, R. Blomquist
   Code used: VARIANT-ISE (nodal spherical harmonics with integral transport), VARIANT-SE (nodal spherical harmonics)
   Solutions provided: 2-D and 3-D

9. ***Los Alamos National Laboratory (LANL), USA***
   Participants: J.A. Dahl, R.E. Alcouffe, R.S. Baker
   Code used: PARTISN (S_N)
   Solutions provided: 2-D and 3-D

10. ***Los Alamos National Laboratory (LANL), USA***
    Participants: T. Wareing, J. McGhee
    Code used: PERICLES (2-D) and ATTILA (3-D) (S_N)
    Solutions provided: 2-D and 3-D

11. ***Oak Ridge National Laboratory (ORNL), USA***
    Participants: Y. Azmy, J. Gehin, R. Orsi (ENEA-Italy)
    Code used: DORT and TORT (S_N)
    Solutions provided: 2-D and 3-D

12. ***Indira Gandhi Centre for Atomic Research (IGCAR), India***
    Participant: P. Mohanakrishnan
    Code used: COHINT (interface current technique with P_2 half space expansion)
    Solutions provided: 2-D

13. ***TEPCO Systems Corporation (TEPSYS), Japan***
    Participant: S. Kosaka
    Code used: CHAPLET (method of characteristics)
    Solutions provided: 2-D

14. ***Russian Research Centre Kurchatov Institue (RRC KI), Russian Federation***
    Participant: V.F. Boyarinov
    Code used: WIMS-SH SUHAM-2D (surface harmonics method)
    Solutions provided: 2-D

15. ***Russian Research Centre Kurchatov Institue (RRC KI), Russian Federation***
    Participants: A.A. Polismakov, A.V. Tchibiniaev
    Code used: STRUCTURE (collision probability, S_N synthesis)
    Solutions provided: 2-D

16. ***Russian Research Centre Kurchatov Institue (RRC KI), Russian Federation***
    Participant: T.S. Poveschenko
    Code used: GEFCOP (first collision probability method)
    Solutions provided: 2-D

17. ***Pennsylvania State University (PSU), USA***
    Participants: B. Ivanov, K. Ivanov, R.J.J. Stamm'ler
    Code used: HELIOS (current coupling collision probability)
    Solutions provided: 2-D

Chapter 4

METHOD OF RESULTS ANALYSIS

The goal set forth to each participant was to provide an eigenvalue and normalised pin power solution (total power = number of fuel pins) for the benchmark problem. The comparison of the eigenvalue result is straightforward since it is a unique number for which a very precise estimate can be obtained using the Monte Carlo code. The comparison of the pin power distribution is not as straightforward, since there are 1 056 total fuel pins (545 unique fuel pins by symmetry reduction) in Figure 3. A direct comparison of all of the pin powers on an individual basis, like that done with the eigenvalue, would result in an overwhelming amount of information and would not be very instructive.

To reduce the amount of information, the following unique pin power per cent error measures were selected: per cent error on maximum pin power (peaking), per cent error on the minimum pin power, maximum per cent error in the distribution and the per cent errors of the individual assembly powers. The importance of these per cent error measures is clear since they represent individual estimates of unique quantities.

To assess the overall pin power distribution, the following collective per cent error measures were selected: average pin power per cent error (AVG), root mean square (RMS) of the pin power per cent error distribution, and mean relative pin power per cent error (MRE). Eq. (1) defines the AVG error, where N is the number of fuel pins and e_n is the calculated per cent error for the nth pin power, p_n.

$$AVG = \frac{\sum_{N} |e_n|}{N} \tag{1}$$

Using similar notation, Eq. (2) defines the RMS per cent error, and Eq. (3) defines the MRE error (p_{avg} is the average pin power).

$$RMS = \frac{\sqrt{\sum_{N} e_n^2}}{N} \tag{2}$$

$$MRE = \frac{\sum_{N} |e_n| \cdot p_n}{N \cdot p_{avg}} \tag{3}$$

From Eq. (1), one can see that the AVG error measure will give a simple average of the pin power per cent error. This is a very useful quantity since it is a straightforward number that gives an overall idea of the pin power distribution accuracy. However the simple average does not indicate the way in which the error is distributed. Thus the RMS and MRE error measures are also needed. The RMS error measure weighs the largest per cent errors more than the smallest ones. Consequently, it gives a better assessment of the distribution of the per cent errors than the AVG error measure can give. The MRE

error measure weights the per cent error with the reference pin power, thereby linking the per cent error distribution to the power distribution. Consequently, the MRE error measure gives an estimate of the total amount of error in the pin power distribution where the RMS error is not linked to the actual power distribution. In effect, the MRE error measure diminishes the importance of error in the low power region in favour of error in the high power region. An instructional example is included in Appendix C for clarity of the three measures of the error distribution.

The last information gathered from the participant solutions was a tally of the number of fuel pin power predictions that made it within the 68%, 90%, 98% and 99.8% confidence intervals of the reference solution pin power prediction. This error measure indicates the percentage of the fuel pins that the participant's code predicts within the levels of precision of the Monte Carlo reference solution.

A comparison of the participant computational times was not carried out for this benchmark. With present-day computational abilities, comparison of computational efficiency between different codes is almost impossible without first performing a series of identical timing benchmarks on all of the various participant platforms. Additionally, some methods are penalised by the computational resources available to them, such as core memory size, available scratch disk space, limited parallel computing capabilities, etc. Such complications quite simply cannot be accounted for in timing benchmarks and would inevitably result in an inadequate estimation of the methods involved. We have therefore chosen to forego a rigorous comparison of computational efficiency and simply report a crude estimate of the CPU time that each participant reported. This result is representative of the time required for the participant to obtain their submitted solution on a regular basis and should not be construed as a figure of merit for computational efficiency.

Chapter 5

COMPARISONS OF THE REFERENCE MONTE CARLO SOLUTIONS

With the error measures selected, we now compare the various Monte Carlo multi-group reference solutions submitted by the participants. Table 1 gives the information about the participants while Table 2 gives the estimated number of histories for all of the Monte Carlo solutions. As can be seen in Table 2, the reference MCNP solution used for this work does not implement the largest number of histories and therefore does not necessarily constitute the best solution. However, it was felt to be sufficient for this benchmark.

Table 3 gives the eigenvalue solutions, the per cent error with respect to the reference MCNP solution, and the 68%, 98% and 99.8% confidence intervals associated with all of the Monte Carlo solutions. As can be seen, only KENO is within the 68% confidence interval of the reference, but all three are close to being within the 99.8% confidence interval. It is important to note that the statistical error associated with both the reference MCNP solution and the participant Monte Carlo solution must be combined to give the overall confidence interval.

Table 4 summarises the information for several specific pin powers selected as error measures in Chapter 4. In Table 4, the per cent error information for the reference MCNP solution represents the 98% confidence intervals associated with the various pin powers. Similarly, the associated reference statistical errors provided with the participant maximum per cent error are the reference MCNP 98% confidence intervals for the fuel pin that had the maximum error. For the maximum pin power and the minimum pin power all three participant Monte Carlo solutions agree with the reference Monte Carlo solution within the 98% confidence interval, but not a 68% confidence interval. For the maximum per cent error, none of the participant Monte Carlo solutions are within the reference 98% confidence interval. However, similar to the eigenvalue, the confidence interval of both solutions must be merged to obtain the true confidence interval. For the VIM result, the statistical error on the pin power with 2.2% error is 1.8% giving an overall 2.4% confidence interval (98%) for this pin and thus the 2.2% error is well within the 98% confidence interval. Unfortunately, statistical error information was only provided for the VIM solution. However, it is reasonable to assume that the MCNP-LANL and KENO solutions display a similar behaviour.

Table 5 gives the assembly powers for the participant reference solutions along with the reference MCNP solution. As can be seen, all of the assembly powers come well within or very close to the 98% confidence intervals of the reference MCNP solution.

Table 6 gives the pin power distribution error measures for the Monte Carlo reference solutions. As can be seen, only the VIM RMS error measure is significantly outside of the 98% confidence interval of the reference MCNP solution. However, this is due to the fact that the VIM solution utilised fewer histories, producing larger statistical errors (RMS of the statistical errors for VIM solution is 1.3%). In short, the RMS of the statistical error on the VIM solution should be used (1.3%) rather than the RMS of the statistical error on the reference MCNP solution (0.34%).

The final error measure to compare is the percentage of fuel pins within the reference MCNP confidence 68%, 90%, 98% and 99.8% confidence intervals tabulated in Table 7. Given that we are comparing Monte Carlo solutions to Monte Carlo solutions we should expect the percentage of fuel pins within the confidence interval to agree with the confidence interval of the reference MCNP solution (68% within the 68% confidence interval). However, this will only be true if the confidence intervals were based on the combined statistical error of the participant solution and the reference MCNP solution, which was not possible for these results. The results shown are only based upon the reference MCNP confidence intervals.

Continuing with the analysis of the three-dimensional Monte Carlo results, Table 8 provides information on the participants and Table 9 gives an estimated number of histories for each Monte Carlo calculation. As can be seen, no VIM solution was provided for the three-dimensional benchmark.

The Monte Carlo eigenvalue solutions and per cent errors with respect to the reference MCNP solution are given in Table 10 along with the 68%, 98% and 99.8% confidence intervals associated. Unlike the two-dimensional results of Table 3, both MCNP-LANL and KENO are within the 68% confidence interval of the reference MCNP for the three-dimensional problem.

The maximum pin power, the minimum pin power and the maximum per cent error are tabulated in Table 11 along with the per cent errors from the reference MCNP. As was the case for the two-dimensional results, the reference MCNP information represents the 98% confidence intervals associated with the error measures. For the maximum pin power and the minimum pin power, both participant Monte Carlo solutions agree with the reference MCNP solution within the 98% confidence interval. For the maximum per cent error, none of the participant reference solutions are within the reference 98% confidence interval, but again, the confidence interval of both solutions must be merged to obtain the true confidence interval. As was concluded for the two-dimensional solution, it is reasonable to assume that the MCNP-LANL and KENO solutions have sufficient statistical error that the combined 98% confidence intervals consume the discrepancies.

Table 12 gives the assembly powers for the participant reference solutions and the reference MCNP. As was the case for the two-dimensional problem, all of the assembly powers come well within the 98% confidence intervals of the reference MCNP solution.

The pin power distribution error measures for the three-dimensional geometry are given in Table 13. In this table, both the MCNP-LANL and KENO solution are within the 98% confidence interval of the reference MCNP solution for the three distribution error measures.

Table 14 gives the percentage of fuel pins that fall within the reference MCNP 68%, 90%, 98% and 99.8% confidence intervals. These results are similar to those seen in Table 7, but a slight improvement is discernible. To obtain a total agreement, however, the statistical error on both the participant solution and the reference MCNP solutions must be combined, which was not done for these results.

We can conclude from the analysis of the above Monte Carlo solutions that they all agree using a 98% confidence interval. Although some of the error measures such as the eigenvalue and assembly powers agreed well using a 68% or 90% confidence interval, only a 98% confidence interval guaranteed that all of the error measures were satisfied. In general, the maximum per cent error was the limiting error measure making the 98% confidence interval essential. Thus, 98% reference MCNP confidence intervals are used throughout the rest of this document to determine whether deterministic calculations are “in agreement” with the Monte Carlo reference solution.

The reference MCNP solution is provided electronically in Appendix D and both the pin power and statistical error tables for the two- and three-dimensional geometries can be printed out using the pre-formatted worksheets in the EXCEL workbooks. Similarly, all of the analysis tools and information used to compare the various Monte Carlo solutions are provided electronically in Appendix E. All of the Monte Carlo pin power solutions and error calculations with respect to the reference MCNP solution can also be printed or viewed if desired.

Table 1. Participant information for the two-dimensional reference solutions

Code names	Institution	Abbreviation	Country	Participants
Reference MCNP	Argonne National Laboratory	ANL	United States	M.A. Smith, N. Tsoulfanidis, R.N. Blomquist, E.E. Lewis
VIM	Argonne National Laboratory	ANL	United States	M.A. Smith, N. Tsoulfanidis, R.N. Blomquist, E. E. Lewis
MCNP-LANL	Los Alamos National Laboratory	LANL	United States	K. Parsons
KENO	Oak Ridge National Laboratory	ORNL	United States	Y. Azmy, J. Gehin, R. Orsi (ENEA)

Table 2. Estimated number of histories for the two-dimensional multi-group reference solutions

Code names	Estimated millions of histories
Reference MCNP	300
VIM	81
MCNP-LANL	100
KENO	1 000

Table 3. Eigenvalue solutions for the two-dimensional multi-group reference solutions

Code names	Eigenvalue	Per cent error	68%	98%	99.8%
Reference MCNP	1.186550		0.003	0.008	0.010
VIM	1.187035	0.041	0.012	0.027	0.036
MCNP-LANL	1.186380	-0.014	0.005	0.012	0.016
KENO	1.186520	-0.003	0.002	0.004	0.005

Table 4. Per cent error results for specific pin powers

Code names	Maximum pin power	*Per cent error*	Minimum pin power	*Per cent error*	Maximum per cent error	*Associated reference MCNP statistical error*
Ref. MCNP	2.498	±0.16	0.23	±0.58		
VIM	2.495	-0.11	0.23	0.27	2.20	±0.56
MCNP-LANL	2.495	-0.11	0.23	0.17	1.02	±0.51
KENO	2.499	0.06	0.23	-0.01	0.76	±0.44

Table 5. Assembly power per cent error for the two-dimensional multi-group reference solutions

Code names	Inner UO_2	*Per cent error*	MOX	*Per cent error*	Outer UO_2	*Per cent error*
Reference MCNP	492.8	±0.10	211.7	±0.18	139.8	±0.20
VIM	492.3	-0.11	211.9	0.08	140.0	0.14
MCNP-LANL	492.8	0.00	211.8	0.05	139.6	-0.13
KENO	493.1	0.06	211.7	-0.02	139.6	-0.14

Table 6. Pin power distribution error measures for the two-dimensional multi-group reference solutions

Code names	AVG	RMS	MRE
Reference MCNP	0.32	0.34	0.27
VIM	0.32	0.42	0.27
MCNP-LANL	0.24	0.31	0.20
KENO	0.14	0.19	0.12

Table 7. Percentage of fuel pins within the reference confidence intervals

Code names	68%	90%	98%	99.8%
VIM	29.0	46.3	59.8	73.7
MCNP-LANL	34.3	55.8	73.1	85.1
KENO	54.4	78.8	93.0	98.5

Table 8. Participant information for the three-dimensional reference solutions

Code names	Institution	Abbreviation	Country	Participants
Reference MCNP	Argonne National Laboratory	ANL	United States	M.A. Smith, N. Tsoulfanidis, R.N. Blomquist, E.E. Lewis
MCNP-LANL	Los Alamos National Laboratory	LANL	United States	K. Parsons
KENO	Oak Ridge National Laboratory	ORNL	United States	Y. Azmy, J. Gehin, R. Orsi (ENEA)

Table 9. Estimated number of histories for the three-dimensional multi-group reference solutions

Code names	Estimated millions of histories
Reference MCNP	300
MCNP-LANL	114
KENO	1 000

Table 10. Eigenvalue solutions for the three-dimensional multi-group reference solutions

Code names	Eigenvalue	Per cent error	68%	98%	99.8%
Reference MCNP	1.183810		0.003	0.008	0.010
MCNP-LANL	1.183800	-0.001	0.012	0.027	0.036
KENO	1.183780	-0.003	0.005	0.012	0.016

Table 11. Per cent error results for specific pin powers

Code names	Maximum pin power	*Per cent error*	Minimum pin power	*Per cent error*	Maximum per cent error	*Associated reference MCNP statistical error*
Reference MCNP	2.500	±0.16	0.23	±0.58		
MCNP-LANL	2.496	-0.17	0.23	0.02	1.08	±0.37
KENO	2.499	-0.05	0.23	0.42	0.64	±0.44

Table 12. Assembly power per cent error for the three-dimensional multi-group reference solutions

Code names	Inner UO_2	*Per cent error*	MOX	*Per cent error*	Outer UO_2	*Per cent error*
Reference MCNP	492.9	±0.10	211.8	±0.18	139.6	±0.20
MCNP-LANL	493.0	0.02	211.7	-0.02	139.6	-0.01
KENO	492.9	0.00	211.7	-0.02	139.7	0.05

Table 13. Pin power distribution error measures for the two-dimensional multi-group reference solutions

Code names	AVG	RMS	MRE
Reference MCNP	0.32	0.34	0.27
MCNP-LANL	0.20	0.26	0.17
KENO	0.12	0.16	0.10

Table 14. Percentage of fuel pins within the reference confidence intervals

Code names	68%	90%	98%	99.8%
MCNP-LANL	42.0	62.7	80.3	91.1
KENO	66.0	87.3	95.9	99.6

Chapter 6

TWO-DIMENSIONAL BENCHMARK RESULTS

Seventeen (17) participants submitted a total of 20 solutions for the two-dimensional benchmark. Table 15 provides the names of the participants along with their institution, home country and the name of the code that produced the results submitted. A brief description of the spatial and angular approximations implemented in each participant's code is given in Table 16. To view a complete summary of the participants' code and method used, refer to the original documentation submitted by each participant in Appendix B.

The purpose of the following analysis is not to point out the weaknesses or successes of any individual participant's code or method, especially considering that minor changes in the spatial and angular approximations implemented in any individual participant's code can substantially change the results shown here. Therefore, the point of this analysis is simply to provide the participants with an objective comparison of the results they submitted with a reference MCNP solution and the solutions submitted by their peers.

For the two-dimensional benchmark, the solutions from 16 first-order codes and four second-order codes were submitted. Five of the first order codes implement a collision probability method and six implement the method of characteristics. The remaining first-order approaches implement a form of discrete ordinates, four of which use a finite difference approach and one which uses a finite element approach. For the second-order codes, one implements a finite element diffusion approach, one implements a finite element discrete ordinates approach and two implement finite element, spherical harmonic nodal approaches.

Table 17 tabulates the participant eigenvalue solutions and the per cent errors with respect to the reference MCNP solution. Again, the statistical errors for the reference MCNP solution are the 98% confidence intervals. Figure 4 displays the eigenvalue solutions ordered with respect to decreasing eigenvalue accuracy where the dashed line represents the reference MCNP solution and the confidence intervals are too small to view. Figure 5 displays the eigenvalue per cent error with respect to decreasing eigenvalue accuracy where the reference MCNP statistical error again is too small to be distinguished. As can be seen in Figures 4 and 5 and Table 17, a wide range of solutions were obtained, but a majority of the solutions are reasonably close to the reference MCNP solution. Only three of the participants' codes are within the 98% confidence interval of the MCNP eigenvalue, however the average error for all the participant solutions is only about 0.08%, with only two of the solutions having substantially large errors.

The specific pin power error measures are tabulated in Table 18. Figure 6 displays the maximum pin power results, Figure 7 the minimum pin power results and Figure 8 the maximum per cent errors found in each participant solution. For each participant solution, the location of the maximum error (with respect to Figure 3) was determined and the statistical error associated with that pin obtained. This statistical error has been tabulated for each participant in Table 18 in the column entitled *Associated reference MCNP statistical error* and included in Figure 8 as *Associated statistical error*. All of the participant solutions in Figures 6-8 are ordered with respect to decreasing solution accuracy.

In Table 18, six participants obtained a maximum pin power within the 98% confidence interval and eight obtained a minimum pin power within the 98% confidence interval. The maximum per cent error results in Figure 8 show that none of the codes succeed in coming within the 98% MCNP confidence intervals. Only three of the participant codes have maximum errors less than 1% and only 15 achieve maximum errors less than 5%. Not surprisingly, maximum per cent error proved to be the most difficult measure for deterministic methods to satisfy in both two- and three-dimensional problems. It also represented the largest deviations between Monte Carlo calculations.

Next, the assembly power error measures are considered, the results of which are tabulated in Table 19. Figure 9 displays the participant results for the inner UO_2 assembly power, Figure 10 the results for the MOX assembly power, and Figure 11 the results of the outer UO_2 assembly power. For the inner UO_2 assembly power five participant solutions are within the 98% confidence interval. A similar result is seen for the outer UO_2 assembly, for which 10 participant solutions are within the 98% confidence interval. For the MOX assembly, seven participant solutions are within the 98% confidence interval.

Table 20 gives the pin power distribution error measures for the two-dimensional benchmark problem. Figure 12 displays the AVG error measure results, Figure 13 the RMS error measure results and Figure 14 the MRE error measure results. Seven of the participants agree to the reference MCNP solution within the 98% confidence interval for the AVG error measure and roughly 15 are less than 1% in error. The results of the RMS error measure are not as good, with only four of the participants within the 98% confidence interval and 12 within 1%. For the MRE error measure, five of the participants are within the 98% confidence interval and 16 are within 1%. It is important to note that the decrease in accuracy from the AVG error to the RMS error is indicative of a presence of more fuel pins with larger errors. However, given that the results of the MRE error measure do not exactly follow the trend seen from the AVG to the RMS error measure, it appears that the increase in fuel pin inaccuracy is occurring in the low power region of the problem geometry (i.e. outer UO_2 pins).

The last information gathered from the participant results is the number of fuel pins that lay within the 68%, 90%, 98% and 99.8% confidence intervals of the reference MCNP solution. Table 21 tabulates the number of fuel pins within the various confidence intervals while Table 22 tabulates the percentage of fuel pins within the confidence intervals. Figure 15 plots the participant results, ordered with respect to the 98% confidence interval results. As can be seen, none of the participants match the 98% confidence interval and relatively few are close. This error measure represents by far the strictest measure of accuracy that can be applied to the pin power distribution; however, it is subject to significant uncertainty from the normalisation procedure applied. For instance, normalisation applied to the peak pin power (a specific location in the pin power distribution) rather than the total power sums can result in 5-15% changes in the participant results shown in Figure 15. For this reason, this error measure should not be assumed essential to guarantee the accuracy of any given solution.

Overall, the inaccuracies in the two-dimensional benchmark can be attributed, in part, to insufficient space-angle approximations implemented by the participants in their codes. In some cases the participants submitted multiple results using coarser mesh or coarser angular approximations than those used in the above analysis. In almost all of those cases the coarser solutions were significantly less accurate than those shown in this chapter. Since all participants did not turn in multiple solutions, a complete analysis of the refinement of the participant solution was not possible and therefore is not included here. However, an electronic copy of the analysis workbook is available under the subdirectory "CoarserAngularAndSpatialResults" in Appendix F. For cross-referencing, the details of the spatial and angular refinements can be found in the participants' original submittal results and documentation provided in Appendix G (see also Appendix B). Also, for completeness, an estimate of each participant's CPU time is provided in Table 23.

It is suggested, as a first approach to improving the accuracy of a solution, that further refinement of the angular and spatial variables be investigated by the participants. The analysis tools used for the two-dimensional benchmark work are provided electronically in Appendix F and can be used by the participants for future comparisons if desired. Also, all of the participants' pin power and per cent error distributions were combined into a single printable worksheet. This worksheet is part of the EXCEL workbook "z.2D.Summary.of.Final.Results" provided in Appendix F.

Additional continuous Monte Carlo solutions provided by some of the participants are not used for comparison in the report. However, they are provided electronically in Appendix H.

Table 15. Participant information for the two-dimensional benchmark problem

Code names	Institution	Abbreviation	Country	Participants
APOLLO2	Commissariat à l'Energie Atomique	CEA	France	S. Santandrea R. Sanchez
CRONOS2	Commissariat à l'Energie Atomique	CEA	France	F. Moreau
CRONOS2-SN	Commissariat à l'Energie Atomique	CEA	France	F. Moreau
DORT-GRS	Gesellschaft fuer Reaktorsicherheit	GRS	Germany	A. Pautz, S. Langenbuch, W. Zwermann, K. Velkov
COHINT	Indira Gandhi Centre for Atomic Research	IGCAR	India	P. Mohanakrishnan
CHAPLET	TEPCO Systems Corporation	TEPSYS	Japan	S. Kosaka
TWODANT	Hanyang University, Dept. Nuclear Engineering	HU-Korea	Korea	J.K. Kim C.Y. Han
DeCART	Korea Atomic Energy Research Institute	KAERI	Korea	H.G. Joo, J.Y. Cho, K.S. Kim, S.Q. Zee
CRX	Korea Advanced Institute of Science and Technology	KAIST	Korea	N.Z. Cho, G.S. Lee, C.J. Park
MCCG3D	Institute of Physic and Power Engineering	IPPE	Russia	I.R. Suslov
WIMS-SH SUHAM-2D	Russian Research Centre "Kurchatov Institute"	RRC KI	Russia	V.F. Boyarinov
UNKGRO	Russian Research Centre "Kurchatov Institute"	RRC KI	Russia	V.D. Davidenko, V.F. Tsibulsky
STRUCTURE	Russian Research Centre "Kurchatov Institute"	RRC KI	Russia	A.A. Polismakov, A.V. Tchibiniaev
GEFCOP	Russian Research Centre "Kurchatov Institute"	RRC KI	Russia	T.S. Poveschenko
VARIANT-ISE	Argonne National Laboratory	ANL	United States	M.A. Smith, N. Tsoulfanidis, E.E. Lewis
VARIANT-SE	Argonne National Laboratory	ANL	United States	M.A. Smith, N. Tsoulfanidis, E.E. Lewis
PARTISN	Los Alamos National Laboratory	LANL	United States	J.A. Dahl, R.E. Alcouffe, R.S. Baker
PERICLES	Los Alamos National Laboratory	LANL	United States	T. Wareing J. McGhee
DORT-ORNL	Oak Ridge National Laboratory	ORNL	United States	Y. Azmy, J. Gehin, R. Orsi (ENEA)
HELIOS	Pennsylvania State Univ., Dept. Nuclear Engineering	PSU-USA	United States	B. Ivanov, K. Ivanov, R.J.J. Stamm'ler

Table 16. Brief code description for each participant two-dimensional benchmark solution

Code names	Angular approximation	Spatial approximation
APOLLO2	Method of characteristics	Flat source arbitrary spatial mesh
CRONOS2	Diffusion	Finite element method
CRONOS2-SN	Discrete ordinates	Finite element method
DORT-GRS	Discrete ordinates	Cartesian finite differences, linear spatial differencing
COHINT	Interface current technique with P_2 half space expansion	Spatial Cartesian mesh with flat spatial differencing
CHAPLET	Method of characteristics	Flat source arbitrary spatial mesh
TWODANT	Discrete ordinates	Spatial Cartesian mesh with linear spatial differencing
DeCART	Method of characteristics	Flat source arbitrary spatial mesh
CRX	Method of characteristics	Flat source arbitrary spatial mesh
MCCG3D	Method of characteristics	QSD-linear arbitrary spatial mesh
WIMS-SH SUHAM-2D	Surface harmonics method; zeroth trial matrix-G_3, first and second-P_2, third-diffusion	Spatial Cartesian mesh with one point per cell, continuous inside each cell
UNKGRO	Method of characteristics with stochastic rays	Flat source arbitrary spatial mesh
STRUCTURE	Collision probability, S_N synthesis	Flat source arbitrary spatial mesh
GEFCOP	First collision probability method	Flat source arbitrary spatial mesh
VARIANT-ISE	Nodal spherical harmonics with integral transport	Finite element method
VARIANT-SE	Nodal spherical harmonics	Finite element method
PARTISN	Discrete ordinates	Spatial Cartesian mesh, diamond differencing
PERICLES	Discrete ordinates	Unstructured quadrilateral mesh with bilinear discontinuous spatial differencing
DORT-ORNL	Discrete ordinates	Cartesian finite differences, linear spatial differencing
HELIOS	Current coupling collision probability	Flat source arbitrary spatial mesh

Table 17. Eigenvalue solutions for the two-dimensional benchmark problem

Code names	Eigenvalue	Per cent error
Reference MCNP	1.186550	±0.008
APOLLO2	1.186180	-0.031
CRONOS2	1.183230	-0.280
CRONOS2-SN	1.183380	-0.267
DORT-GRS	1.184818	-0.146
COHINT	1.175300	-0.948
CHAPLET	1.186560	0.001
TWODANT	1.186677	0.011
DeCART	1.186600	0.004
CRX	1.188130	0.133
MCCG3D	1.186570	0.002
WIMS-SH SUHAM-2D	1.186284	-0.022
UNKGRO	1.185230	-0.111
STRUCTURE	1.185228	-0.111
GEFCOP	1.186300	-0.021
VARIANT-ISE	1.187454	0.076
VARIANT-SE	1.184945	-0.135
PARTISN	1.186370	-0.015
PERICLES	1.186580	0.003
DORT-ORNL	1.184960	-0.134
HELIOS	1.193299	0.569

Figure 4. Eigenvalue solutions for the two-dimensional benchmark

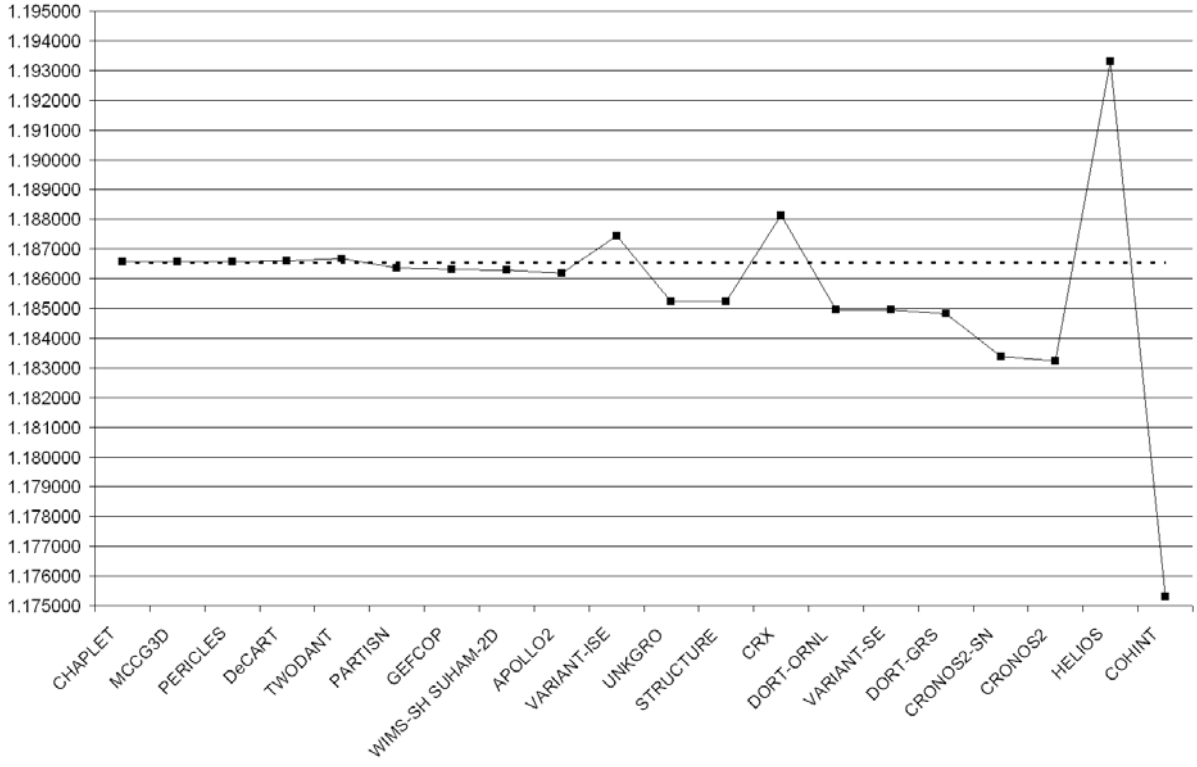

Figure 5. Eigenvalue per cent errors for the two-dimensional benchmark

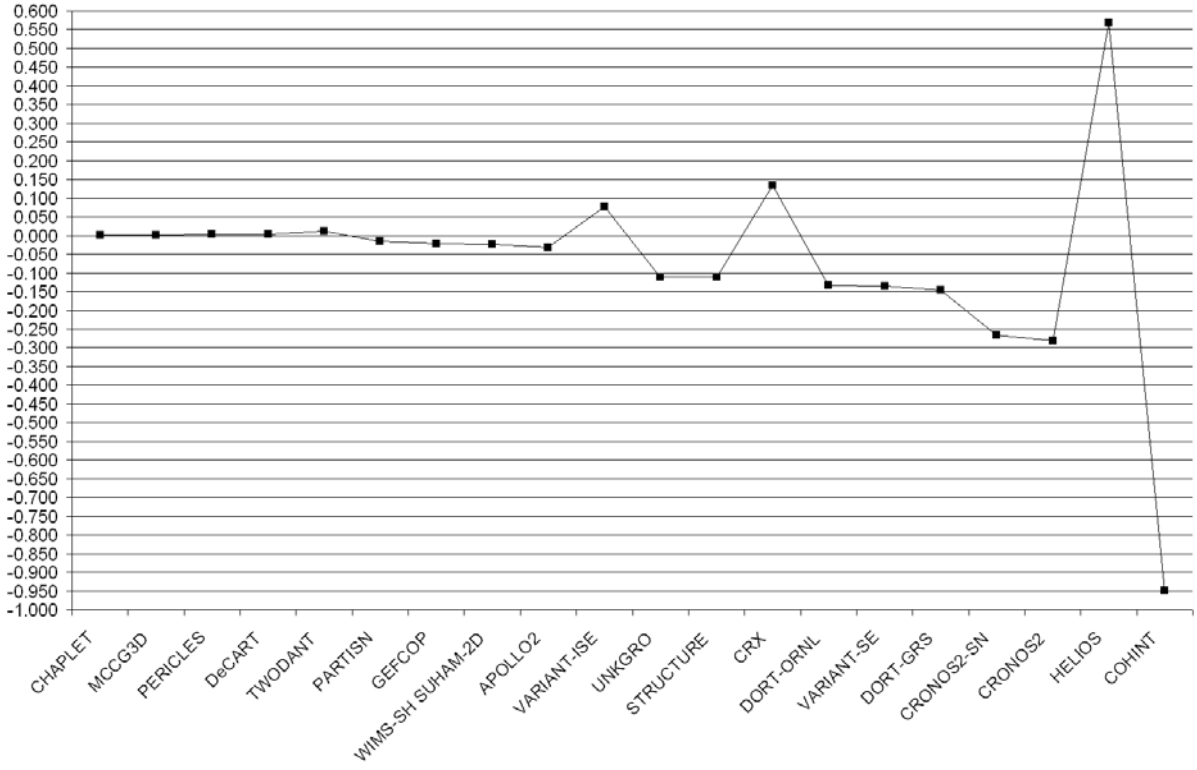

Table 18. Participant results for specific pin powers in the two-dimensional benchmark

Code names	Maximum pin power	Per cent error	Minimum pin power	Per cent error	Maximum per cent error	Associated reference MCNP statistical error
Ref. MCNP	2.498	±0.16	0.232	±0.58		
APOLLO2	2.499	0.03	0.239	3.10	4.16	±0.58
CRONOS2	2.520	0.90	0.241	4.00	5.95	±0.58
CRONOS2-SN	2.506	0.34	0.241	4.00	4.98	±0.58
DORT-GRS	2.510	0.48	0.232	0.02	1.21	±0.44
COHINT	2.395	-4.11	0.250	8.11	11.36	±0.40
CHAPLET	2.495	-0.13	0.233	0.69	0.93	±0.56
TWODANT	2.534	1.43	0.231	-0.03	2.32	±0.44
DeCART	2.492	-0.23	0.235	1.68	1.84	±0.56
CRX	2.498	0.01	0.233	0.71	1.07	±0.40
MCCG3D	2.498	-0.01	0.233	0.47	0.63	±0.56
WIMS-SH SUHAM-2D	2.525	1.07	0.228	-1.32	4.38	±0.40
UNKGRO	2.503	0.19	0.236	1.94	4.21	±0.47
STRUCTURE	2.480	-0.71	0.242	4.36	4.52	±0.56
GEFCOP	2.495	-0.10	0.228	-1.32	10.16	±0.21
VARIANT-ISE	2.496	-0.07	0.232	0.22	0.54	±0.44
VARIANT-SE	2.508	0.39	0.232	0.11	1.13	±0.44
PARTISN	2.503	0.18	0.232	0.18	5.23	±0.23
PERICLES	2.494	-0.16	0.231	-0.21	0.92	±0.56
DORT-ORNL	2.512	0.57	0.231	-0.22	1.30	±0.44
HELIOS	2.510	0.49	0.233	0.54	2.27	±0.44

Figure 6. Maximum pin power results for the two-dimensional benchmark

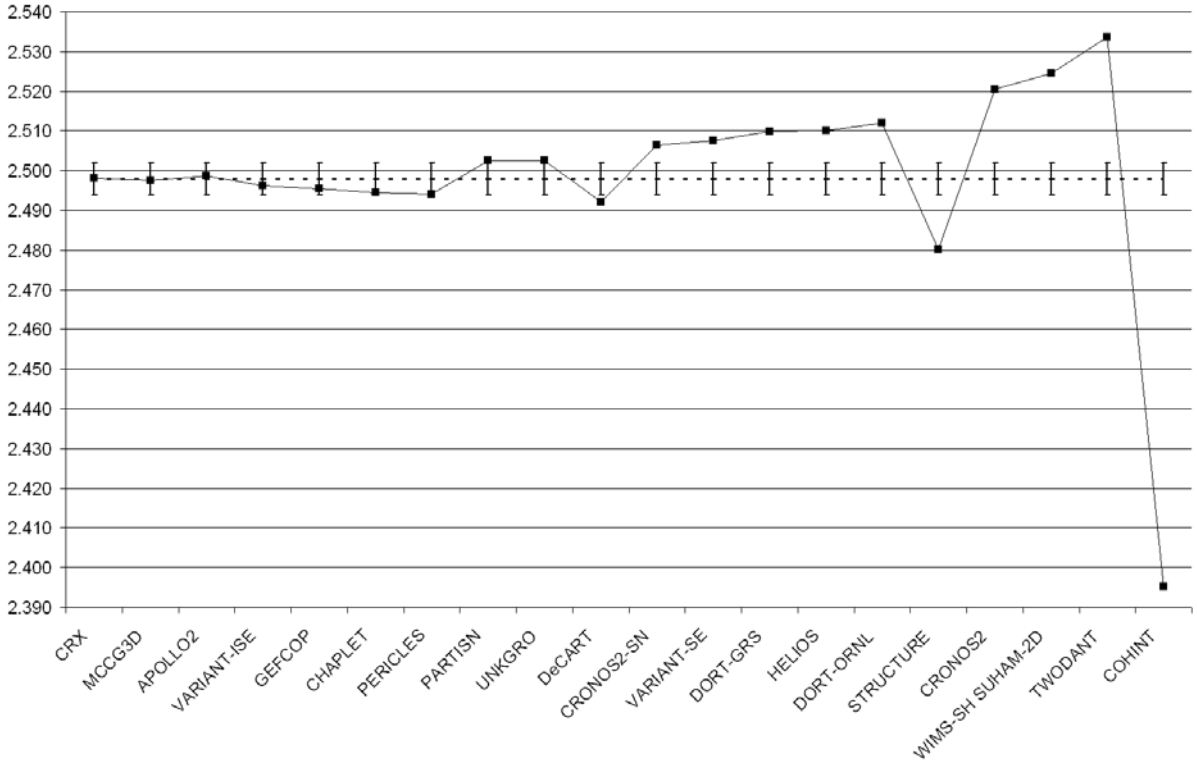

Figure 7. Minimum pin power results for the two-dimensional benchmark

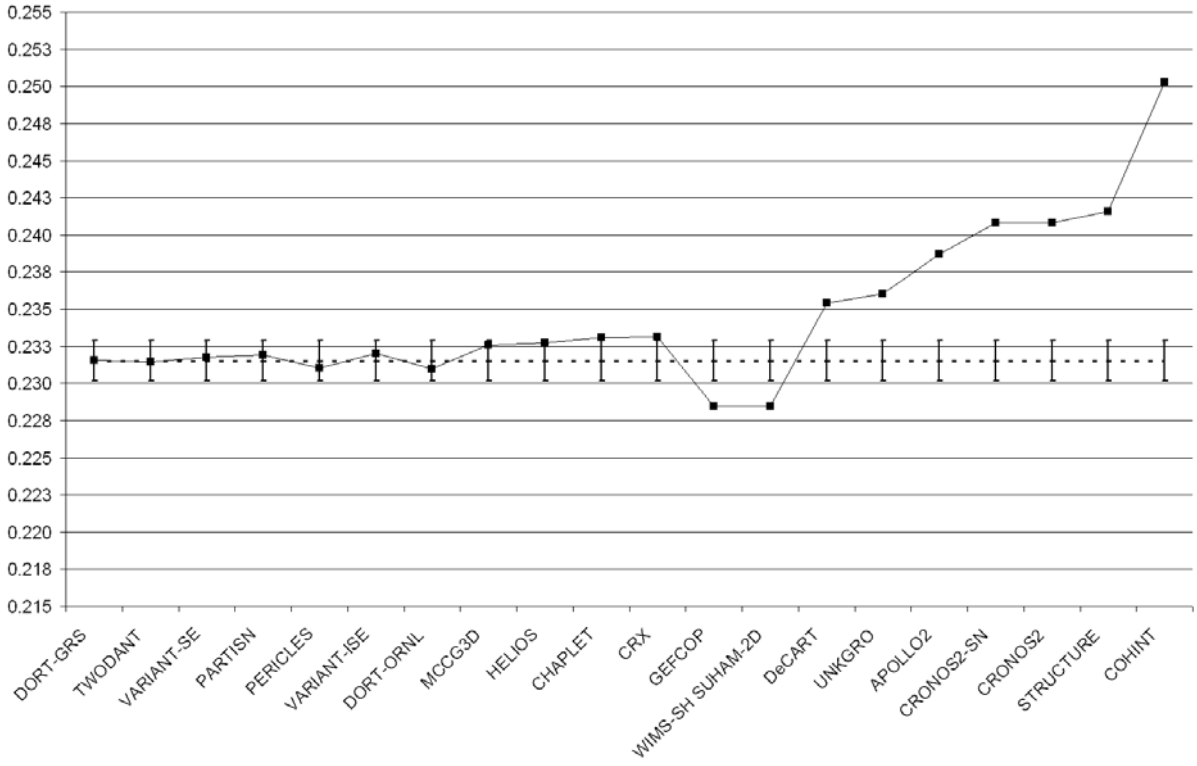

Figure 8. Maximum per cent errors for the two-dimensional benchmark

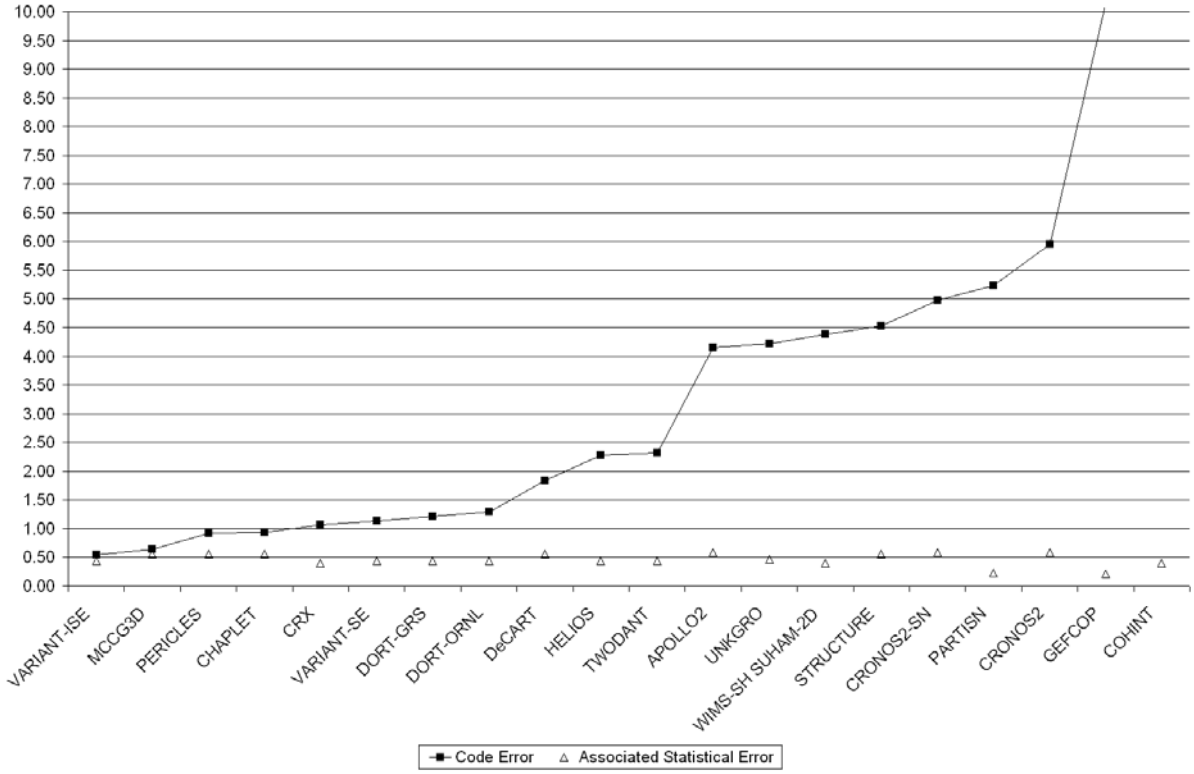

Table 19. Assembly power per cent errors for the two-dimensional benchmark

Code names	Inner UO_2	*Per cent error*	MOX	*Per cent error*	Outer UO_2	*Per cent error*
Reference MCNP	492.8	±0.10	211.7	±0.18	139.8	±0.20
APOLLO2	492.3	-0.10	211.7	0.01	140.3	0.34
CRONOS2	495.4	0.53	210.8	-0.41	138.9	-0.61
CRONOS2-SN	494.0	0.24	211.0	-0.34	140.0	0.16
DORT-GRS	494.5	0.34	211.0	-0.34	139.5	-0.20
COHINT	486.8	-1.22	213.8	0.97	141.7	1.36
CHAPLET	492.3	-0.10	211.9	0.10	139.9	0.05
TWODANT	497.5	0.95	209.6	-1.01	139.4	-0.30
DeCART	491.9	-0.18	212.0	0.15	140.0	0.19
CRX	492.9	0.01	211.8	0.03	139.6	-0.15
MCCG3D	492.8	-0.01	211.8	0.02	139.7	-0.03
WIMS-SH SUHAM-2D	494.9	0.43	211.3	-0.21	138.5	-0.89
UNKGRO	489.3	-0.70	212.9	0.57	140.8	0.73
STRUCTURE	490.2	-0.52	212.5	0.37	140.8	0.71
GEFCOP	490.8	-0.40	213.8	0.97	137.7	-1.50
VARIANT-ISE	492.6	-0.04	211.8	0.06	139.7	-0.03
VARIANT-SE	494.2	0.28	211.1	-0.27	139.5	-0.18
PARTISN	493.3	0.11	211.5	-0.12	139.8	-0.02
PERICLES	491.9	-0.17	212.4	0.33	139.3	-0.38
DORT-ORNL	494.9	0.42	210.8	-0.41	139.4	-0.26
HELIOS	494.4	0.32	211.1	-0.30	139.5	-0.20

Figure 9. Inner UO_2 assembly power per cent errors for the two-dimensional benchmark

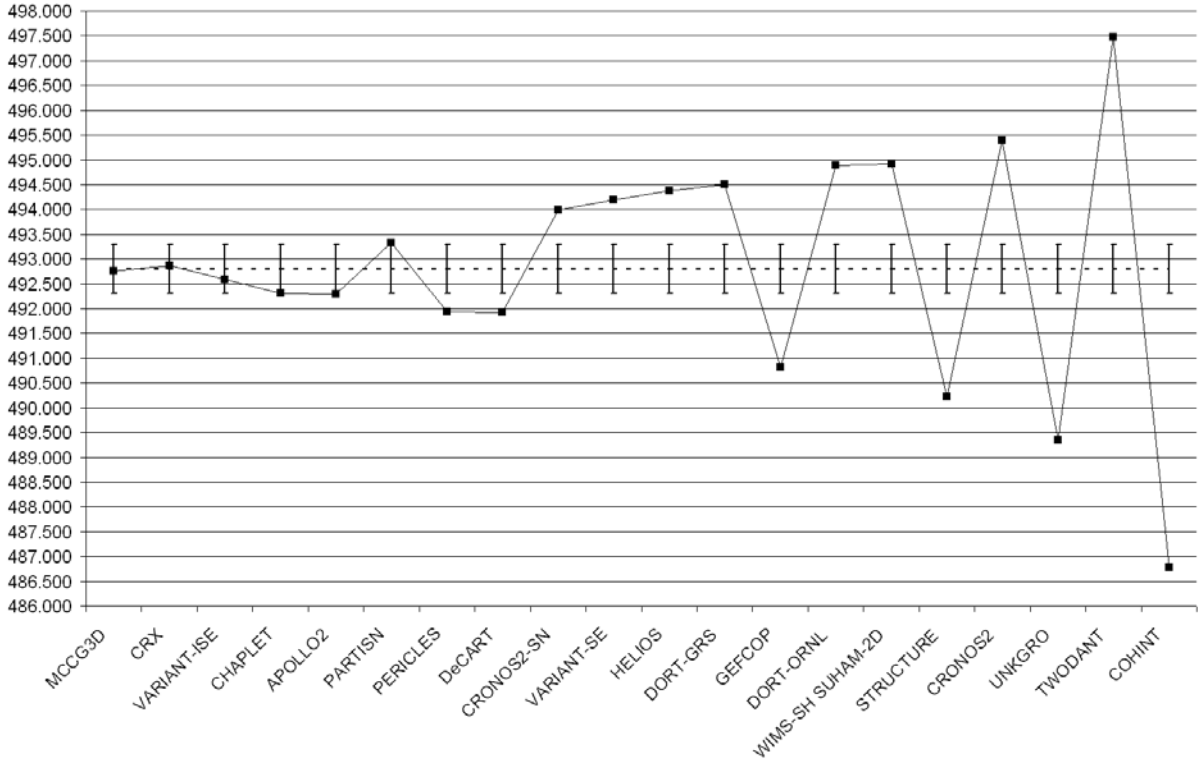

Figure 10. MOX assembly power per cent errors for the two-dimensional benchmark

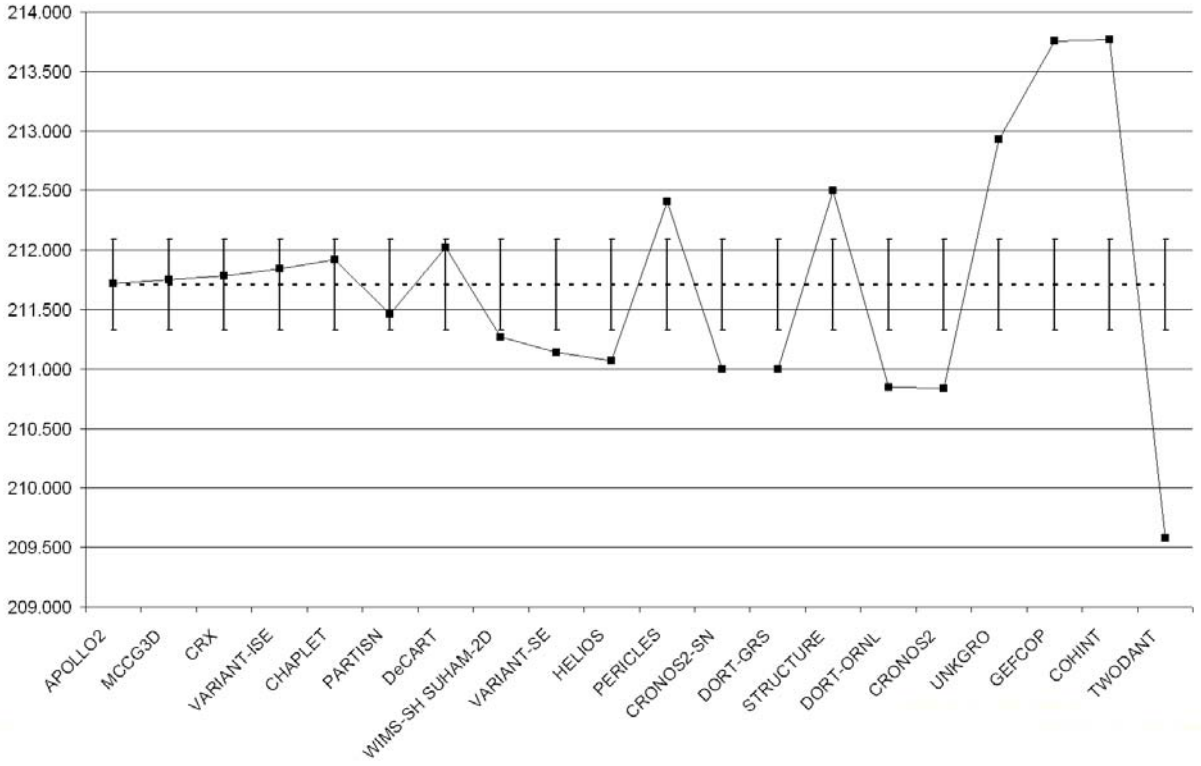

Figure 11. Outer UO_2 assembly power per cent errors for the two-dimensional benchmark

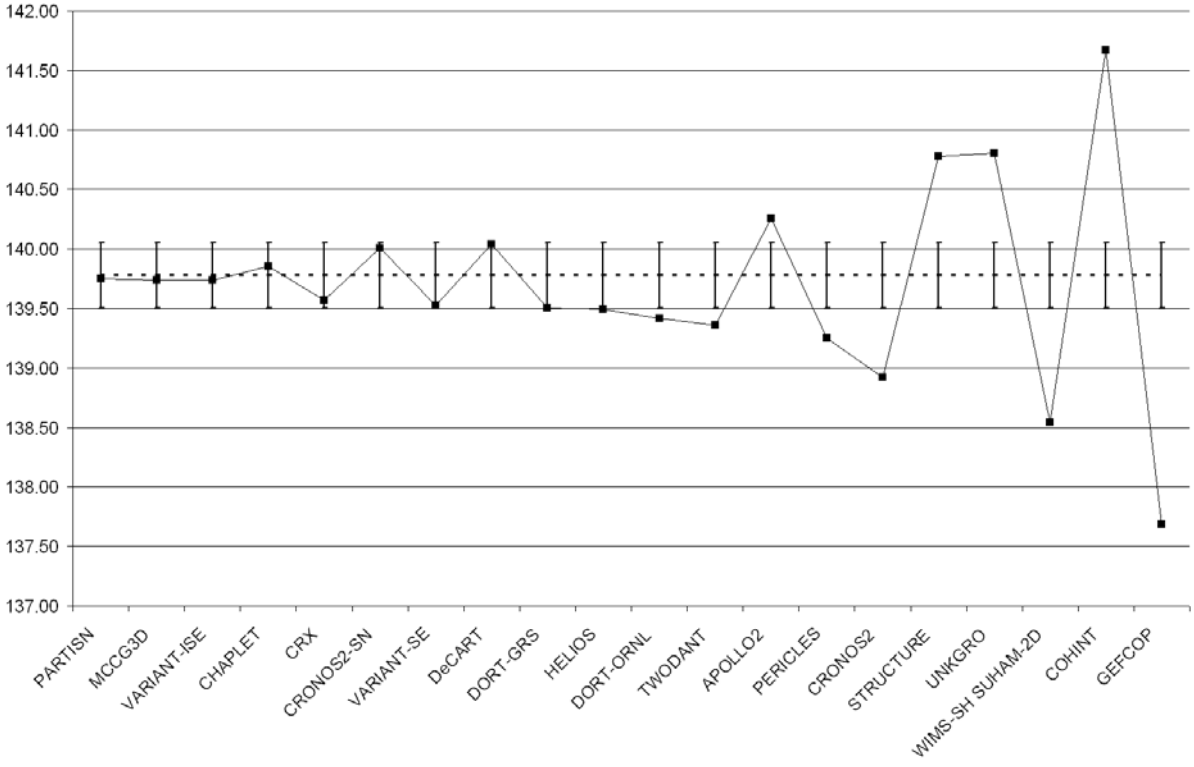

Table 20. Pin power distribution error measures for the two-dimensional benchmark

Code names	AVG	RMS	MRE
Reference MCNP	0.32	0.34	0.27
APOLLO2	0.51	0.78	0.36
CRONOS2	1.42	1.73	1.21
CRONOS2-SN	0.77	1.00	0.60
DORT-GRS	0.35	0.41	0.34
COHINT	2.66	3.58	2.34
CHAPLET	0.18	0.24	0.15
TWODANT	0.89	1.04	0.90
DeCART	0.31	0.46	0.24
CRX	0.23	0.30	0.19
MCCG3D	0.13	0.17	0.11
WIMS-SH SUHAM-2D	1.24	1.57	1.04
UNKGRO	1.01	1.28	0.91
STRUCTURE	0.82	1.24	0.62
GEFCOP	1.88	2.54	1.50
VARIANT-ISE	0.13	0.17	0.11
VARIANT-SE	0.29	0.35	0.28
PARTISN	0.22	0.33	0.23
PERICLES	0.31	0.37	0.28
DORT-ORNL	0.42	0.49	0.41
HELIOS	0.61	0.77	0.52

Figure 12. AVG per cent error for the two-dimensional benchmark

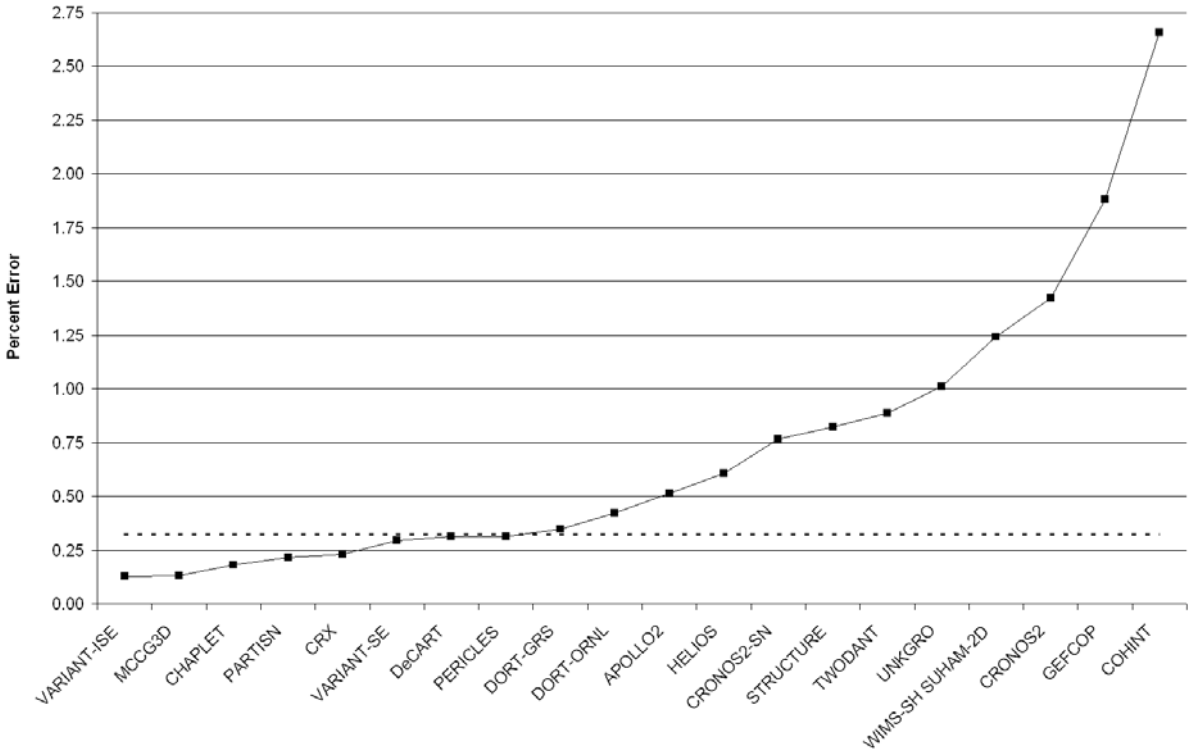

Figure 13. RMS per cent error for the two-dimensional benchmark

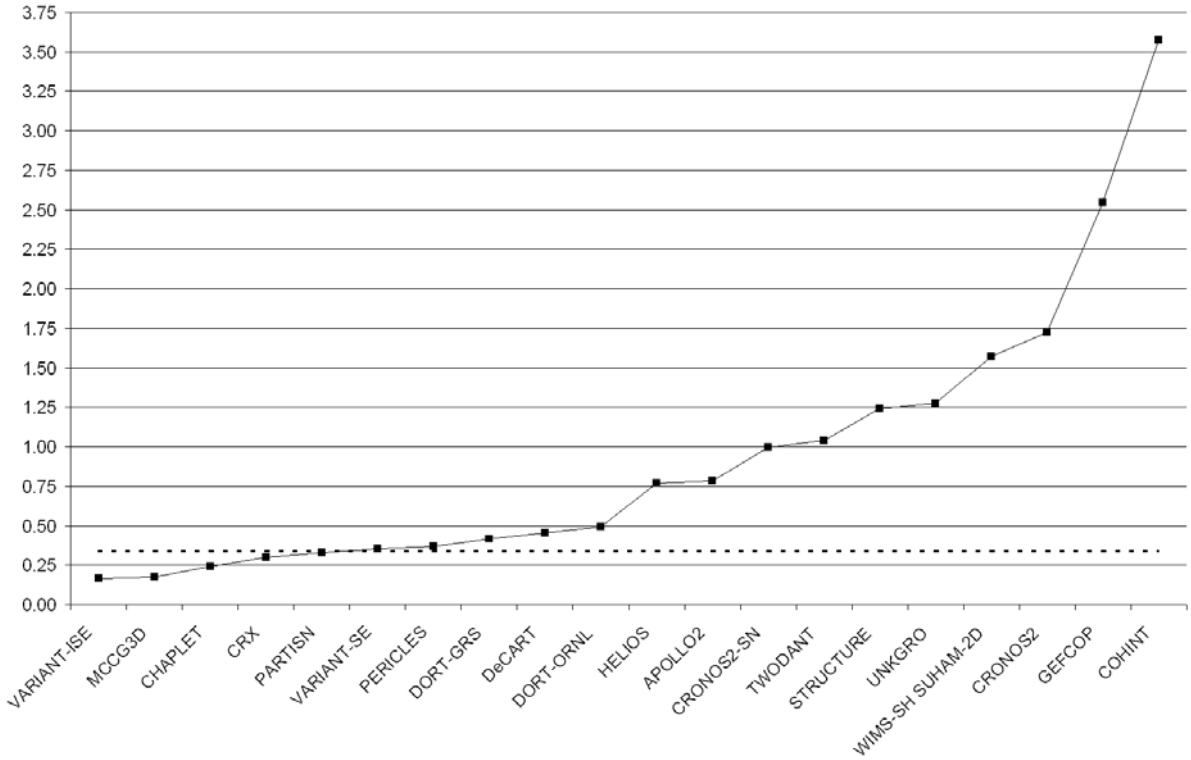

Figure 14. MRE per cent error for the two-dimensional benchmark

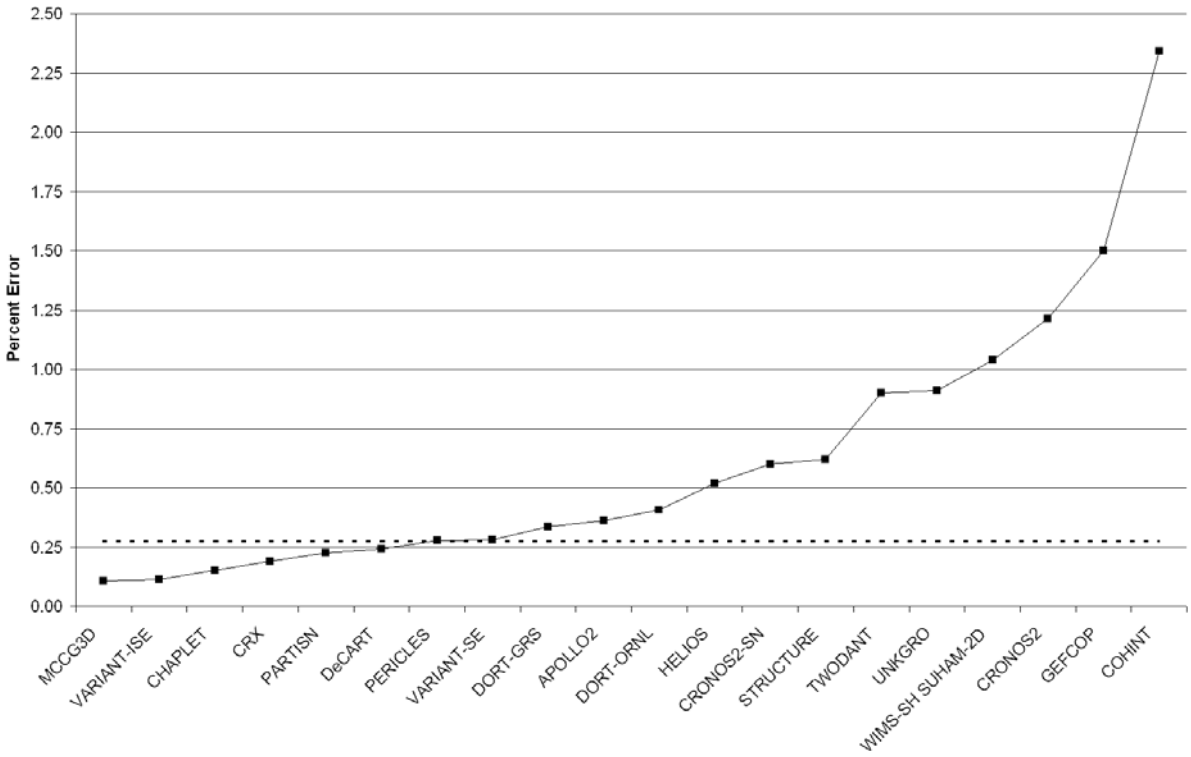

Table 21. Number of fuel pins within the reference confidence intervals for the two-dimensional benchmark

Code names	68%	90%	98%	99.8%
APPOLLO2	223	389	517	628
CRONOS2	60	101	147	173
CRONOS2-SN	100	150	224	305
DORT-GRS	203	361	486	661
COHINT	30	50	84	107
CHAPLET	485	734	911	1002
TWODANT	121	159	199	263
DeCART	338	519	696	833
CRX	376	569	784	942
MCCG3D	655	884	1013	1050
WIMS-SH SUHAM-2D	68	108	174	209
UNKGRO	91	143	195	273
STRUCTURE	120	217	316	422
GEFCOP	48	90	132	192
VARIANT-ISE	660	879	1008	1054
VARIANT-SE	247	403	597	781
PARTISN	412	621	817	933
PERICLES	165	344	576	783
DORT-ORNL	159	245	393	530
HELIOS	142	217	324	437

Table 22. Percentage of fuel pins within the reference confidence intervals for the two-dimensional benchmark

Code names	68%	90%	98%	99.8%
APPOLLO2	21.1	36.8	49.0	59.5
CRONOS2	5.7	9.6	13.9	16.4
CRONOS2-SN	9.5	14.2	21.2	28.9
DORT-GRS	19.2	34.2	46.0	62.6
COHINT	2.8	4.7	8.0	10.1
CHAPLET	45.9	69.5	86.3	94.9
TWODANT	11.5	15.1	18.8	24.9
DeCART	32.0	49.1	65.9	78.9
CRX	35.6	53.9	74.2	89.2
MCCG3D	62.0	83.7	95.9	99.4
WIMS-SH SUHAM-2D	6.4	10.2	16.5	19.8
UNKGRO	8.6	13.5	18.5	25.9
STRUCTURE	11.4	20.5	29.9	40.0
GEFCOP	4.5	8.5	12.5	18.2
VARIANT-ISE	62.5	83.2	95.5	99.8
VARIANT-SE	23.4	38.2	56.5	74.0
PARTISN	39.0	58.8	77.4	88.4
PERICLES	15.6	32.6	54.5	74.1
DORT-ORNL	15.1	23.2	37.2	50.2
HELIOS	13.4	20.5	30.7	41.4

Figure 15. Percentage of fuel pins within the two-dimensional benchmark confidence intervals

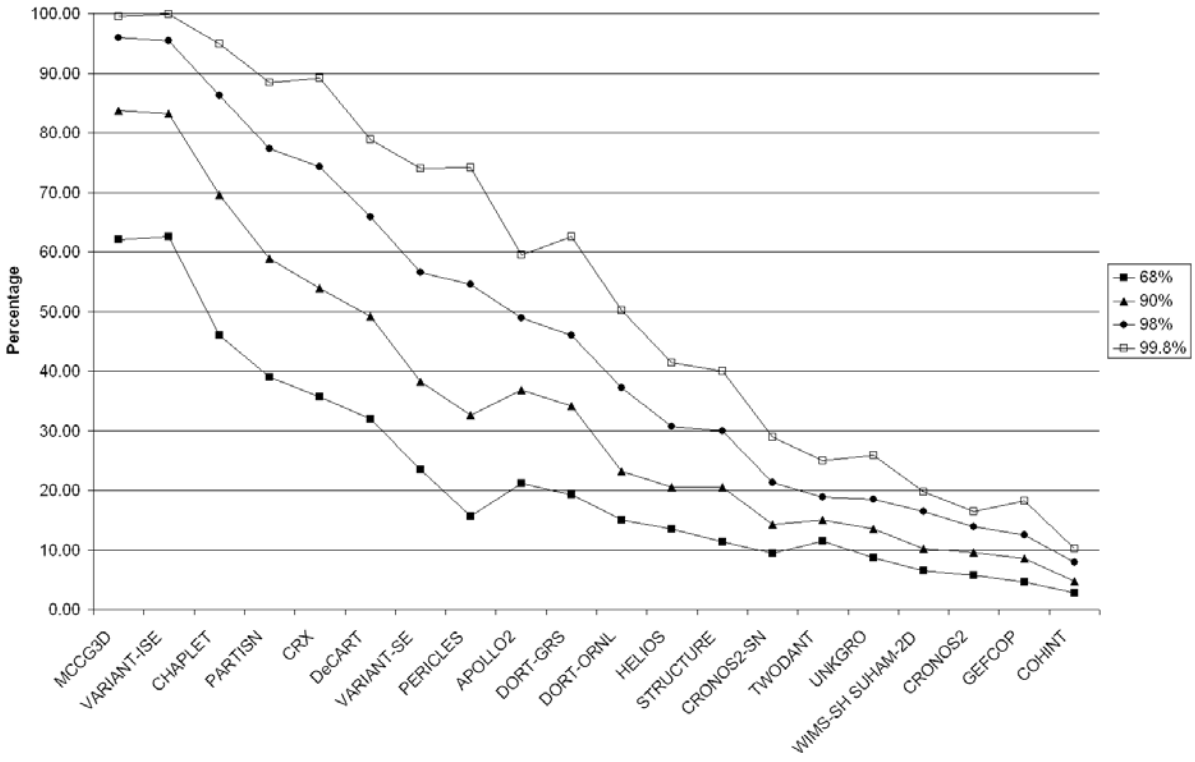

Table 23. Estimated CPU time for the two-dimensional benchmark

Code names	Estimated CPU time
APOLLO2	Hours
CRONOS2	Minutes
CRONOS2-SN	Minutes
DORT-GRS	Hours
COHINT	Hours
CHAPLET	Hours
TWODANT	Minutes
DeCART	Hour
CRX	*Not given*
MCCG3D	*Not given*
WIMS-SH SUHAM-2D	Minutes
UNKGRO	Days
STRUCTURE	Days
GEFCOP	Hours
VARIANT-ISE	Hours
VARIANT-SE	Days
PARTISN	Minutes
PERICLES	Hours
DORT-ORNL	Days
HELIOS	Minutes

Chapter 7

THREE-DIMENSIONAL BENCHMARK RESULTS

A total of 11 participants submitted results for the three-dimensional benchmark. Table 24 gives the names of the participants along with their institution, their home country and the name of the code that produced the results submitted. A brief description of the spatial and angular approximations implemented in each participant's code is given in Table 25. To view a complete summary of the participants' codes and methods used, refer to the original documentation submitted by each participant in Appendix B.

For the three-dimensional benchmark, the results from nine first-order codes and two second-order codes were submitted. Four of the first-order codes are collision probability methods, two of which break down the three-dimensional problem into two-dimensional planer coupled-characteristics calculations. The remaining first-order approaches are discrete ordinates methods, four of which implement a finite-difference approach and one which implements a finite-element approach. As for the second-order codes, one is a discrete ordinates method and the other is a nodal spherical harmonics approach, and both implement finite element spatial approximations.

Table 26 provides the participant eigenvalue solutions and the per cent error with respect to the reference MCNP solution. Figure 16 displays the eigenvalue solutions and Figure 17 the eigenvalue per cent errors; both are ordered with respect to decreasing eigenvalue accuracy. As can be seen in Figures 16 and 17 and Table 26, a wide range of solutions were obtained. Only one of the participants' codes is within the 98% confidence interval of the MCNP reference. The average error on the eigenvalue solution for all the participant solutions is about 0.1%.

The specific pin power error measures are tabulated in Table 27. Figure 18 plots the maximum pin power results, Figure 19 the minimum pin power results, and Figure 20 the maximum per cent errors found in each participant solution along with the statistical error associated with that pin power. All of the participant solutions in Figures 6-8 are ordered with respect to decreasing solution accuracy. In Table 27, four participants obtained a maximum pin power within the 98% confidence interval and six obtained a minimum pin power within the 98% confidence interval. The maximum per cent error results in Figure 20 are much worse, with none of the codes succeeding in coming within the reference MCNP confidence intervals. Only two of the participant codes have maximum errors less than 1% and only seven achieve maximum errors less than 5%.

The assembly power error measures are tabulated in Table 28. Figure 21 plots the participant results for the inner UO_2 assembly power, Figure 22 the results for the MOX assembly power and Figure 23 the results of the outer UO_2 assembly power. For the inner UO_2 assembly power, four participant solutions are within the 98% confidence interval. For the MOX assembly, seven participant solutions are within the 98% confidence interval. For the outer UO_2 assembly, eight of the participant solutions are within the 98% confidence interval.

Table 29 gives the pin power distribution error measures for the three-dimensional benchmark problem. Figure 24 displays the AVG per cent error results, Figure 25 the RMS per cent error results and Figure 26 the MRE per cent error results. Four of the participant results agree within the 98% confidence interval for the AVG error measure and nine are less than 1% in error. The results of the RMS error measure are slightly worse as four of the participants are within the 98% confidence interval and eight are less than 1% in error. The results for the MRE error measure are similar to the results of the AVG error measure with four participants within the 98% confidence interval and nine less than 1% in error.

Table 30 tabulates the number of fuel pins within the various confidence intervals while Table 31 tabulates the percentage of fuel pins within the confidence intervals. Figure 15 plots the participant results, ordered with respect to the 98% confidence interval results. As can be seen, none of the participants match the 98% confidence interval and relatively few are close.

As for the two-dimensional benchmark, Table 32 gives a crude estimate of each participant's CPU time. Also similar to the two-dimensional benchmark, the inaccuracies in the three-dimensional benchmark can be attributed to insufficient space-angle approximations implemented by the participants. It is suggested that to improve any of the results, further refinements of the angular and spatial variable be applied by the participants. The analysis tools used for the three-dimensional benchmark are provided electronically in Appendix I and can be used by the participants for future comparisons if desired. Also, the table of all of the participant pin power distributions and pin power per cent error distributions is included as a worksheet of the EXCEL workbook "z.3D.Summary.of.Final.Results" provided in Appendix I.

Additional continuous Monte Carlo solutions provided by some of the participants are not used for comparison in the report. However, they are provided electronically in Appendix H.

Table 24. Participant information for the three-dimensional benchmark problem

Code names	Institution	Abbreviation	Country	Participants
CRONOS2-SN	Commissariat à l'Energie Atomique	CEA	France	F. Moreau
TORT-GRS	Gesellschaft fuer Reaktorsicherheit	GRS	Germany	A. Pautz, S. Langenbuch, W. Zwermann, K. Velkov
THREEDANT	Hanyang University, Dept. Nuclear Engineering	HU-Korea	Korea	J.K. Kim, C.Y. Han
DeCART	Korea Atomic Energy Research Institute	KAERI	Korea	H.G. Joo, J.Y. Cho, K.S. Kim S.Q. Zee
CRX	Korea Advanced Institute of Science and Technology	KAIST	Korea	N.Z. Cho, G.S. Lee, C.J. Park
MCCG3D	Institute of Physic and Power Engineering	IPPE	Russia	I.R. Suslov
UNKGRO	Russian Research Centre "Kurchatov Institute"	RRC KI	Russia	V.D. Davidenko, V.F. Tsibulsky
VARIANT-SE	Argonne National Laboratory	ANL	United States	M.A. Smith, N. Tsoulfanidis, E.E. Lewis
PARTISN	Los Alamos National Laboratory	LANL	United States	J.A. Dahl, R.E. Alcouffe, R.S. Baker
ATTILA	Los Alamos National Laboratory	LANL	United States	T. Wareing, J. McGhee
TORT-ORNL	Oak Ridge National Laboratory	ORNL	United States	Y. Azmy, J. Gehin, R. Orsi (ENEA)

Table 25. Brief code description for each participant three-dimensional benchmark solution

Code names	Angular approximation	Spatial approximation
CRONOS2-SN	Discrete ordinates	Finite element method
TORT-GRS	Discrete ordinates	Cartesian finite differences, linear spatial differencing
THREEDANT	Discrete ordinates	Spatial Cartesian mesh with linear spatial differencing
DeCART	Method of characteristics-2-D diffusion-1-D	Flat source arbitrary spatial mesh
CRX	Method of characteristics-2-D S_N-1-D	Flat source arbitrary spatial mesh
MCCG3D	Method of characteristics	QSD-Linear arbitrary spatial mesh
UNKGRO	Method of characteristics with stochastic rays	Flat source arbitrary spatial mesh
VARIANT-SE	Nodal spherical harmonics	Finite element method
PARTISN	Discrete ordinates	Spatial Cartesian mesh, diamond differencing
ATTILA	Discrete ordinates	Unstructured tetrahedral mesh with linear discontinuous spatial differencing
TORT-ORNL	Discrete ordinates	Cartesian finite differences, linear spatial differencing

Table 26. Eigenvalue solutions for the three-dimensional benchmark problem

Code names	Eigenvalue	Per cent error
Reference MCNP	1.183810	±0.008
CRONOS2-SN	1.177230	-0.556
TORT-GRS	1.180450	-0.284
THREEDANT	1.183919	0.009
DeCART	1.183860	0.004
CRX	1.185360	0.131
MCCG3D	1.183450	-0.030
UNKGRO	1.181040	-0.234
VARIANT-SE	1.178243	-0.470
PARTISN	1.183620	-0.016
ATTILA	1.183480	-0.028
TORT-ORNL	1.182340	-0.124

Figure 16. Eigenvalue solutions for the three-dimensional benchmark

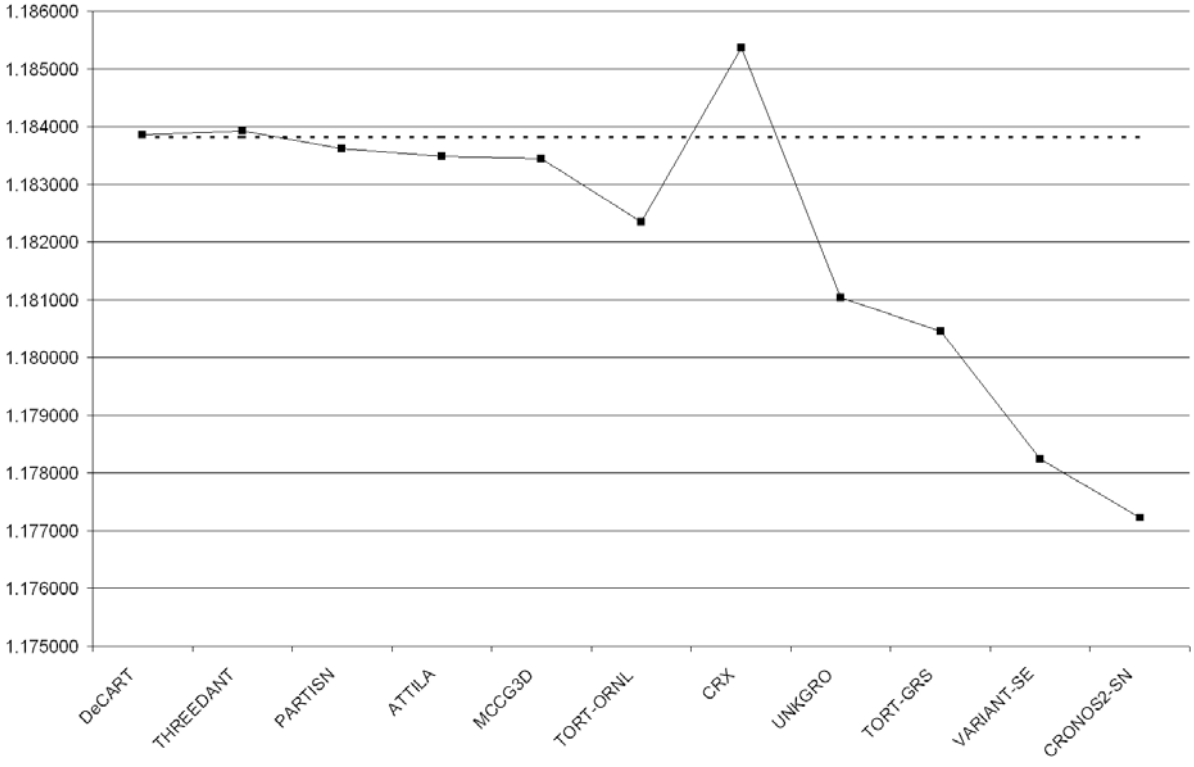

Figure 17. Eigenvalue per cent errors for the three-dimensional benchmark

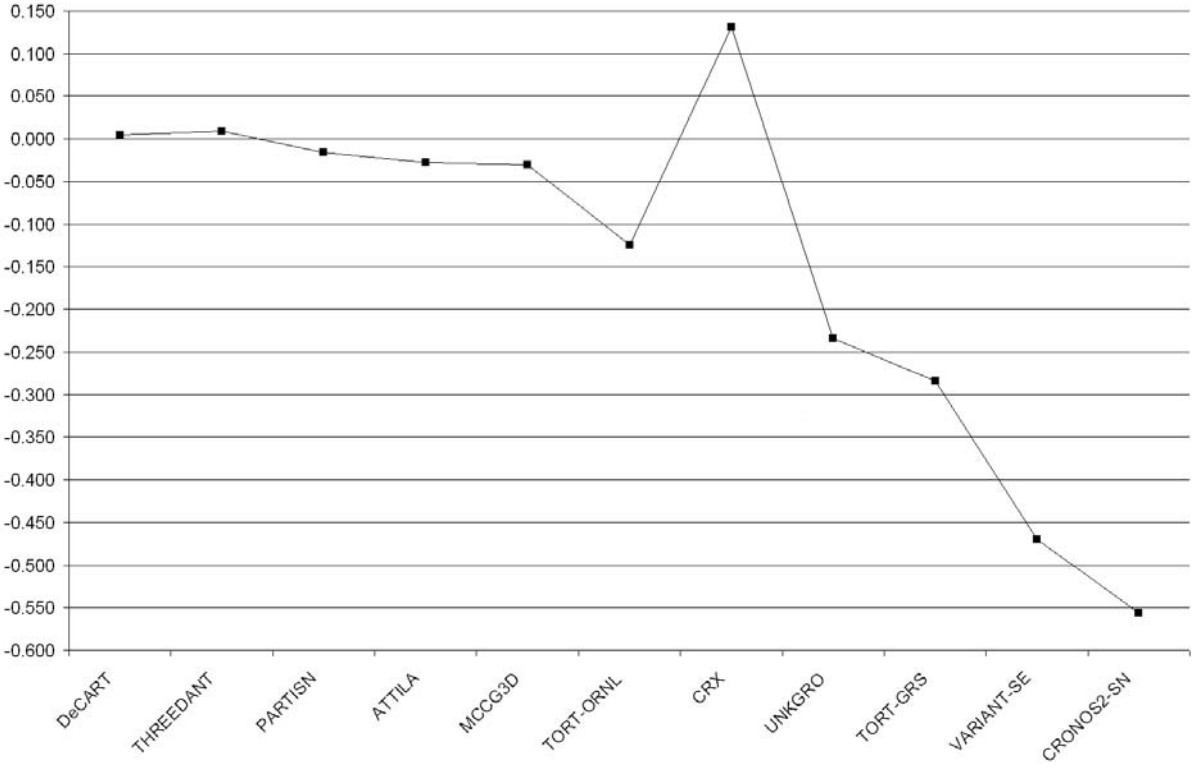

Table 27. Participant results for specific pin powers in the three-dimensional benchmark

Code names	Maximum pin power	Per cent error	Minimum pin power	Per cent error	Maximum per cent error	Associated reference MCNP statistical error
Ref. MCNP	2.500	±0.16	0.23	±0.58		
CRONOS2-SN	2.513	0.53	0.24	3.80	6.47	±0.40
TORT-GRS	2.520	0.82	0.23	0.08	1.71	±0.44
THREEDANT	2.533	1.32	0.23	0.16	2.15	±0.44
DeCART	2.491	-0.35	0.24	1.89	1.89	±0.58
CRX	2.496	-0.14	0.23	0.87	1.05	±0.40
MCCG3D	2.494	-0.24	0.23	1.29	1.59	±0.58
UNKGRO	2.454	-1.82	0.25	8.00	9.18	±0.40
VARIANT-SE	2.509	0.37	0.23	0.35	1.45	±0.37
PARTISN	2.502	0.07	0.23	0.36	5.27	±0.23
ATTILA	2.499	-0.04	0.23	0.29	0.58	±0.44
TORT-ORNL	2.505	0.20	0.23	0.46	0.84	±0.44

Figure 18. Maximum pin power results for the three-dimensional benchmark

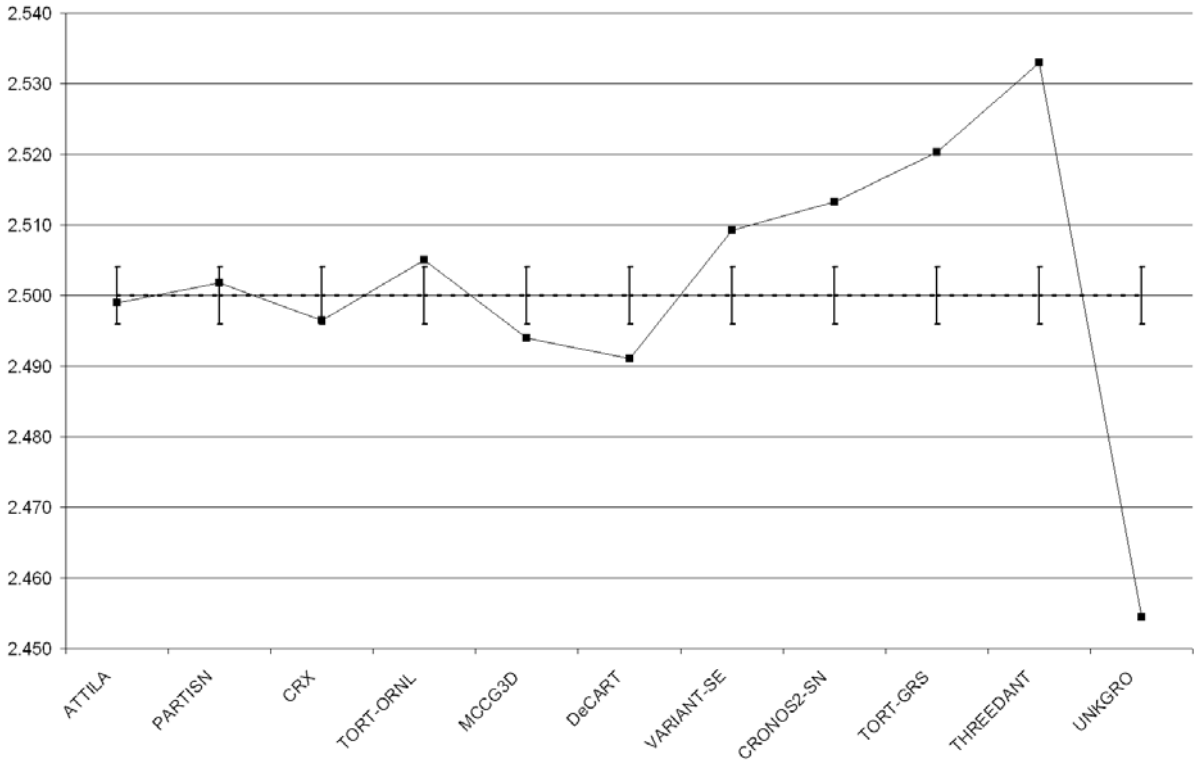

Figure 19. Minimum pin power results for the three-dimensional benchmark

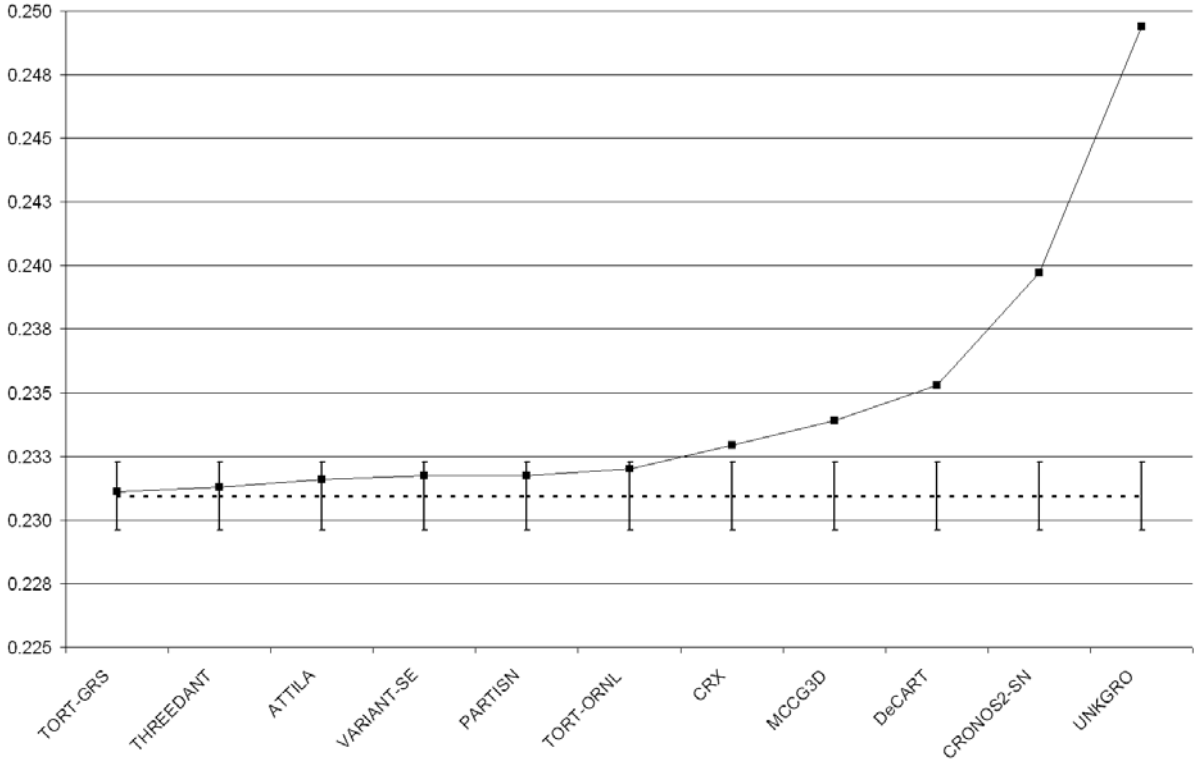

Figure 20. Maximum per cent errors for the three-dimensional benchmark

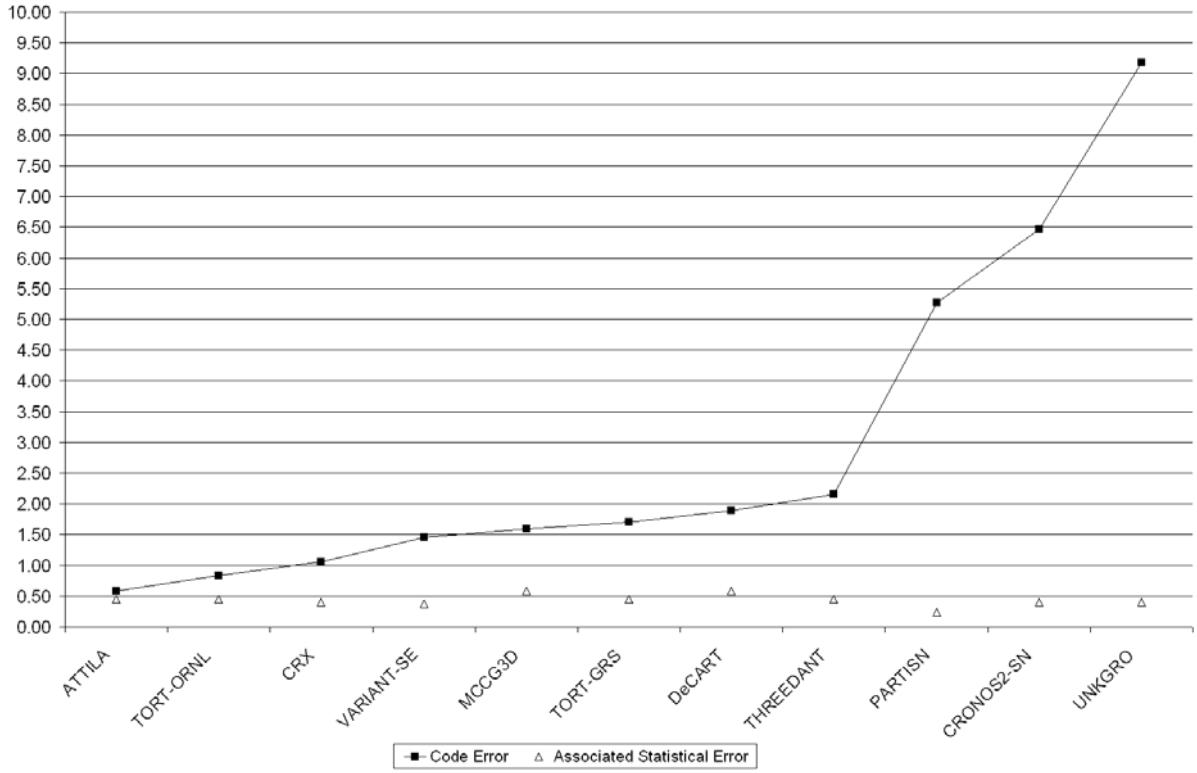

Table 28. Assembly power per cent errors for the three-dimensional benchmark

Code names	Inner UO_2	*Per cent error*	MOX	*Per cent error*	Outer UO_2	*Per cent error*
Reference MCNP	492.9	±0.10	211.8	±0.18	139.6	±0.20
CRONOS2-SN	492.0	-0.17	212.0	0.12	140.0	0.26
TORT-GRS	495.5	0.52	210.5	-0.56	139.4	-0.12
THREEDANT	497.4	0.91	209.6	-0.99	139.3	-0.19
DeCART	491.8	-0.23	212.1	0.16	140.0	0.30
CRX	492.7	-0.05	211.9	0.07	139.5	-0.05
MCCG3D	491.7	-0.24	212.2	0.21	139.9	0.22
UNKGRO	484.3	-1.75	214.7	1.40	142.3	1.93
VARIANT-SE	494.1	0.24	211.2	-0.27	139.6	-0.03
PARTISN	493.2	0.07	211.5	-0.11	139.7	0.08
ATTILA	493.0	0.02	211.7	-0.02	139.6	-0.02
TORT-ORNL	493.7	0.16	211.4	-0.18	139.6	-0.01

Figure 21. Inner UO_2 assembly power per cent errors for the three-dimensional benchmark

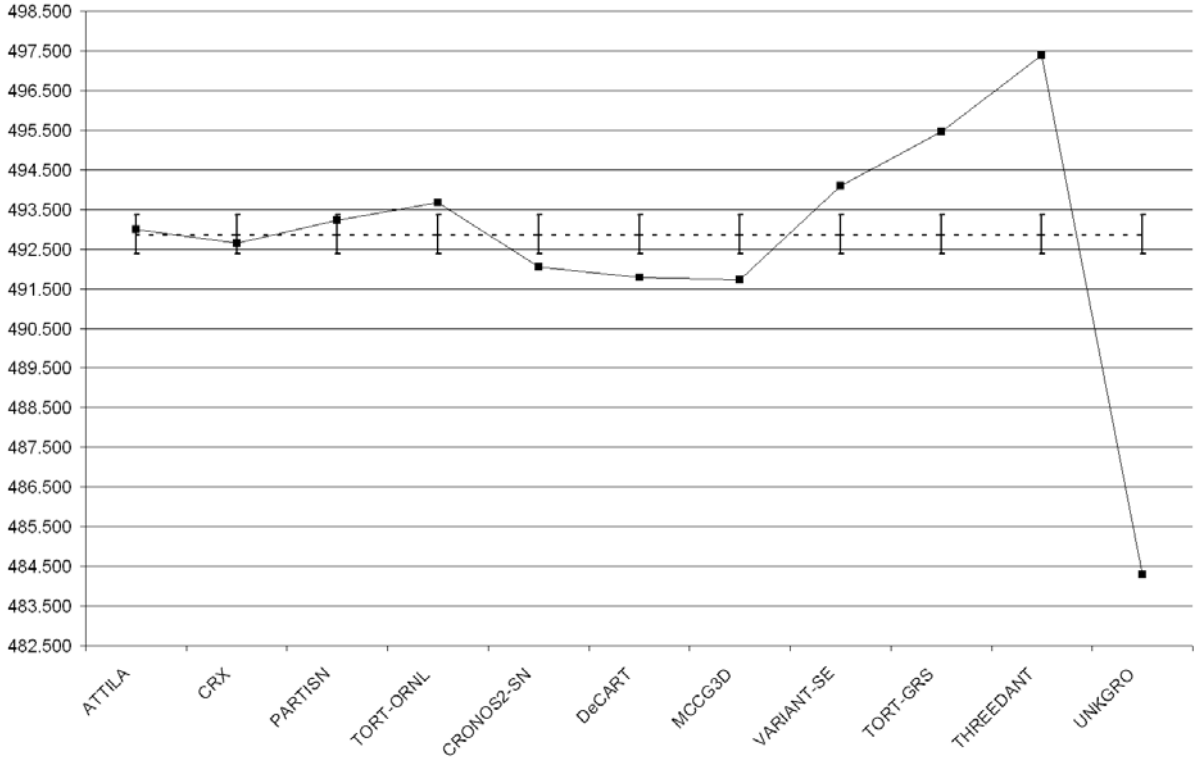

Figure 22. MOX assembly power per cent errors for the three-dimensional benchmark

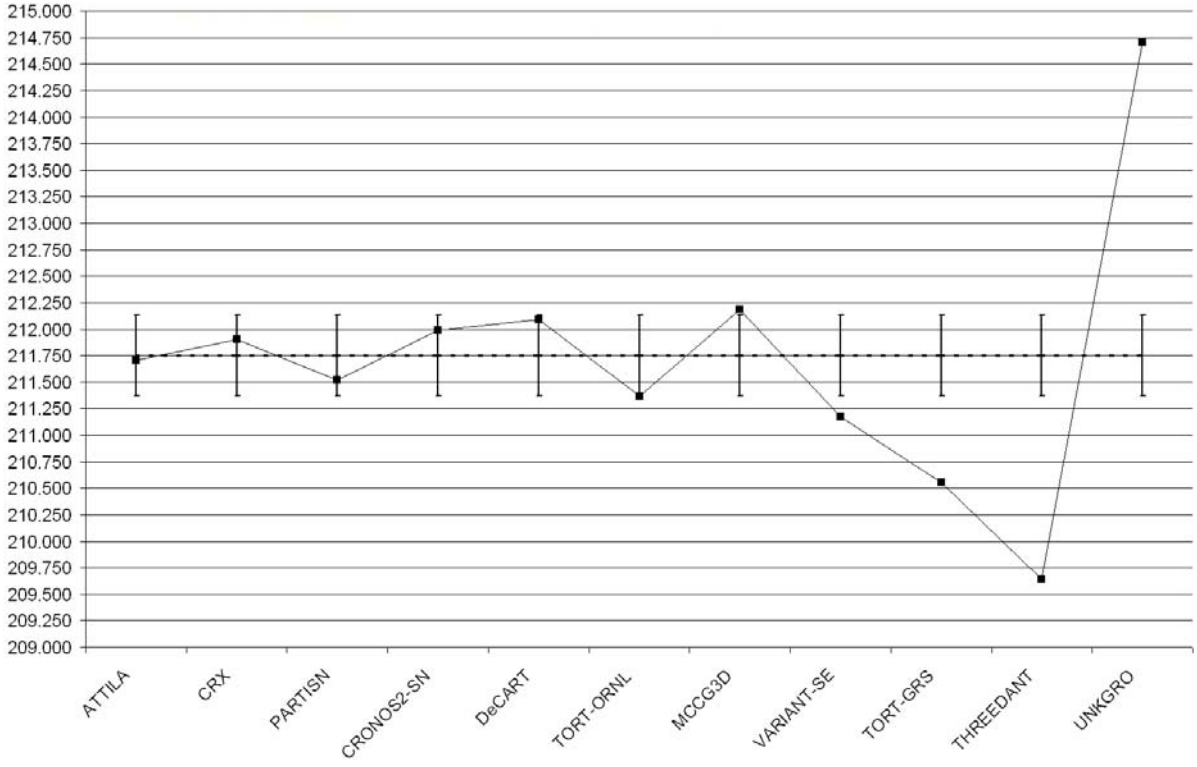

Figure 23. Outer UO_2 assembly power per cent errors for the three-dimensional benchmark

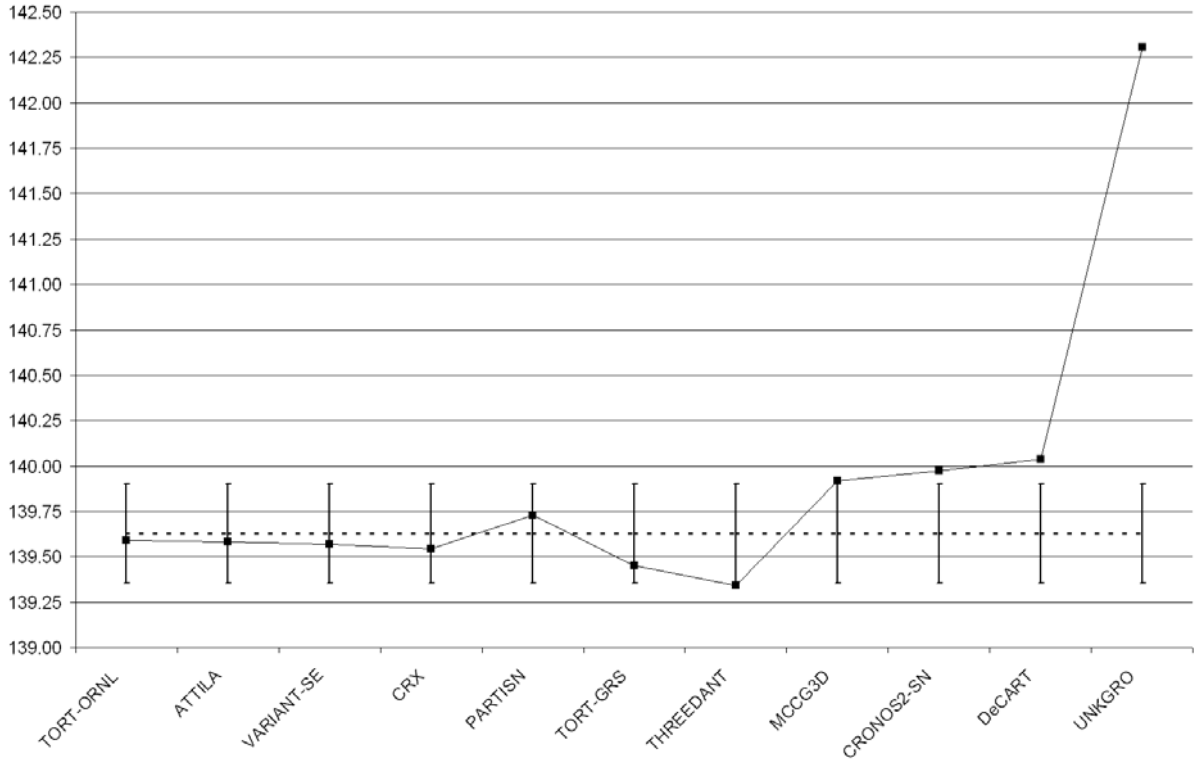

Table 29. Pin power distribution error measures for the three-dimensional benchmark

Code names	AVG	RMS	MRE
Reference MCNP	0.32	0.34	0.27
CRONOS2-SN	1.62	2.00	1.37
TORT-GRS	0.51	0.62	0.52
THREEDANT	0.84	0.99	0.87
DeCART	0.36	0.50	0.27
CRX	0.22	0.29	0.18
MCCG3D	0.34	0.46	0.27
UNKGRO	2.09	2.82	1.75
VARIANT-SE	0.48	0.59	0.47
PARTISN	0.18	0.30	0.20
ATTILA	0.11	0.14	0.09
TORT-ORNL	0.19	0.24	0.18

Figure 24. AVG per cent error for the three-dimensional benchmark

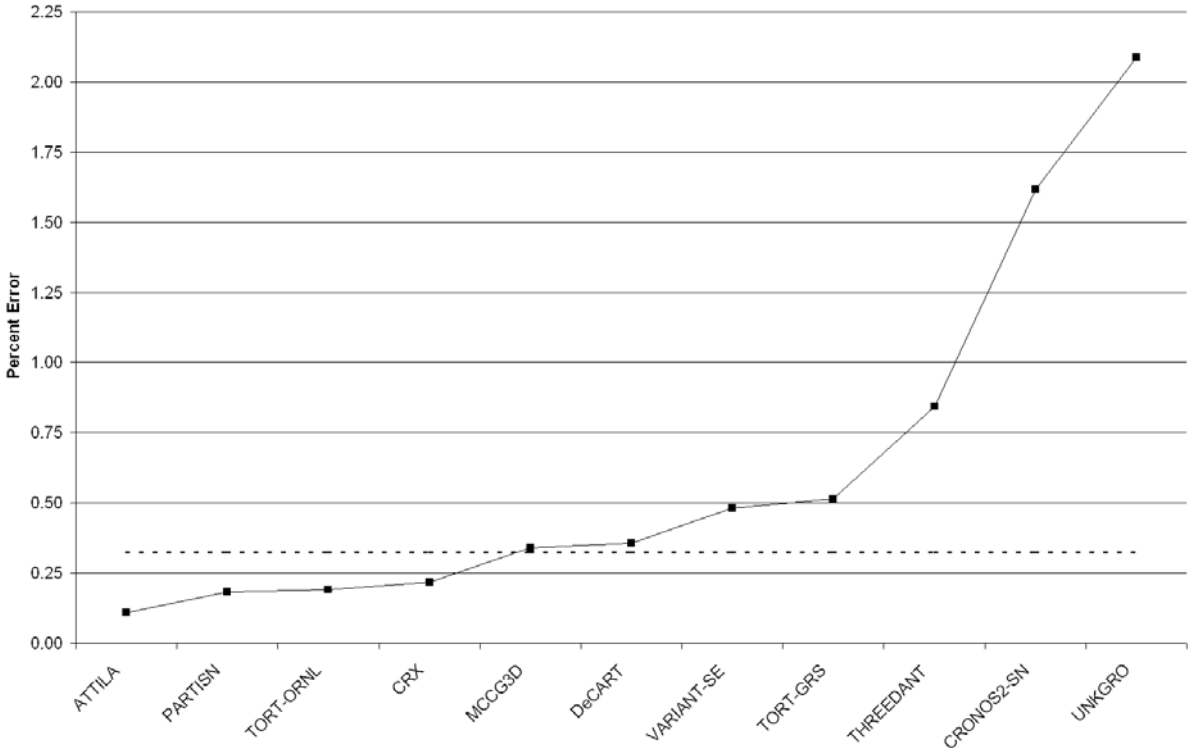

Figure 25. RMS per cent error for the three-dimensional benchmark

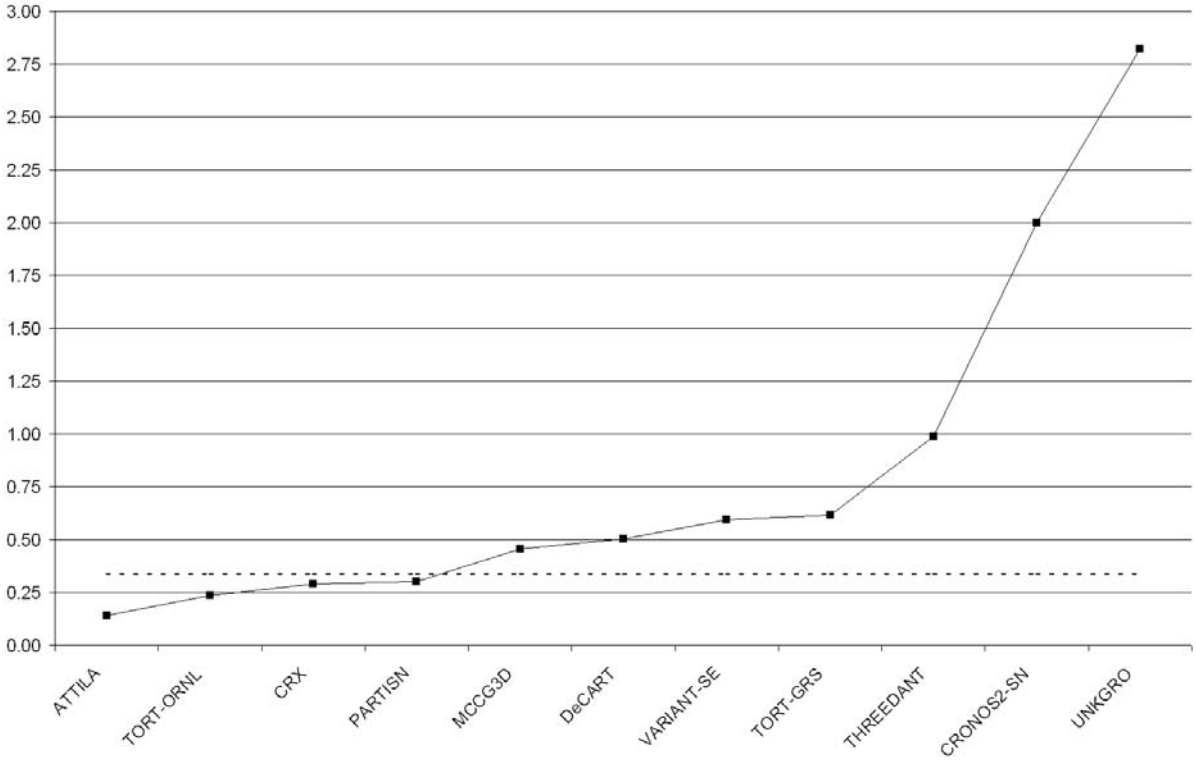

Figure 26. MRE per cent error for the three-dimensional benchmark

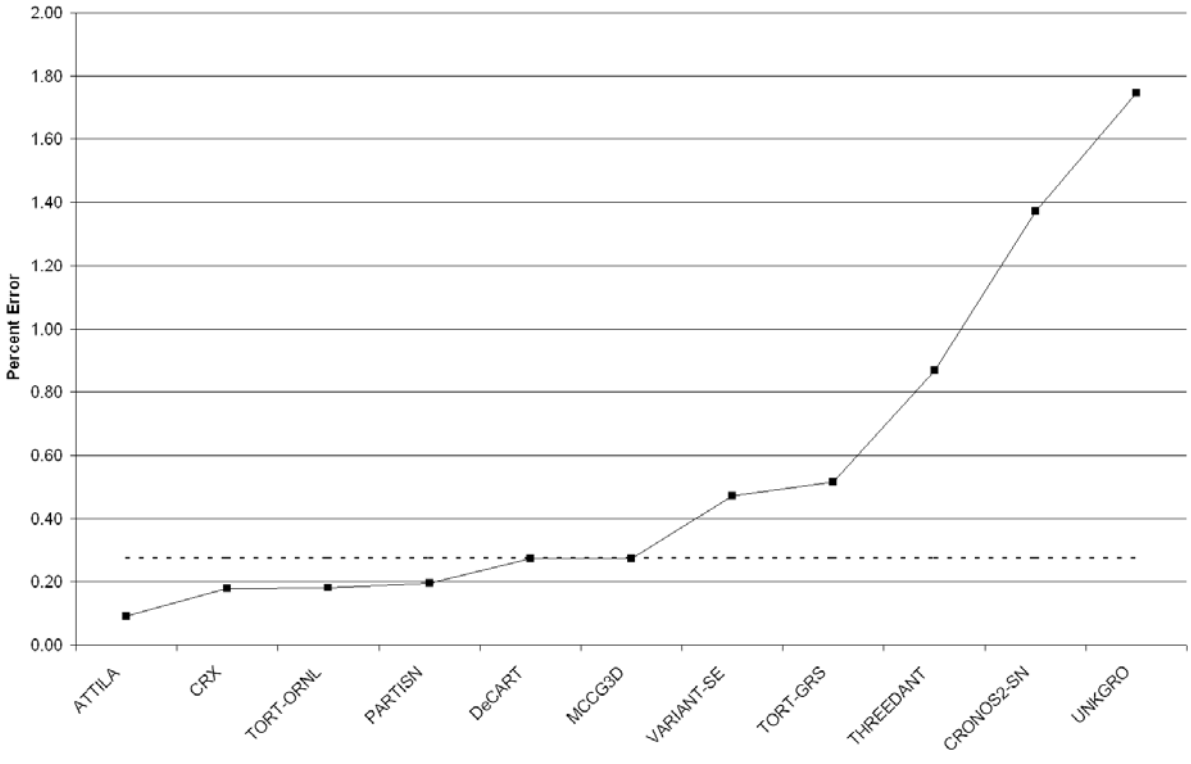

Table 30. Number of fuel pins within the reference confidence intervals for the three-dimensional benchmark

Code names	68%	90%	98%	99.8%
CRONOS2-SN	32	72	96	131
TORT-GRS	164	263	357	435
THREEDANT	121	169	225	287
DeCART	276	458	613	751
CRX	401	629	848	963
MCCG3D	252	438	588	755
UNKGRO	45	69	91	119
VARIANT-SE	168	282	421	580
PARTISN	488	724	885	981
ATTILA	725	949	1036	1056
TORT-ORNL	428	668	844	972

Table 31. Percentage of fuel pins within the reference confidence intervals for the three-dimensional benchmark

Code names	68%	90%	98%	99.8%
CRONOS2-SN	3.0	6.8	9.1	12.4
TORT-GRS	15.5	24.9	33.8	41.2
THREEDANT	11.5	16.0	21.3	27.2
DeCART	26.1	43.4	58.0	71.1
CRX	38.0	59.6	80.3	91.2
MCCG3D	23.9	41.5	55.7	71.5
UNKGRO	4.3	6.5	8.6	11.3
VARIANT-SE	15.9	26.7	39.9	54.9
PARTISN	56.2	68.6	83.8	92.9
ATTILA	68.7	89.9	98.1	100.0
TORT-ORNL	40.5	63.3	79.9	92.0

Figure 27. Percentage of fuel pins within the three-dimensional benchmark confidence intervals

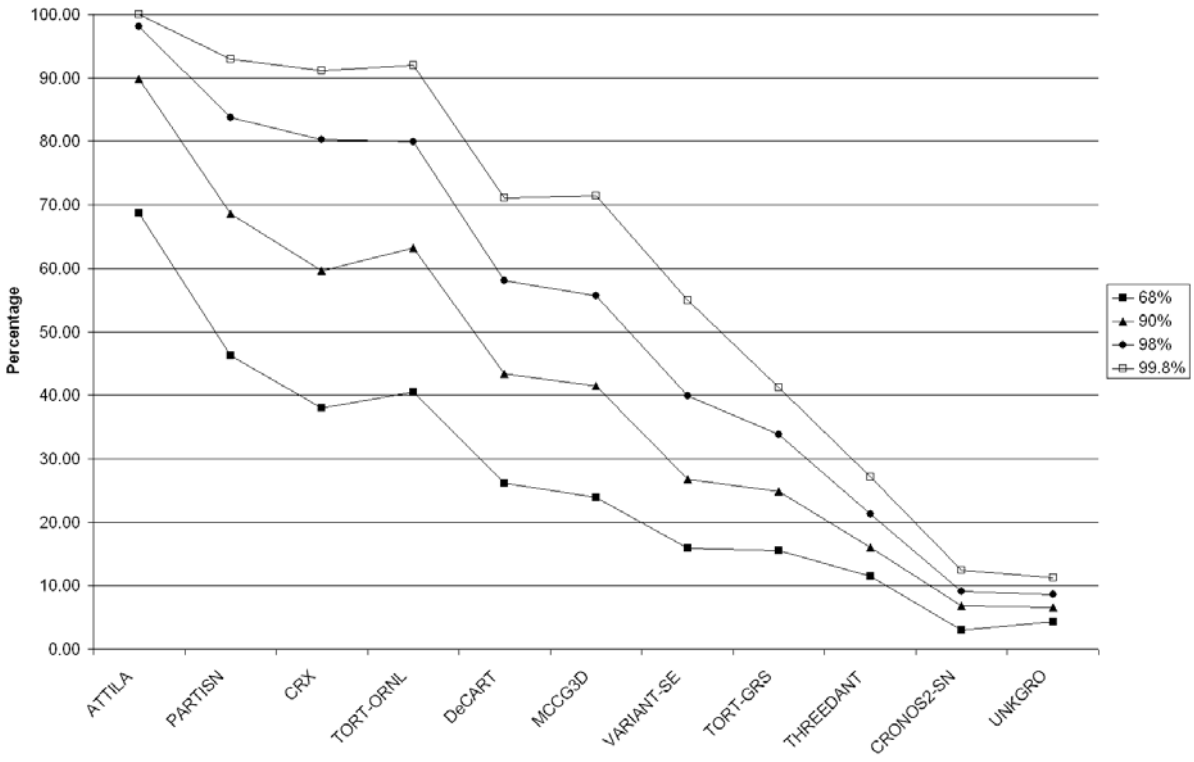

Table 32. Estimated CPU time for the two-dimensional benchmark

Code names	Estimated CPU time
CRONOS2-SN	Hours
TORT-GRS	Days
THREEDANT	Hours
DeCART	Hours
CRX	*Not given*
MCCG3D	*Not given*
UNKGRO	Days
VARIANT-SE	Days
PARTISN	Minutes
ATTILA	Days
TORT-ORNL	*Not given*

Chapter 8

CONCLUSIONS

To test the ability of current deterministic transport codes treating reactor core problems without spatial homogenisation, an OECD/NEA international benchmark problem was undertaken. A total of 20 participant contributions were provided for the 2-D configuration and a total of 11 were provided for the 3-D configuration. The submitted results were compared against Monte Carlo reference solutions.

Overall all the results submitted were good; a majority of the participants obtained solutions that were comparable to the reference MCNP solution. Most of the errors in the participant solutions can be attributed to the high-order space-angle approximations necessary for this benchmark. It is important to note however, that the high-order space-angle approximations needed for this benchmark may not be necessary in all heterogeneous whole-core problems. This benchmark cannot therefore be taken as a representative calculation for all heterogeneous problems. In conclusion, the preceding analysis shows that modern deterministic transport codes can calculate the flux distribution reasonably well without relying upon spatial homogenisation techniques.

As a follow-up to the current benchmark, an extension of the three-dimensional calculations will be proposed to provide a more challenging test of present day three-dimensional methods' abilities to handle spatial heterogeneities while still allowing participants to investigate sensitivities to spatial and angular approximations implemented in their codes.

REFERENCES

[1] Kobayashi, K., N. Sugimura and Y. Nagaya, *3-D Radiation Transport Benchmarks for Simple Geometries with Void Regions*, OECD/NEA report, ISBN 92-64-18274-8, November 2000.

[2] Kobayashi, K. and E. Sartori (eds.), "3-D Radiation Transport Benchmarks for Simple Geometries with Void Regions", *Progress in Nuclear Energy*, Volume 39, Number 2, 2001.

[3] Cavarec, C. *et al*., *The OECD/NEA Benchmark Calculations of Power Distributions within Assemblies*, Electricité de France, Sept. 1994.

[4] Cathalau, S., J.C. Lefebvre, J.P. West, *Proposal for a Second Stage of the Benchmark on Power Distributions within Assemblies*, an earlier version of the published OECD/NEA benchmark, April 1996.

[5] Marleau, G., A. Hébert, R. Roy, *A User's Guide for DRAGON*, ecole Polytechnique de Montréal, December 1997.

[6] Briesmeister, J.F., *MCNP^{TM} – A General Monte Carlo N-particle Transport Code*, Los Alamos National Laboratory, LA-12625-M, March 1997.

APPENDIX A

Benchmark Specification for Deterministic 2-D/3-DMOX Fuel Assembly Transport Calculations without Spatial Homogenisation

C5G7 MOX Benchmark

E.E. Lewis
Northwestern University
Department of Mechanical Engineering
Evanston, Illinois 60208

M.A. Smith, N. Tsoulfanidis
University of Missouri, Rolla
Department of Nuclear Engineering
Rolla, Missouri 65409

G. Palmiotti, T.A. Taiwo, R.N. Blomquist
Argonne National Laboratory
9700 South Cass Avenue
Argonne, Illinois 60439

Outline

- Benchmark specification
- Appendix 1 – Description of computational model used to obtain benchmark solutions
- Appendix 2 – Results to be reported

Problem specification

We hereby propose that a seven-group form of the C5 MOX fuel assembly problem specified by Cavarec, *et. al*. be used as a basis to test the ability of current transport codes to treat reactor core problems without spatial homogenisation. The two-dimensional and three-dimensional configurations are shown in Figure 1. For the two-dimensional domain, vacuum boundary conditions are applied to the right and to the bottom of the geometry while reflected boundary conditions are applied to the top and left of the geometry as indicated. The overall dimensions of the two-dimensional problem geometry, as seen in Figure 1, are 64.26 × 64.26 cm, while each assembly is 21.42 × 21.42 cm. For the three-dimensional configuration, the fuel assemblies are extended in the *z* direction 192.78 cm and an additional 21.42 cm water reflector is added above them. The *z* boundary conditions are reflected below and vacuum above as indicated in Figure 1. The overall dimensions for the three-dimensional configuration, also as seen in Figure 1, are 64.26 × 64.26 × 214.20 cm, while each assembly is 21.42 × 21.42 × 192.78 cm.

Each fuel assembly is made up of a 17 × 17 lattice of square fuel pin cells, as seen in Figure 2. The side length of every fuel pin cell is 1.26 cm and every cylinder is of radius 0.54 cm. As indicated in Figure 2, there are two compositions for every fuel pin cell. For this benchmark problem a single moderator composition is provided for use in all of the fuel-pin cells and in the water reflector (moderator) surrounding the assemblies. The composition layout for the fuel-pin cell *cylinders* is provided in Figure 3 for all four assemblies.

Table 1 provides seven-group, transport-corrected, isotropic-scattering cross-sections for UO_2, the three enrichments of MOX, the guide tubes and fission chamber, and the moderator described in the problem specification. To obtain these cross-sections, the number densities and the dimensions of the fuel, cladding and assemblies specified by S. Cathalau, *et al*. were used with the collision probability code DRAGON (G. Marleau, *et al*.) and the WIMS-AECL 69-group library. Each fuel type was represented as a single pin cell in an infinite-lattice fine-mesh collision probability calculation. A full anisotropic collision probability calculation was performed and standard flux weighting was used to collapse to seven energy groups and to homogenise fuel, gap and cladding materials into homogenised fuel compositions. The seven-group moderator cross-sections in Table 1 were obtained using the UO_2 pin cell spectrum. The cross-sections for the homogenised guide tube and fission chamber regions were also obtained using a UO_2 fuel spectrum to be consistent with the moderator cross-sections.

Problem objectives

Stage I. Two-dimensional configuration

Calculate:

(a) The eigenvalue.

(b) Each of the pin powers (with average pin power normalised to 1 fission/sec/cell).

Stage II. Three-dimensional configuration

Calculate:

(a) The eigenvalue

(b) Each of the pin powers (with average pin power normalised to 1 fission/sec/cell)

It is suggested that the eigenvalue be compared to that of the approximate reference solution eigenvalues provided below to ensure that the geometry is set up correctly (actual reference eigenvalues are known to ±0.00004). For either, configuration an Excel spreadsheet is provided for the insertion of pin power information as indicated by the numbering convention in Figure 3. If you are unable to obtain pin powers and can only obtain pin production rates, accommodations are available. Both the pin power and pin production rate reference solutions for the two- and three-dimensional configurations were obtained via a multi-group Monte Carlo calculation utilising 300 million histories. A 0.14% RMS statistical pin power per cent error was achieved for both two- and three-dimensional configurations.

Reference seven-group Monte Carlo eigenvalue answers

- Approximate eigenvalue for the two-dimensional configuration: 1.19.
- Approximate eigenvalue for the three-dimensional configuration: 1.18.

Comments

We are well aware that the homogenisation and group collapse introduced some error into the cross-sections. Our object, however, is not to examine the validity of the group collapse, or fuel-cladding homogenisation. Instead, it is to provide a reasonable set of multi-group cross-sections in which there is no fuel-coolant homogenisation. Moreover, for brevity in data input we utilise a single set of water cross-sections in both the UO_2 and MOX assembles and in the reflector. The geometry specification combined with these transport-corrected, isotropic-scattering, seven-group cross-sections provides a basis for comparing the accuracy of deterministic transport codes with reference seven-group Monte Carlo solutions. Each reference solution required approximately one week of CPU time on a Sun 60. The solutions may also serve to test the validity of spatial fuel-coolant homogenisation procedures at the fuel pin cell and/or at the fuel assembly level.

REFERENCES

Cathalau, S., J.C. Lefebvre, J.P. West, *Proposal for a Second Stage of the Benchmark on Power Distributions within Assemblies*, an earlier version of the published OECD/NEA benchmark, April 1996.

Cavarec, C., *et al*., *The OECD/NEA Benchmark Calculations of Power Distributions within Assemblies*, Electricité de France, September 1994.

Marleau, G., A. Hébert, R. Roy, *A User's Guide for DRAGON*, Ecole Polytechnique de Montréal, December 1997.

Figure 1. Core configuration for the C5 benchmark problem

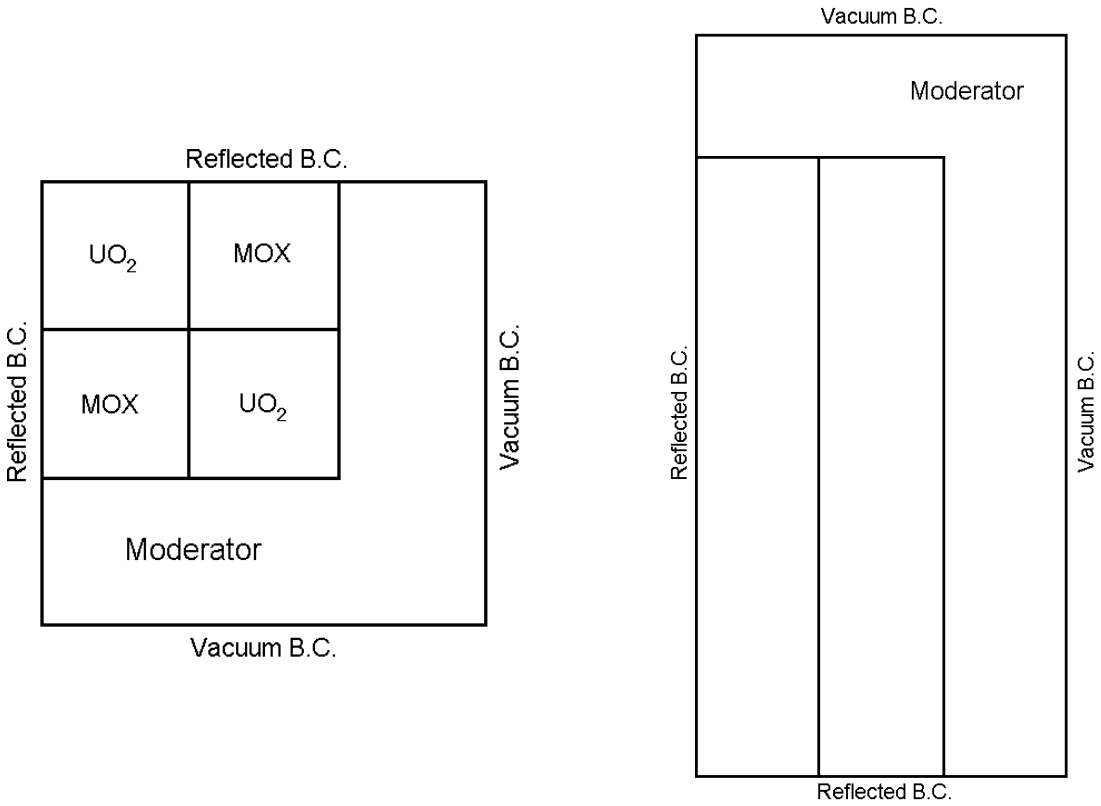

Figure 2. Fuel pin layout

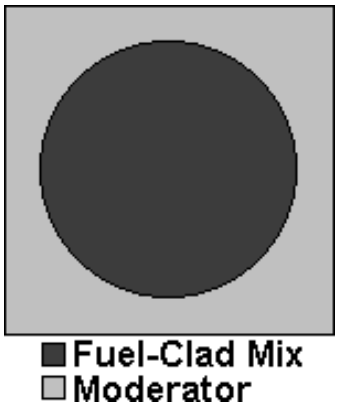

Figure 3. Benchmark fuel pin compositions and numbering scheme

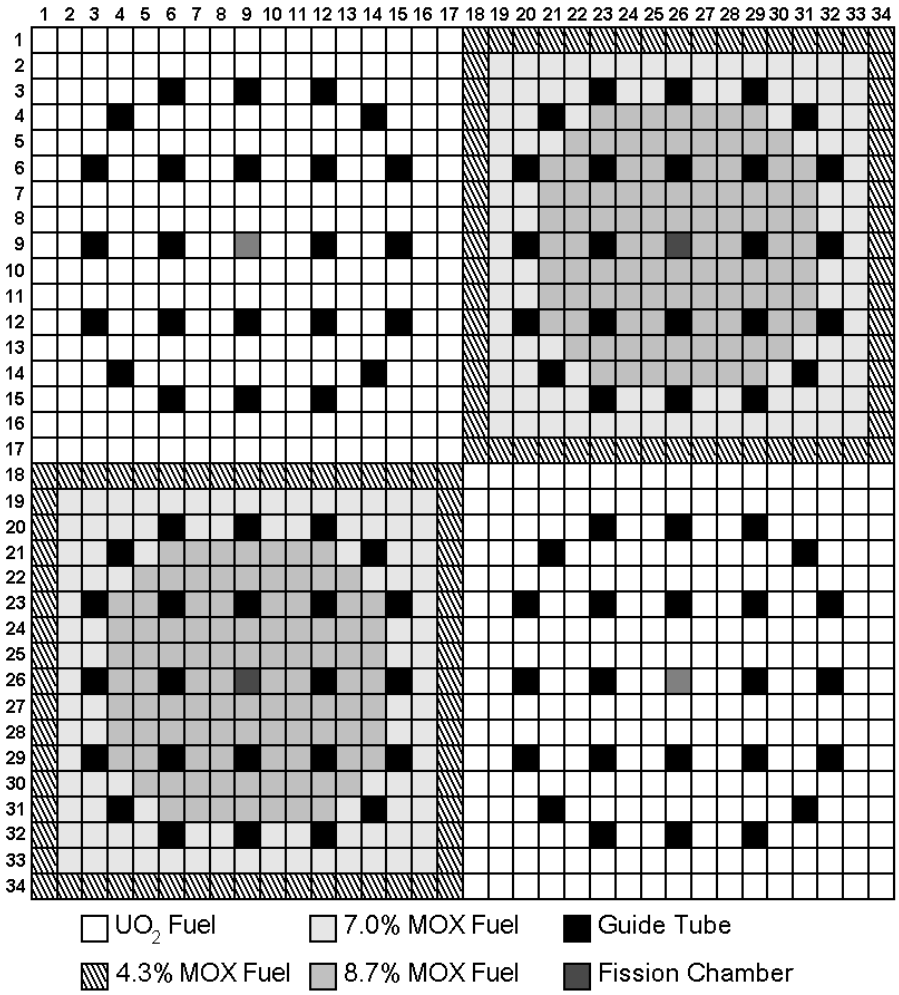

Table 1(a). UO_2 fuel-clad macroscopic cross-sections

	Total cross-section	Transport cross-section	Absorption cross-section	Capture cross-section	Fission cross-section	Nu	Chi
Group 1	2.12450E-01	1.77949E-01	8.02480E-03	8.12740E-04	7.21206E-03	2.78145E+00	5.87910E-01
Group 2	3.55470E-01	3.29805E-01	3.71740E-03	2.89810E-03	8.19301E-04	2.47443E+00	4.11760E-01
Group 3	4.85540E-01	4.80388E-01	2.67690E-02	2.03158E-02	6.45320E-03	2.43383E+00	3.39060E-04
Group 4	5.59400E-01	5.54367E-01	9.62360E-02	7.76712E-02	1.85648E-02	2.43380E+00	1.17610E-07
Group 5	3.18030E-01	3.11801E-01	3.00200E-02	1.22116E-02	1.78084E-02	2.43380E+00	0.00000E+00
Group 6	4.01460E-01	3.95168E-01	1.11260E-01	2.82252E-02	8.30348E-02	2.43380E+00	0.00000E+00
Group 7	5.70610E-01	5.64406E-01	2.82780E-01	6.67760E-02	2.16004E-01	2.43380E+00	0.00000E+00

Scattering block

	to Group 1	to Group 2	to Group 3	to Group 4	to Group 5	to Group 6	to Group 7
Group 1	1.27537E-01	4.23780E-02	9.43740E-06	5.51630E-09	0.00000E+00	0.00000E+00	0.00000E+00
Group 2	0.00000E+00	3.24456E-01	1.63140E-03	3.14270E-09	0.00000E+00	0.00000E+00	0.00000E+00
Group 3	0.00000E+00	0.00000E+00	4.50940E-01	2.67920E-03	0.00000E+00	0.00000E+00	0.00000E+00
Group 4	0.00000E+00	0.00000E+00	0.00000E+00	4.52565E-01	5.56640E-03	0.00000E+00	0.00000E+00
Group 5	0.00000E+00	0.00000E+00	0.00000E+00	1.25250E-04	2.71401E-01	1.02550E-02	1.00210E-08
Group 6	0.00000E+00	0.00000E+00	0.00000E+00	0.00000E+00	1.29680E-03	2.65802E-01	1.68090E-02
Group 7	0.00000E+00	0.00000E+00	0.00000E+00	0.00000E+00	0.00000E+00	8.54580E-03	2.73080E-01

Table 1(b). 4.3% MOX fuel-clad macroscopic cross-sections

	Total cross-section	Transport cross-section	Absorption cross-section	Capture cross-section	Fission cross-section	Nu	Chi
Group 1	2.11920E-01	1.78731E-01	8.43390E-03	8.06860E-04	7.62704E-03	2.85209E+00	5.87910E-01
Group 2	3.55810E-01	3.30849E-01	3.75770E-03	2.88080E-03	8.76898E-04	2.89099E+00	4.11760E-01
Group 3	4.88900E-01	4.83772E-01	2.79700E-02	2.22717E-02	5.69835E-03	2.85486E+00	3.39060E-04
Group 4	5.71940E-01	5.66922E-01	1.04210E-01	8.13228E-02	2.28872E-02	2.86073E+00	1.17610E-07
Group 5	4.32390E-01	4.26227E-01	1.39940E-01	1.29177E-01	1.07635E-02	2.85447E+00	0.00000E+00
Group 6	6.84950E-01	6.78997E-01	4.09180E-01	1.76423E-01	2.32757E-01	2.86415E+00	0.00000E+00
Group 7	6.88910E-01	6.82852E-01	4.09350E-01	1.60382E-01	2.48968E-01	2.86780E+00	0.00000E+00

Scattering block

	to Group 1	to Group 2	to Group 3	to Group 4	to Group 5	to Group 6	to Group 7
Group 1	1.28876E-01	4.14130E-02	8.22900E-06	5.04050E-09	0.00000E+00	0.00000E+00	0.00000E+00
Group 2	0.00000E+00	3.25452E-01	1.63950E-03	1.59820E-09	0.00000E+00	0.00000E+00	0.00000E+00
Group 3	0.00000E+00	0.00000E+00	4.53188E-01	2.61420E-03	0.00000E+00	0.00000E+00	0.00000E+00
Group 4	0.00000E+00	0.00000E+00	0.00000E+00	4.57173E-01	5.53940E-03	0.00000E+00	0.00000E+00
Group 5	0.00000E+00	0.00000E+00	0.00000E+00	1.60460E-04	2.76814E-01	9.31270E-03	9.16560E-09
Group 6	0.00000E+00	0.00000E+00	0.00000E+00	0.00000E+00	2.00510E-03	2.52962E-01	1.48500E-02
Group 7	0.00000E+00	0.00000E+00	0.00000E+00	0.00000E+00	0.00000E+00	8.49480E-03	2.65007E-01

Table 1(c). 7.0% MOX fuel-clad macroscopic cross-sections

	Total cross-section	Transport cross-section	Absorption cross-section	Capture cross-section	Fission cross-section	Nu	Chi
Group 1	2.14540E-01	1.81323E-01	9.06570E-03	8.11240E-04	8.25446E-03	2.88498E+00	5.87910E-01
Group 2	3.59350E-01	3.34368E-01	4.29670E-03	2.97105E-03	1.32565E-03	2.91079E+00	4.11760E-01
Group 3	4.98910E-01	4.93785E-01	3.28810E-02	2.44594E-02	8.42156E-03	2.86574E+00	3.39060E-04
Group 4	5.96220E-01	5.91216E-01	1.22030E-01	8.91570E-02	3.28730E-02	2.87063E+00	1.17610E-07
Group 5	4.80350E-01	4.74198E-01	1.82980E-01	1.67016E-01	1.59636E-02	2.86714E+00	0.00000E+00
Group 6	8.39360E-01	8.33601E-01	5.68460E-01	2.44666E-01	3.23794E-01	2.86658E+00	0.00000E+00
Group 7	8.59480E-01	8.53603E-01	5.85210E-01	2.22407E-01	3.62803E-01	2.87539E+00	0.00000E+00

Scattering block

	to Group 1	to Group 2	to Group 3	to Group 4	to Group 5	to Group 6	to Group 7
Group 1	1.30457E-01	4.17920E-02	8.51050E-06	5.13290E-09	0.00000E+00	0.00000E+00	0.00000E+00
Group 2	0.00000E+00	3.28428E-01	1.64360E-03	2.20170E-09	0.00000E+00	0.00000E+00	0.00000E+00
Group 3	0.00000E+00	0.00000E+00	4.58371E-01	2.53310E-03	0.00000E+00	0.00000E+00	0.00000E+00
Group 4	0.00000E+00	0.00000E+00	0.00000E+00	4.63709E-01	5.47660E-03	0.00000E+00	0.00000E+00
Group 5	0.00000E+00	0.00000E+00	0.00000E+00	1.76190E-04	2.82313E-01	8.72890E-03	9.00160E-09
Group 6	0.00000E+00	0.00000E+00	0.00000E+00	0.00000E+00	2.27600E-03	2.49751E-01	1.31140E-02
Group 7	0.00000E+00	0.00000E+00	0.00000E+00	0.00000E+00	0.00000E+00	8.86450E-03	2.59529E-01

Table 1(d). 8.7% MOX fuel-clad macroscopic cross-sections

	Total cross-section	Transport cross-section	Absorption cross-section	Capture cross-section	Fission cross-section	Nu	Chi
Group 1	2.16280E-01	1.83045E-01	9.48620E-03	8.14110E-04	8.67209E-03	2.90426E+00	5.87910E-01
Group 2	3.61700E-01	3.36705E-01	4.65560E-03	3.03134E-03	1.62426E-03	2.91795E+00	4.11760E-01
Group 3	5.05630E-01	5.00507E-01	3.62400E-02	2.59684E-02	1.02716E-02	2.86986E+00	3.39060E-04
Group 4	6.11170E-01	6.06174E-01	1.32720E-01	9.36753E-02	3.90447E-02	2.87491E+00	1.17610E-07
Group 5	5.08900E-01	5.02754E-01	2.08400E-01	1.89142E-01	1.92576E-02	2.87175E+00	0.00000E+00
Group 6	9.26670E-01	9.21028E-01	6.58700E-01	2.83812E-01	3.74888E-01	2.86752E+00	0.00000E+00
Group 7	9.60990E-01	9.55231E-01	6.90170E-01	2.59571E-01	4.30599E-01	2.87808E+00	0.00000E+00

Scattering block

	to Group 1	to Group 2	to Group 3	to Group 4	to Group 5	to Group 6	to Group 7
Group 1	1.31504E-01	4.20460E-02	8.69720E-06	5.19380E-09	0.00000E+00	0.00000E+00	0.00000E+00
Group 2	0.00000E+00	3.30403E-01	1.64630E-03	2.60060E-09	0.00000E+00	0.00000E+00	0.00000E+00
Group 3	0.00000E+00	0.00000E+00	4.61792E-01	2.47490E-03	0.00000E+00	0.00000E+00	0.00000E+00
Group 4	0.00000E+00	0.00000E+00	0.00000E+00	4.68021E-01	5.43300E-03	0.00000E+00	0.00000E+00
Group 5	0.00000E+00	0.00000E+00	0.00000E+00	1.85970E-04	2.85771E-01	8.39730E-03	8.92800E-09
Group 6	0.00000E+00	0.00000E+00	0.00000E+00	0.00000E+00	2.39160E-03	2.47614E-01	1.23220E-02
Group 7	0.00000E+00	0.00000E+00	0.00000E+00	0.00000E+00	0.00000E+00	8.96810E-03	2.56093E-01

Table 1(e). Fission chamber macroscopic cross-sections

	Total cross-section	Transport cross-section	Absorption cross-section	Capture cross-section	Fission cross-section	Nu	Chi
Group 1	1.90730E-01	1.26032E-01	5.11320E-04	5.11315E-04	4.79002E-09	2.76283E+00	5.87910E-01
Group 2	4.56520E-01	2.93160E-01	7.58130E-05	7.58072E-05	5.82564E-09	2.46239E+00	4.11760E-01
Group 3	6.40700E-01	2.84250E-01	3.16430E-04	3.15966E-04	4.63719E-07	2.43380E+00	3.39060E-04
Group 4	6.49840E-01	2.81020E-01	1.16750E-03	1.16226E-03	5.24406E-06	2.43380E+00	1.17610E-07
Group 5	6.70630E-01	3.34460E-01	3.39770E-03	3.39755E-03	1.45390E-07	2.43380E+00	0.00000E+00
Group 6	8.75060E-01	5.65640E-01	9.18860E-03	9.18789E-03	7.14972E-07	2.43380E+00	0.00000E+00
Group 7	1.43450E+00	1.17214E+00	2.32440E-02	2.32419E-02	2.08041E-06	2.43380E+00	0.00000E+00

Scattering block

	to Group 1	to Group 2	to Group 3	to Group 4	to Group 5	to Group 6	to Group 7
Group 1	6.61659E-02	5.90700E-02	2.83340E-04	1.46220E-06	2.06420E-08	0.00000E+00	0.00000E+00
Group 2	0.00000E+00	2.40377E-01	5.24350E-02	2.49900E-04	1.92390E-05	2.98750E-06	4.21400E-07
Group 3	0.00000E+00	0.00000E+00	1.83425E-01	9.22880E-02	6.93650E-03	1.07900E-03	2.05430E-04
Group 4	0.00000E+00	0.00000E+00	0.00000E+00	7.90769E-02	1.69990E-01	2.58600E-02	4.92560E-03
Group 5	0.00000E+00	0.00000E+00	0.00000E+00	3.73400E-05	9.97570E-02	2.06790E-01	2.44780E-02
Group 6	0.00000E+00	0.00000E+00	0.00000E+00	0.00000E+00	9.17420E-04	3.16774E-01	2.38760E-01
Group 7	0.00000E+00	0.00000E+00	0.00000E+00	0.00000E+00	0.00000E+00	4.97930E-02	1.09910E+00

Table 1(f). Guide tube macroscopic cross-sections

	Total cross-section	Transport cross-section	Absorption cross-section	Capture cross-section
Group 1	1.90730E-01	1.26032E-01	5.11320E-04	5.11320E-04
Group 2	4.56520E-01	2.93160E-01	7.58010E-05	7.58010E-05
Group 3	6.40670E-01	2.84240E-01	3.15720E-04	3.15720E-04
Group 4	6.49670E-01	2.80960E-01	1.15820E-03	1.15820E-03
Group 5	6.70580E-01	3.34440E-01	3.39750E-03	3.39750E-03
Group 6	8.75050E-01	5.65640E-01	9.18780E-03	9.18780E-03
Group 7	1.43450E+00	1.17215E+00	2.32420E-02	2.32420E-02

Scattering block

	to Group 1	to Group 2	to Group 3	to Group 4	to Group 5	to Group 6	to Group 7
Group 1	6.61659E-02	5.90700E-02	2.83340E-04	1.46220E-06	2.06420E-08	0.00000E+00	0.00000E+00
Group 2	0.00000E+00	2.40377E-01	5.24350E-02	2.49900E-04	1.92390E-05	2.98750E-06	4.21400E-07
Group 3	0.00000E+00	0.00000E+00	1.83297E-01	9.23970E-02	6.94460E-03	1.08030E-03	2.05670E-04
Group 4	0.00000E+00	0.00000E+00	0.00000E+00	7.88511E-02	1.70140E-01	2.58810E-02	4.92970E-03
Group 5	0.00000E+00	0.00000E+00	0.00000E+00	3.73330E-05	9.97372E-02	2.06790E-01	2.44780E-02
Group 6	0.00000E+00	0.00000E+00	0.00000E+00	0.00000E+00	9.17260E-04	3.16765E-01	2.38770E-01
Group 7	0.00000E+00	0.00000E+00	0.00000E+00	0.00000E+00	0.00000E+00	4.97920E-02	1.09912E+00

Table 1(g). Moderator macroscopic cross-sections

	Total cross-section	Transport cross-section	Absorption cross-section	Capture cross-section
Group 1	2.30070E-01	1.59206E-01	6.01050E-04	6.01050E-04
Group 2	7.76460E-01	4.12970E-01	1.57930E-05	1.57930E-05
Group 3	1.48420E+00	5.90310E-01	3.37160E-04	3.37160E-04
Group 4	1.50520E+00	5.84350E-01	1.94060E-03	1.94060E-03
Group 5	1.55920E+00	7.18000E-01	5.74160E-03	5.74160E-03
Group 6	2.02540E+00	1.25445E+00	1.50010E-02	1.50010E-02
Group 7	3.30570E+00	2.65038E+00	3.72390E-02	3.72390E-02

Scattering block

	to Group 1	to Group 2	to Group 3	to Group 4	to Group 5	to Group 6	to Group 7
Group 1	4.44777E-02	1.13400E-01	7.23470E-04	3.74990E-06	5.31840E-08	0.00000E+00	0.00000E+00
Group 2	0.00000E+00	2.82334E-01	1.29940E-01	6.23400E-04	4.80020E-05	7.44860E-06	1.04550E-06
Group 3	0.00000E+00	0.00000E+00	3.45256E-01	2.24570E-01	1.69990E-02	2.64430E-03	5.03440E-04
Group 4	0.00000E+00	0.00000E+00	0.00000E+00	9.10284E-02	4.15510E-01	6.37320E-02	1.21390E-02
Group 5	0.00000E+00	0.00000E+00	0.00000E+00	7.14370E-05	1.39138E-01	5.11820E-01	6.12290E-02
Group 6	0.00000E+00	0.00000E+00	0.00000E+00	0.00000E+00	2.21570E-03	6.99913E-01	5.37320E-01
Group 7	0.00000E+00	0.00000E+00	0.00000E+00	0.00000E+00	0.00000E+00	1.32440E-01	2.48070E+00

Appendix A.1

DESCRIPTION OF COMPUTATIONAL MODEL USED TO OBTAIN BENCHMARK SOLUTIONS

(*Preferred format is WORD*)

We would like to have as detailed a description as you are able to provide on your treatment of the space-angle variables and the procedures by which you carried out the calculations (but limited to five pages). Please include the following:

1. Name of participant(s).

2. Establishment(s).

3. Name of code system(s) used.

4. Computational method used (e.g. S_N, P_N, collision probability, characteristic, etc.).

5. Type and level of angular approximation (e.g. S_8, P_7, number of characteristic angles, etc.).

6. Type and level of spatial discretisation (e.g. linear-triangular finite elements, flat source region collision probabilities, etc.). Provide number of mesh points, source regions, tracking pitch, etc., per lattice cell. If possible include a drawing or diagram of the spatial mesh for one lattice cell.

7. Convergence:

   – Eigenvalue (at least 10 E-5).

   – Pointwise (e.g. flux, fission source, etc.).

8. Machine on which the calculations were performed and (if possible) CPU time.

9. Other assumptions and characteristics, comments useful for interpreting correctly the results.

Appendix A. 2

RESULTS TO BE REPORTED*

(*Requested format is EXCEL*)

1. Stage I: Two-dimensional configuration

Table I.1. Eigenvalue

Eigenvalue	

Table I.2. UO_2 Normalised pin powers

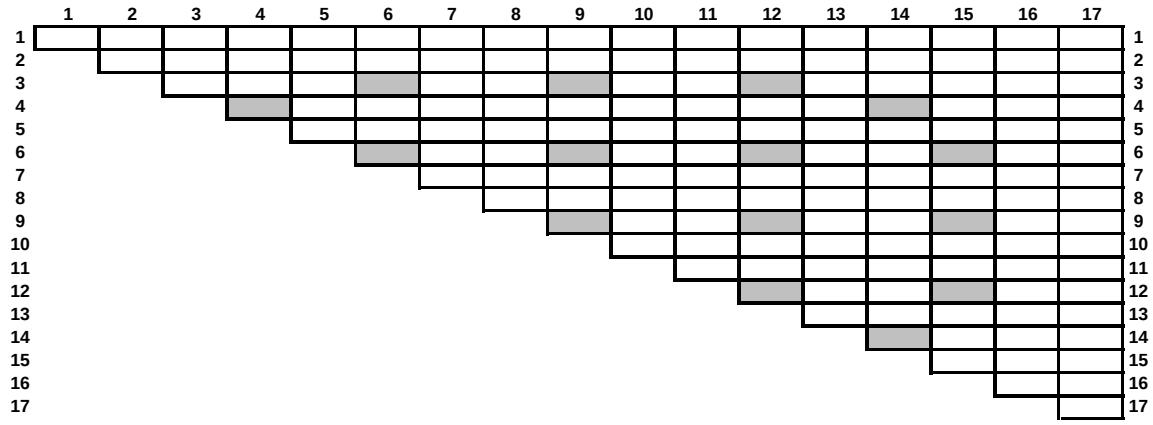

Table I.3. UO_2 Normalised pin powers

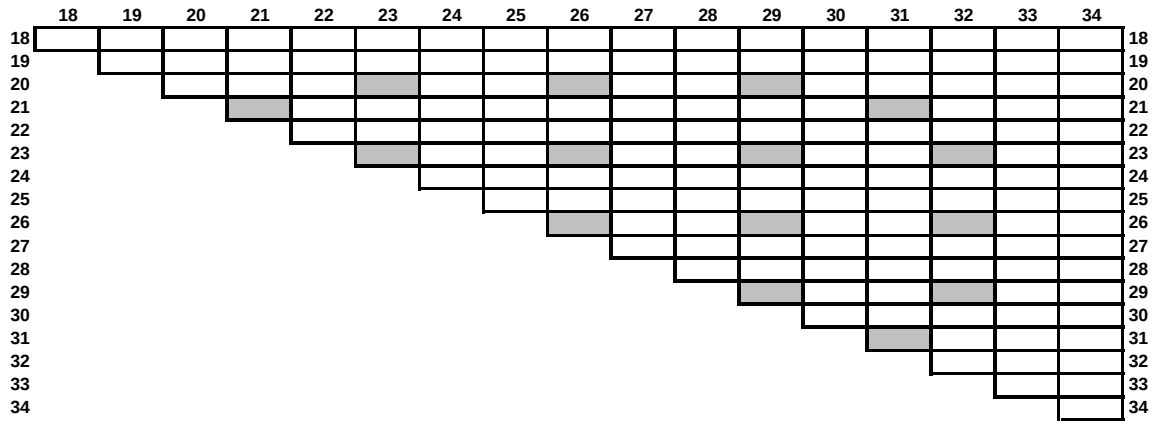

* Tables I.2 to I.4 are shown here only to clarify their from. For result submittal, the EXCEL templates should be used.

Table I.4. MOX normalised pin powers

	18	19	20	21	22	23	24	25	26	27	28	29	30	31	32	33	34	
1																		1
2																		2
3																		3
4																		4
5																		5
6																		6
7																		7
8																		8
9																		9
10																		10
11																		11
12																		12
13																		13
14																		14
15																		15
16																		16
17																		17

2. Stage II: Three-dimensional configuration

The following tables are to be filled in as in Stage I: Two-dimensional configuration:

- Table II.1. Eigenvalue
- Table II.2. UO_2 normalised pin powers
- Table II.3. UO_2 normalised pin powers
- Table II.4. MOX normalised pin powers

APPENDIX B

Calculation Details Provided by the Participants

1. Commissariat à l'Énergie Atomique (CEA), France

Name of participant(s)

Frédéric Moreau – diffusion and S_N calculation
Simone Santandrea – characteristic and Monte Carlo calculation
Richard Sanchez – characteristic

Establishment(s)

Commissariat à l'Energie Atomique
CEA SACLAY
DEN/DM2S/SERMA/LENR
F-91191 Gif-sur-Yvette Cedex

Name of code system(s) used

APOLLO2 and CRONOS2 of the SAPHYR system.

Computational method used for two-dimensional configuration

A reference calculation was performed with TRIPOLI4 (Monte Carlo) to purchase a reference. Errors in per cent mentioned below are comparisons with these results.

- Method used: Monte Carlo.
- Ninety-two (92) million histories.
- ±51 pcm to 99%.
- Fission rate ±1%.

Results in file 2D_solution_S8_L25m.xls were obtained with CRONOS2 code:

- Method used: S_8 with even parity formulation (20 directions).
- Eigenvalue = 1.18338.
- Relative error in fission rate between +3.690% in (32;32) and -2.057% in (29;5).
- Mean of absolute values for the relative errors in fission rate 0.72%.
- Pointwise: fission source.
- Calculation performed on DEC Alpha EV6 500 Mhz in 1 100 seconds.
- Spatial discretisation is obtained with isoparametric linear triangular finite elements with 36 triangles and 25 nodes by cell described below.
- Flux nodes: 3 472 560 (24 804 for one direction and one group).

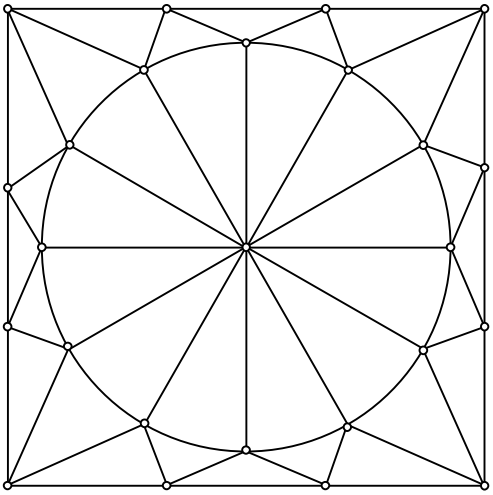

Results in file 2D_solution_diffu_P85m.xls were obtained with CRONOS2 code:

- Method used: Diffusion.
- Eigenvalue = 1.18323.
- Relative error in fission rate between +4.010% in (34;32) and -3.538% in (30;1).
- Mean of absolute values for the relative errors in fission rate 1.30%.
- Pointwise: fission source.
- Calculation performed on DEC Alpha EV6 500 Mhz in 370 seconds.
- Spatial discretisation is obtained with isoparametric parabolic triangular finite elements with 36 triangles and 85 nodes by cell described below.
- Flux nodes: 691 159 (98 737 for one group).

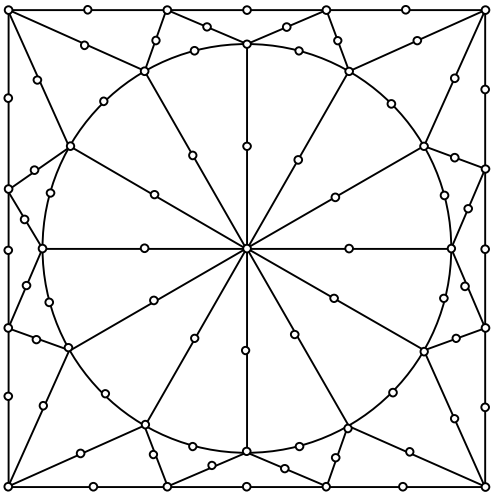

Results in file 2D_solution_A.xls were obtained with APOLLO2 code:

- Eigenvalue = 1.18634.
- Maximum relative error in fission rate -3.2% in (32;32).
- Mean of absolute values for the relative errors in fission rate 0.50%.
- Number of characteristic angles: The angular quadrature consisted of eight nearly uniformly distributed azimuthal angles and two polar angles, obtained from an optimised Bickley-Naylor formula.
- Distance between trajectories of $\delta = 0.05$ resulted in 8 234 trajectories with a total of 3 073 110 region intersections.
- Number of points per group: 19 188.

Computational method used for three-dimensional configuration

Results in file 3D_solution_S4_L13m.xls were obtained with CRONOS2 code:

- Method used: S_4 with even parity formulation (12 directions).
- Eigenvalue = 1.17723.
- Pointwise: fission source.
- Calculation performed on DEC Alpha EV6 500 Mhz in 8 500 seconds.
- Nine (9) axial nodes.
- Spatial radial discretisation is obtained with isoparametric linear triangular finite elements with 20 triangles and 13 nodes by cell described below
- Flux nodes: 9 909 648 (117 972 for one direction and one group).

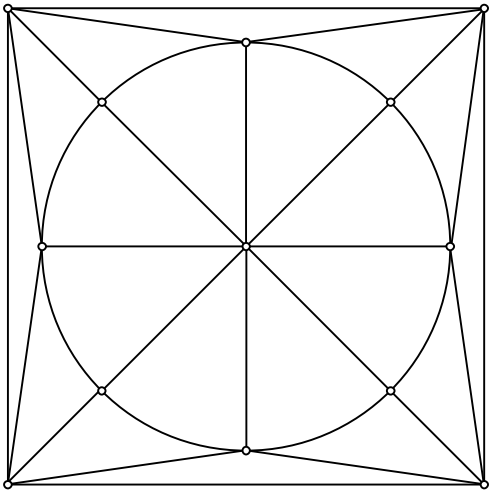

2. Gesellschaft für Reaktorsicherheit (GRS), Germany

Name of participant(s)

A.Pautz, S. Langenbuch, W. Zwermann, K. Velkov

Establishment(s)

Gesellschaft für Anlagen- und Reaktorsicherheit (GRS) mbH
Forschungsgelaende
D-85748 Garching
E-Mail: pat@grs.de

Name of code system(s) used

DORT/TORT (from DOORS 3.3).

Computational method used

Discrete ordinates (S_N).

Type and level of angular approximation

S_4,S_8,S_{16} ⇒ 16(32), 48(96), 160(320) discrete directions in 2(3) spatial dimensions.

Type and level of spatial discretisation

2-D: Representation of each pin cell by a Cartesian mesh, ranging from 3×3 to 17×17 grid points per pin-cell ⇒ Overall dimension (including reflector): ~ (120×120) – (650×650).

3-D: Representation of each pin cell by a 5×5 grid in x-y-plane, z-dimension divided into 12 axial nodes => Overall dimension: $185 \times 185 \times 12 = 410\,700$ nodes.

Convergence

DORT (2-D): Eigenvalue 5E-8, fission source: 5E-7, pointwise fluxes: 1E-6.

TORT (3-D): Eigenvalue 1E-6, fission source: 1E-5, pointwise fluxes: 2E-5.

Machine on which the calculations were performed and (if possible) CPU time

COMPAQ Professional Workstation XP 1000, 500 MHz, EV6 processor, COMPAQ TRU64 UNIX operating system.

Largest 2-D case (~420 000 meshes, S_{16}): 387 min.

Largest 3-D case (~410 000 meshes, S_{16}): 1 005 min.

Other assumptions and characteristics, comments useful for interpreting correctly the results

Since DORT and TORT only provide regular mesh features, the circular fuel pin had to be approximated by a Cartesian mesh, the simplest case being a square fuel pin such that each pin cell would be represented by 3×3 meshes. The approximation of the fuel pin was gradually

improved up to 17 × 17 meshes per pin cell. Figure 1 shows the nodalisation of the pin cell for a typical mesh (7 × 7). The mesh was chosen such that the averaged distance between the circular fuel pin borderline and the "staircase" approximation is minimised.

Figure 1. Example of typical pin cell nodalisation by a 7 × 7 Cartesian mesh

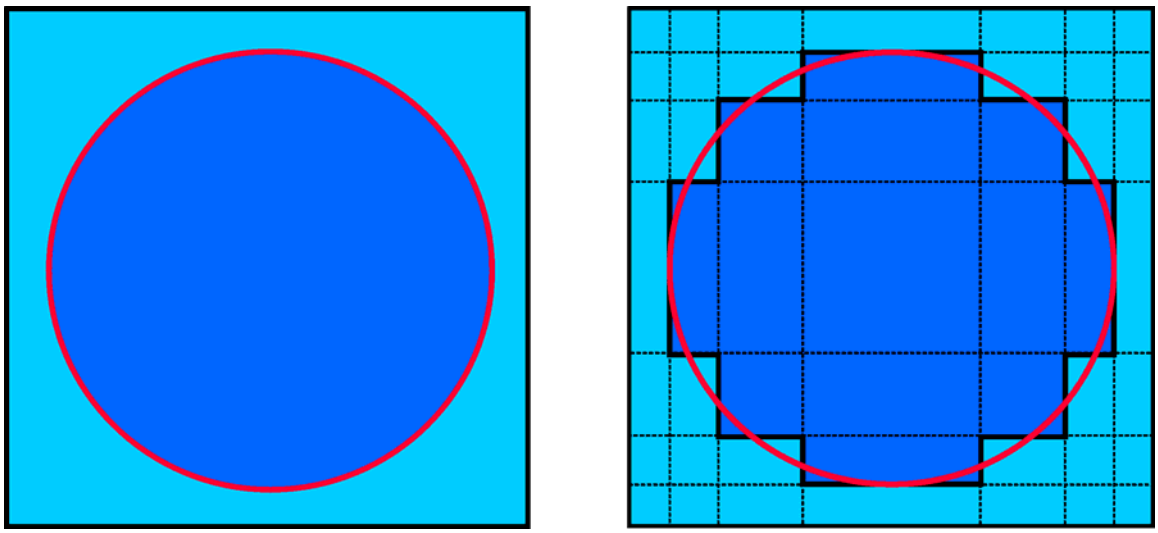

For the 2-D case, several calculations with different spatial resolutions and different angular approximations were performed, the most exact one being a calculation with roughly 400 000 mesh points and a fully symmetrical S_{16} quadrature set. Considering this as the reference case, the effect of lower order spatial and angular approximations was investigated, comparing eigenvalues and pin powers. The resulting eigenvalues are compared in Figure 2 for S_4, S_8 and S_{16} quadrature and different spatial resolutions (the number of nodes per pin cell is in one direction only).

Figure 2. Eigenvalue dependence on spatial and angular approximation

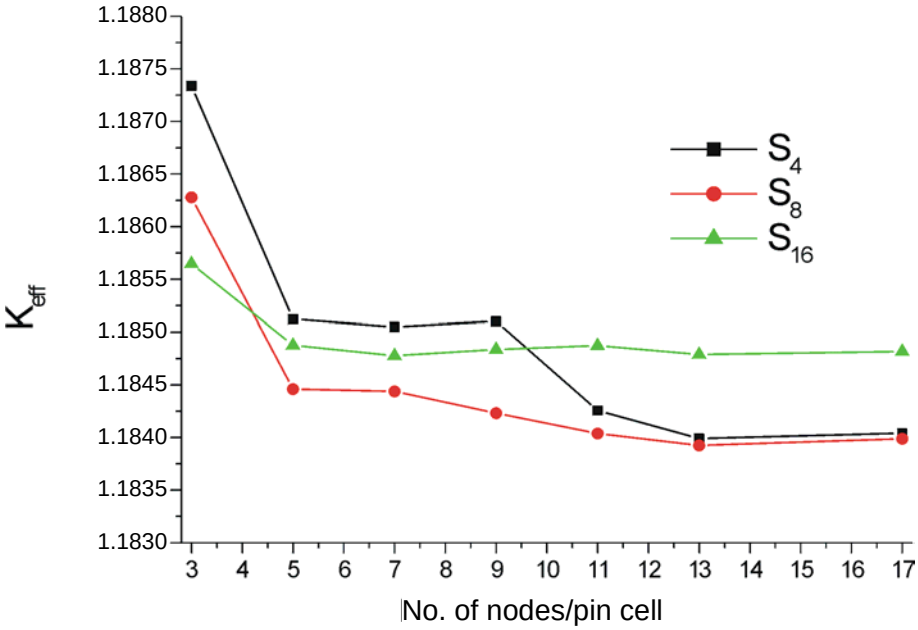

While the simple square cell representation of the fuel pin obviously yields larger deviations in the eigenvalue, higher spatial approximations, especially for large quadrature sets are very consistent, the differences in the eigenvalue being only 1E-3. A further spatial improvement is not necessary, however, there is a systematic effect on quadrature order.

We also considered the deviations in pin power distributions for the different cases from Figure 2. Figure 3 shows the average pin power deviation (in %), as compared to the reference case. Again, it can be seen that already for low order spatial and angular approximation, the agreement is quite good (i.e. far below 1%).

Figure 3. Averaged pin power deviation for several angular and spatial approximations

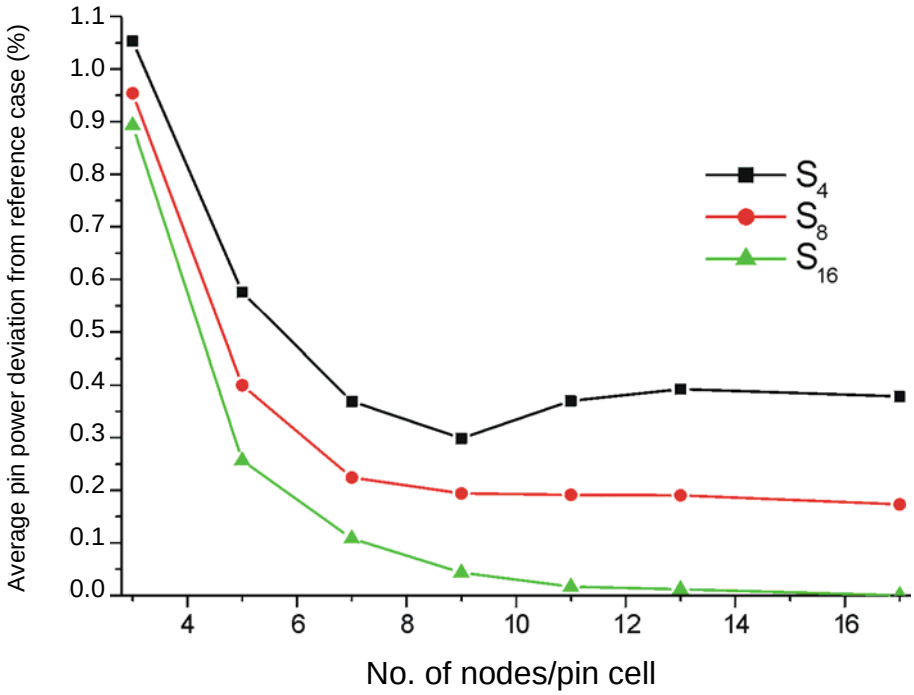

For the 3-D case, we restricted ourselves to a rather coarse (5 × 5) pin cell nodalisation to keep the numerical effort reasonable. Only 12 axial nodes (two for the axial reflector) were employed, thus giving an overall number of ~400 000 spatial nodes. The resulting eigenvalues for S_4, S_8 and S_{16} calculations are in good agreement (cf. Table 1).

Table 1. 3-D eigenvalues for different angular approximations

S_4	S_8	S_{16}
1.18012	1.18014	1.18045

The 3-D results are preliminary and will be improved by further calculations with a better spatial approximation and better convergence of fluxes and fission rates.

3. Hanyang University (HU), Korea

Name of participant(s)

Jong Kyung Kim, Chi Young Han

Establishment(s)

Department of Nuclear Engineering
Hanyang University
Seoul, Korea

Name of code system(s) used

TWODANT and THREEDANT within the DANTSYS 3.0 code system.

Computational method used

Discrete ordinates method (S_N method).

Type and level of angular approximation

S_8, P_0.

Type and level of spatial discretisation

The circular fuel pin was modelled on an equivalent-area square pin and the number of fine mesh per lattice pin cell is 4 × 4 as per the following drawing:

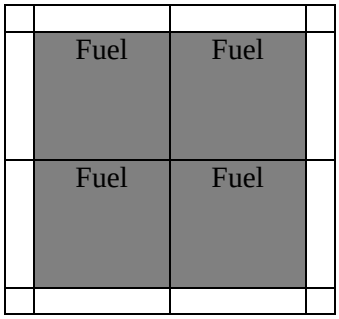

Convergence

- Eigenvalue: 1.0E-5.
- Pointwise flux and fission source: 1.0E-5.

Machine on which the calculations were performed and (if possible) CPU time

- For the 2-D calculations: HP Workstation C3700, CPU time of 77.3 seconds.
- For the 3-D calculations: HP Workstation C3700, CPU time of 17 463 seconds (about 291 minutes).

4. Korea Atomic Energy Research Institute (KAERI), Korea

Name of participant(s)

Han Gyu Joo, JinYoung Cho, Kang Seog Kim, Sung Quun Zee

Establishment(s)

Korea Atomic Energy Research Institute

Name of code system(s) used

DeCART (Deterministic Core Analysis based on Ray Tracing).

Computational method used

2-D MOC (Method of Characteristics)/1-D Nodal Diffusion Kernel Based 3-D Coarse Mesh Finite Difference (CMFD) Formulation.

Method Summary

Suppose a 3-D neutron transport problem consisting of several planes. As is normally done in the transverse-integrated method, the transport equation can be integrated over the axial direction for a plane. After the integration, the axial dependence disappears and instead, the axial leakage term defined as the following appears:

$$L_{z,k}^{m}(x,y) = \frac{\mu_m}{h_{z,k}}\left(\phi_m^{t,k}(x,y) - \phi_m^{b,k}(x,y)\right) \quad (1)$$

where indices *m*, *k*, *t* and *b* stand for (angular) direction *m*, plane *k*, *top* and *bottom* of the plane, and μ and h_z are the angle cosine and the axial plane thickness, respectively. By moving the axial leakage term to the right hand side, a 2-D problem is formulated with the axially averaged angular fluxes as the unknowns. Once the spatial and angular dependence of the axial leakage term is given, the 2-D problem can be solved using a 2-D MOC solver having angle-dependent sources.

In order to obtain the axial leakage source information, parallel 1-D problems are constructed with the radial leakages as the source. In the work here, the plain diffusion formulation is applied which gives the P_1 angular dependence. Specifically, the 1-D nodal (NEM) diffusion solution is obtained for every pin in the core and the angular flux distribution at the top and bottom of each plane is approximated by the P_1 relation involving the net current and surface flux.

Once the axial leakage sources are defined, the 2-D MOC solution can be obtained for each plane. The planar MOC solution is then used to generate homogenised cell cross-sections and radial cell coupling coefficient for use in the subsequent 3-D pin cell based CMFD formulation as well as for use in the axial nodal diffusion calculation. In the 3-D CMFD formulation, the axial coupling coefficients are also required and they come from the 1-D nodal diffusion solutions. The 3-D CMFD problem is solved to newly determine the cell-averaged fluxes in the 3-D domain. The CMFD solution is then used to update the axial and radial leakages for the subsequent 1-D NEM and 2-D MOC kernel calculations. The alternate CMFD and kernel calculations are repeated until convergence with partially converged solutions at each stage.

Type and level of angular approximation

- Number of azimuthal angles: 16 for 180°.
- Number of polar angles: 8 for 90°.

Type and level of spatial discretisation

- Ray spacing: 0.2 mm in average.
- Number of source regions in a cell: 40.
- Number of planes: 12 (= 9 × 20 cm + 1 × 12.78 cm + 1 × 10 cm + 1 × 11.42 cm).

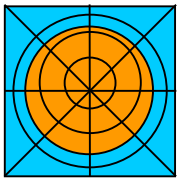

Convergence

- Eigenvalue:

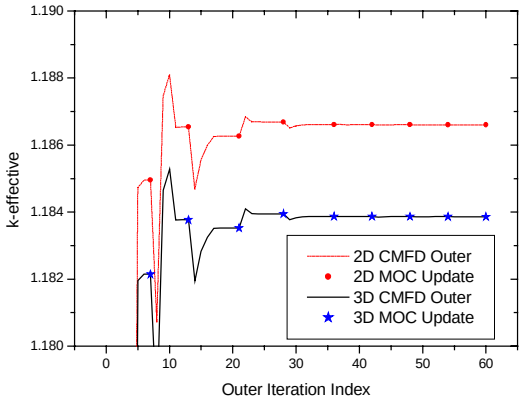

- Pointwise:

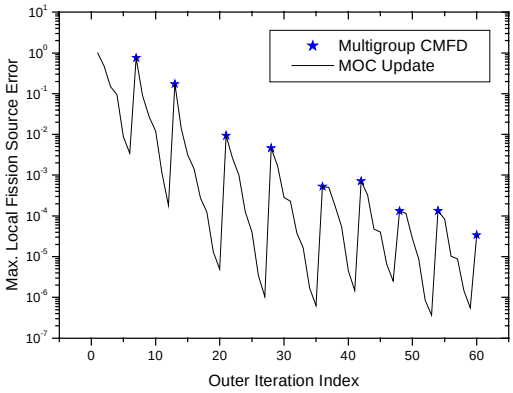

	2D		3D	
	k-eff	Local FS Err	k-eff	Local FS Err
1	1.0000000	1.000000E+00	1.0000000	1.000000E+00
2	1.1403439	4.146554E-01	1.1347834	4.704383E-01
3	1.1493933	9.907043E-02	1.1433375	1.479915E-01
4	1.1593687	6.365263E-02	1.1532931	9.423468E-02
5	1.1847350	8.320791E-03	1.1819613	8.781641E-03
6	1.1849592	2.959370E-03	1.1821466	3.426526E-03
7	1.1849592	8.185127E-01	1.1821466	7.575092E-01
8	1.1807278	5.556894E-02	1.1779500	8.877448E-02
9	1.1874609	1.986861E-02	1.1846560	2.645167E-02
10	1.1881015	7.815129E-03	1.1852807	1.196876E-02
11	1.1865270	4.899410E-04	1.1837597	1.079572E-03
12	1.1865382	1.494405E-04	1.1837693	1.822407E-04
13	1.1865382	1.677845E-01	1.1837693	1.734116E-01
14	1.1846816	1.397117E-02	1.1819444	1.398045E-02
15	1.1855759	3.002944E-03	1.1828323	3.137844E-03
16	1.1859958	1.406769E-03	1.1832493	1.420682E-03
17	1.1862573	2.714409E-04	1.1835189	2.765414E-04
18	1.1862647	1.192796E-04	1.1835260	1.242538E-04
19	1.1862631	1.217372E-05	1.1835245	1.321156E-05
20	1.1862633	4.665696E-06	1.1835246	4.965846E-06
21	1.1862633	9.394693E-03	1.1835246	9.405033E-03
22	1.1868412	2.293776E-03	1.1841001	2.607735E-03
23	1.1866956	9.938332E-04	1.1839542	1.013843E-03
24	1.1866908	1.220952E-04	1.1839487	1.251961E-04
25	1.1866886	3.778328E-05	1.1839465	3.974089E-05
26	1.1866906	3.164658E-06	1.1839486	3.437141E-06
27	1.1866906	8.797077E-07	1.1839486	1.045821E-06
28	1.1866906	4.435175E-03	1.1839486	4.631065E-03
29	1.1865126	1.572607E-03	1.1837714	1.660907E-03
30	1.1865707	2.848132E-04	1.1838295	2.858851E-04
31	1.1865992	2.249075E-04	1.1838578	2.292892E-04
32	1.1866121	3.722954E-05	1.1838705	3.812924E-05
33	1.1866126	1.557261E-05	1.1838711	1.621721E-05
34	1.1866120	1.619264E-06	1.1838705	1.692571E-06
35	1.1866120	5.804732E-07	1.1838705	6.247343E-07
36	1.1866120	4.164919E-04	1.1838705	5.237001E-04
37	1.1866147	4.983169E-04	1.1838730	4.989359E-04
38	1.1866053	1.627867E-04	1.1838637	1.717287E-04
39	1.1866062	4.889314E-05	1.1838646	5.423033E-05
40	1.1866134	3.886550E-06	1.1838718	4.490787E-06
41	1.1866134	1.472656E-06	1.1838718	1.463775E-06
42	1.1866134	7.007503E-04	1.1838718	7.143842E-04
43	1.1865949	3.262967E-04	1.1838533	3.271139E-04
44	1.1866010	4.461671E-05	1.1838595	4.719647E-05
45	1.1866050	3.783211E-05	1.1838635	4.012758E-05
46	1.1866075	6.364414E-06	1.1838659	6.512143E-06
47	1.1866076	2.457036E-06	1.1838660	2.564800E-06
48	1.1866076	1.325028E-04	1.1838660	1.327231E-04
49	1.1866024	1.124240E-04	1.1838608	1.161037E-04
50	1.1866022	2.354612E-05	1.1838606	2.803590E-05
51	1.1866031	8.546678E-06	1.1838614	8.633681E-06
52	1.1866047	8.636721E-07	1.1838631	8.615421E-07
53	1.1866047	3.596965E-07	1.1838631	3.673712E-07
54	1.1866047	1.359356E-04	1.1838631	1.341719E-04
55	1.1866014	8.334188E-05	1.1838598	8.367872E-05
56	1.1866024	9.963653E-06	1.1838608	1.011500E-05
57	1.1866032	8.265960E-06	1.1838616	8.912132E-06
58	1.1866038	1.435824E-06	1.1838622	1.484320E-06
59	1.1866038	5.216732E-07	1.1838622	5.577623E-07
60	1.1866038	3.398829E-05	1.1838622	3.400864E-05

Machine on which the calculations were performed and (if possible) CPU time

- Machine: 1 GHz Pentium-III PC and IBM SMP Regatta (1.3 GHz Power4 CPU).
- CPU time: 2-D – 48.5 minutes (PC), 3-D – 63.4 minutes (IBM with six CPUs).

Other assumptions and characteristics, comments useful for interpreting correctly the results

Sensitivity study on angular and spatial discretisation parameters has been performed for the 2-D and 3-D problems. The results are summarised in the following table. As shown in the table the most refined DeCART solution has about 140 pcm error in the eigenvalue and about 1.4% error in the pin power for both 2-D and 3-D cases. There is little dependence noted on the plane thickness for this problem. This is probably due to the fact that this core is quite uniform axially except for the axial reflector region. For rodded and thermal feedbacked cases, however, stronger dependence is expected. Thus the primary plane thickness was chosen to be 20 cm.

Table 1. Sensitivity study summary

Dim.	N_{Azi}	N_{Pol}	δ_R mm	N_{FSR} Fuel+Mod	N_{pl}	N_{RT}	N_{CMFD}	ε_k pcm	ε_p^{max} %	ε_p^{RMS} %	T_{RT} sec.	T_{tot} sec.
2-D	8	2	0.3	3+8	1	9	48	-31	5.11	1.39	138.6	149.3
				24+8		9	50	33	1.39	0.44	203.8	214.8
				40+8		9	50	33	1.31	0.43	259.2	270.2
	8		0.5	32		9	48	62	1.31	0.38	119.5	129.4
			0.2			9	50	28	1.39	0.45	293.6	304.3
			0.1			9	50	28	1.39	0.45	560.2	571.3
	4		0.3	32		9	50	-19	1.58	0.68	96.8	107.0
	12					9	50	73	1.35	0.41	282.0	292.6
	16					9	48	139	1.39	0.39	373.2	384.0
	20					9	50	110	1.39	0.40	458.2	468.8
	32					9	50	154	1.43	0.40	738.1	748.7
	64					9	50	144	1.39	0.40	1471	1482
	16	2	0.3	24+16		9	50	99	0.93	0.30	455.5	465.4
	16	8	0.3	24+16		9	50	10	1.84	0.46	1968	1979
3-D	16	2	0.2	24+8	8	9	50	136	1.42	0.39	5601	5780
					12	9	50	135	1.42	0.39	9029	8731
					24	9	50	134	1.42	0.39	1569*	1350*

N_{Azi} – number of azimuthal angles, δ_R – ray spacing, N_{FSR} – number of flat source regions, N_{pl} – number of planes, N_{RT} – number of ray tracing sweeps, N_{CMFD} – number of CMFD outers, ε_k – eigenvalue error (k_{2D} = 1.18655, k_{3D} = 1.18381), ε_p^{max}, ε_p^{RMS} – max and RMS pin power error, T_{RT} – CPU time spent for ray tracing on a 1 GHz Pentium III PC, T_{RT} – total CPU time.

* Performed on an IBM Regatta system with six CPUs.

5. Korea Advanced Institute of Science and Technology (KAIST), Korea

Name of participant(s)

Nam Zin Cho

Establishment(s)

Korea Advanced Institute of Science and Technology (KAIST)

Name of code system(s) used

CRX code.

Computational method used

Method of characteristics.

Type and level of angular approximation

Eight (8) azimuthal × 2 polar angles per octant.

Type and level of spatial discretisation

- Number of meshes per cell: 48 (see figure below).
- Number of fuel regions: 32 (see figure below).
- Number of rays/cell/direction: 50.

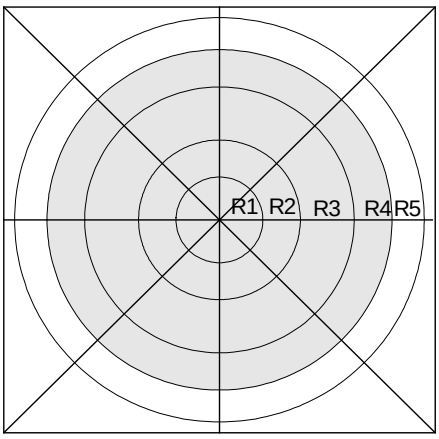

Convergence

- Eigenvalue: 1.0E-5 (2.19E-9 eigenvalue relative error when converged).
- Pointwise: 1.0E-5.

Machine on which the calculations were performed and (if possible) CPU time

KAIST*GALAXY cluster system (using four CPUs of 48 Intel Pentium III and IV machines).

6. Institute of Physics and Power Engineering (IPPE), Russian Federation

Name of participant(s)

Igor R. Suslov

Establishment(s)

IPPE, Obninsk, Russia

Name of code system(s) used

MCCG3D.

Computational method used

Method of long characteristics (LgC) with DD-scheme for integration along characteristics for 2-D and plane-tracing method for 3-D.

Type and level of angular approximation

S_{32} Gauss formula for azimuthal angle, 16 equidistant polar directions in symmetry sector (45 grads) in 2-D calculation. Only simplest S_2 quadrature in azimuthal angle and one direction in 45-grad sector were used in 3-D calculation.

Type and level of spatial discretisation

Forty-five (45) grads symmetry sector was used in calculations.

Each square fuel pin cell was modelled by four regions:

- Central part of pin: single cell (cylindrical) with external radii 0.45 cm.
- Peripheral part of pin: ring (sector for diagonal cells) with inner radii 0.45 cm and external radii 0.54 cm described as 1 × 4 cell block with one cell in radial and four cells in polar variable.
- Inner part of moderator: ring (sector for diagonal cells) with inner radii 0.54 cm and external radii 0.62 cm described as 1 × 4 cell block with one cell in radial and four (two for diagonal cells) cells in polar variable.
- Peripheral part of moderator: ring (sector for diagonal cells) with inner radii 0.62 and external radii $0.63\sqrt{2}$ cm described as 1 × 4 cell block with one cell in radial and four cells in polar variable, limited by square 1.26 × 1.26.

The quadrilateral grid 17 × 17 was used for reflector.

Tracing step (distance between trajectories) for 2-D was 0.1 cm, for 3-D, 0.5 cm.

The non-uniform mesh was used Z-direction with number of layers equal to 17 for 192.78 cm and total number of layers 34 as symmetry in Z-direction is not implemented.

Convergence

2-D calculations:

- Eigenvalue: 10E-7.
- Pointwise: flux 10E-5, fission source 10E-5.

3-D calculation:

- Eigenvalue: 10E-7.
- Pointwise: flux 10E-5, fission source 10E-5.

Machine on which the calculations were performed and (if possible) CPU time

Sun Ultra 1.

Other assumptions and characteristics, comments useful for interpreting correctly the results

Cross-sections used

The following set of cross-sections were used: Transport, Nu*fission, Chi, Scattering.

Pin power is not implemented in MCCG3D up to now and *pin production rates* are presented.

Mesh refinement

A rather significant number of calculations were performed in 2-D to evaluate error due to space, tracing and angular approximation and efficiency of different numerical approaches. A brief summary will be presented here, as the evaluation is not yet finalised. Thus, presented results should be considered as preliminary ones.

Two extra sub-problems were considered in addition to the benchmark problem: a pin cell problem with a single pin in a square "cell" and "supercell" 6 × 6. These small problems offer the possibility of applying more fine mesh and quadratures to improve understanding of convergence with space and angular refinement and efficiency of different techniques. Some calculations were also performed with coarse space mesh for the main 2-D benchmark (core) – one mesh for pin and one mesh for moderator.

The pin production rates were rather stable so only eigenvalue results are presented.

- *Convergence in azimuthal variable*. This is presented in Table 1 for cell, supercell and core calculation. It seems that Gauss's S_{16} quadrature provides an accuracy near 1 pcm in 2-D calculations.
- *Convergence in polar angle*. This is presented in Table 2. It is to be pointed out that the difference between simplified ("cell" and "supercell" models) and main ("core") benchmark – 16 polar angles in 45 grads sector provides 1 pcm accuracy for simple problem but 13 pcm for "core" calculations.

- *Convergence in tracing*. This is presented in Table 3 both with use tracing normalisation techniques and without. It seems that normalisation is very efficient for "cell" scale, less efficient for supercell scale and not important for core scale. It seems that tracing step 0.1 cm provides an accuracy near 1-2 pcm.

- *Space mesh refinement*. Some results are presented in Table 4. It seems that for "core" calculation the same space mesh provides less accurate results than for "simple" problems and mesh refinement affects much more strongly in moderator (with refinement both in radial and polar directions!) than in the pin. It is necessary to use more fine meshes to reach accuracy near 1 pcm or use more advanced space approximation.

- *Iteration convergence*. C5G7 benchmark problems display very slow iteration convergence, especially for outer iterations in 3-D problem and inner iterations for 7th group. For the 2-D problem the Algebraic Collapsing Acceleration technique was very effective for time reducing. Unfortunately this technique is not implemented for large-scale 3-D iterations.

Table 1. Convergence in azimuthal variable

N_μ	Cell	Supercell	Core
1	–	–	1.18396
2	–	1.23591	1.18425
4	1.325982	1.23622	1.18421
8	1.325989	1.23639	1.18423
16	1.326009	1.23644	–
24	1.326014	1.23645	–

Table 2. Convergence in polar angle

N_μ	Cell	Supercell	Core
1	–	–	1.18185
2	1.325882	–	1.18228
4	1.325982	1.23554	1.18408
8	1.325989	1.23584	1.18421
16	1.325991	1.23591	1.18434
32	1.326014	1.23591	–

Table 3. Convergence in tracing

Step	Cell	Cell,Norm	SCell	Scell,Norm	Core	Core,Norm
0.5	1.310358	1.327018	1.23455	1.23533	1.18388	1.18390
0.25			1.23515	1.23556	1.18396	1.18396
0.1	1.324918	1.327056	1.23549	1.23552	1.18392	1.18394
0.05			1.23547	1.23554		
0.025	1.326758	1.327073	1.23554	1.23554		
0.01	1.326996	1.327078				
0.003	1.327065	1.327079				

Table 4. Convergence with mesh refinement

Space meshes per pin/moderator in cell	Cell	Supercell	Core
1/1	1.32680	1.23425	1.18464
1+1 × 4/1		1.23429	
1+2 × 4/1		1.23430	
2/2		–	1.18375
4/4	1.32603		
4 × 2/4 × 4	1.32547		
1+1 × 4/2 × 4			1.18599
1+1 × 4/2 × 2		1.23395	
1+1 × 4/4 × 2		1.23362	
1+1 × 4/8 × 2		1.23339	
1+1 × 4/16 × 2		1.23329	
1+1 × 4/32 × 2		1.23324	
1+1 × 4/32 × 4		1.23322	
1+1 × 4/16 × 8		1.23311	
1+1 × 4/16 × 16		1.23292	
8 × 4/8 × 8	1.32542		
16 × 4/16 × 16	1.32537		–

Future work

More extended calculation with code MCCG3D and with more fine meshes and more accurate angular quadratures are planned in the near future.

7. Russian Research Centre "Kurchatov Institue" (RRC KI), Russian Federation

Name of participant(s)

V.D. Davidenko, V.F. Tsibulsky

Establishment(s)

RRC KI, Russia

The neutron transport problem solution by a characteristics method

A series of characteristics along which the change of a neutron flux for fixed source function is calculated are selected in computational volume. Neutrons of an external source and neutrons of inner groups scattering are considered to be a source of neutrons. After calculation along all of the characteristics, the average value of the neutron flux in different zones of the computational volume is calculated. The average value obtained for the neutron flux is used for inner groups of scattering calculations, which is a source in the following iteration. This iterative procedure lasts until the spatial distribution of neutrons' stabilisation with the necessary accuracy is reached.

The equation along the characteristic is:

$$\frac{d\varphi(x,\vec{\Omega})}{dx} + \Sigma_{tot}\varphi(x,\vec{\Omega}) = \frac{1}{4\pi}\int_{4\pi}\Sigma_s\varphi(x,\vec{\Omega}^{\copyright})d\vec{\Omega}^{\copyright} + Q(x,\vec{\Omega}) \qquad (1)$$

(*Standard labels are used here*.)

Boundary conditions for $\varphi(x,\Omega) = \varphi_0(x,\Omega)$, for $(x\in\Gamma)$ $(\Omega,n) < 0$ (n – external normal to the boundary of computational area, $\varphi_0(x,\Omega)$ – boundary condition).

At a numerical realisation all computational volume is divided into zones and Eq. (1) is integrated along each direction. A crossing each zone by rays is fixed. An average value of neutron flux in a zone j is determined, as the average value of a flux of the all rays crossing a zone:

$$\Phi(\vec{r}_j) = \frac{\sum_m \int_{lj} \omega_i \varphi_i(x)dx}{\sum_m \omega_i l_j} \qquad (2)$$

The summation is carried out on all rays $i \subset (1\ldots\ldots m)$, crossing a zone j, a length of a segment of crossing lj, (mj – full number of rays crossing the zone j), weight coefficients describing each direction contribution in a total flux. $\Phi(r_j)$, the neutron flux in a zone j, is considered to be a constant inside a zone ($r_j \in V_j$).

Eq. (1) has the simple analytical solution:

$$\varphi_i(x) = \varphi_0\exp(-\Sigma_{tj}x) + Q_{ji}/\Sigma_{tj}*(1 - \exp(-\Sigma_{tj}x))$$

where $x\in[0,l_i]$, φ_0 is the value of $\varphi(0)$ on the boundary of a zone, and Qji is a constant source of neutrons in a zone j, for direction i.

Eqs. (1) and (2) are solved by a method of series approach calculation an integral of scattering (in the case of isotropic scattering) the average value of a neutron flux in a zone obtained in the previous iteration is used.

To select rays' directions the stochastic algorithm ensuring a uniform density function with an angular variable in 4π is realised in the UNKGRO code. At a preliminary stage of calculation for fixed geometry the calculation of rays (points where rays cross zones) is carried out, the consequent iterative procedure is performed using these previous computations.

For the solution to small group problems, problems with an external neutron source the effective iteration scheme of acceleration inner groups is applied. For multi-group problems on an eigenvalue, the practice of calculations has shown that the most effective algorithm is the overlapping inner group of iterations with iterations on a source of division, i.e. without internal iterations.

The UNKGRO program solves three-dimensional problems with any geometry using the multi-group approach, and also with an anisotropic source of neutrons. The size of problems is determined by the main memory of the computer. Personally for PC-650 with the main memory 256 Mb it is possible to receive the solution of a problem with a total number of registration zones about 500 000 in 15 energy groups. As the information about the characteristic interceptions of computational volume is kept on the hard disk, in fact, there is no limit on the number of characteristics.

The calculation of problems shown in the test C5G7 MOX was made with a spatial partition 289 377 registration zones and 70 000 characteristics for a two-dimensional problem and 598 650 registration zones and 120 000 characteristics for a three-dimensional problem. It took about 36 hours to solve the 2-D problem, for 3-D it took about 42 hours, CPU on PC-650.

8. Argonne National Laboratory (ANL), USA

ANL-1

Name of participant(s)

Micheal A. Smith,[1,†] Nicholas Tsoulfanidis,[1] Elmer E. Lewis,[2]
Giuseppe Palmiotti,[3] Temitope Taiwo,[3] Roger Blomquist[3]

Establishment(s)

[1]University of Missouri-Rolla
[2]Northwestern University
[3]Argonne National Laboratory

[†]*Now at Argonne National Laboratory*

Name of code system(s) used

VARIANT-ISE: A prototypic version of the VARIANT code.

Computational method used

Response matrix form of the variational nodal method. The nodal flux is solved with an integral transport treatment coupled to interface spherical harmonics. These interface nodal spherical harmonics are then coupled together via red-black partial current iterations.

Type and level of angular approximation

P_7 in 2-D, Square Legendre-Chebychev S_{16}.
P_{11} in 2-D, Square Legendre-Chebychev S_{16}.
P_{11} in 2-D, Square Legendre-Chebychev S_{26}.

Type and level of spatial discretisation

A variational nodal method utilising finite element sub-elements within each node.

- Two-dimensional:
  - A cubic Lagrange multiplier nodal interface approximation (spatial).
  - A consistent source approximation of the finite element mesh.
  - A triangular finite element mesh with quadratic basis functions: 113 DOF (degrees of freedom).

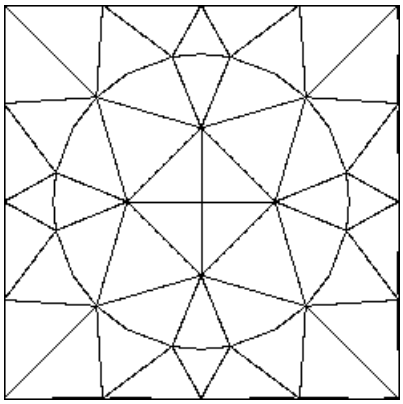

Convergence

- Eigenvalue = 10E-6.
- Pointwise:
  - Pointwise fission source = 10E-5.
  - Average fission source = 10E-5.

Machine on which the calculations were performed and (if possible) CPU time

Sun Sparcstation 60 running Solaris 8.

S_{16} P_7 2-D = 24453.24 seconds/9 hours.

S_{16} P_{11} 2-D = 80532.43 seconds/23 hours.

S_{26} P_{11} 2-D = 79284.06 seconds/22 hours.

All times are total computational times. The excessive times reported are caused by the lack of acceleration on the partial current and source and a poor draft of the FORTRAN used to get the response matrices. With improvements we expect to see a factor of 10-50 decrease in computational time. Response matrix formation times are very small as compared to those of the standard P_N variational treatment. Recent improvements in the source implementation reduced the computational time of the S_{16} P_{11} 2-D solution to less than three hours.

Other assumptions and characteristics, comments useful for interpreting correctly the results

The three different results are shown to give a sense of the dependence of the solution on the internal and external angular approximations. The spatial mesh and Lagrange multiplier approximation are sufficiently refined such that very little benefit is gained by improving either of the two approximations.

Work is progressing to refine the response matrix formation routine and implement an acceleration scheme for the source and partial currents. For the most part the times reported above are not a fair estimate of the ability of the new method.

ANL-2

Name of participant(s)

Micheal A. Smith,[1,†] Nicholas Tsoulfanidis,[1] Elmer E. Lewis,[2]
Giuseppe Palmiotti,[3] Temitope Taiwo,[3] Roger Blomquist[3]

Establishment(s)

[1]University of Missouri-Rolla
[2]Northwestern University
[3]Argonne National Laboratory

[†]*Now at Argonne National Laboratory*

Name of code system(s) used

VARIANT-SE: A prototypic version of the VARIANT code.

Computational method used

Response matrix form of the variational nodal method with a spherical harmonics angular approximation.

Type and level of angular approximation

P_{11} in 2-D and P_5 in 3-D.

Type and level of spatial discretisation

A variational nodal method utilising finite element sub-elements within each node.

- Two-dimensional:
  - A quadratic Lagrange multiplier nodal interface approximation (spatial).
  - A lumped source approximation of the finite element mesh (eight regions with flat spatial dependence).
  - A triangular finite element mesh with quadratic basis functions: 113 DOF (degrees of freedom.

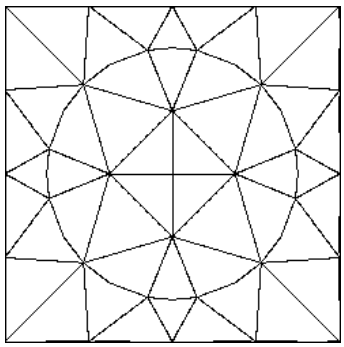

- Three-dimensional:
  - A linear Lagrange multiplier nodal approximation.
  - A lumped source approximation of the finite element mesh (10 regions).
  - A prismatic finite element mesh with quadratic basis functions in *xy* and linear basis functions in *z*: 339 DOF.

Convergence

- Eigenvalue = 10E-6.
- Pointwise:
  - Pointwise fission source = 10E-5.
  - Average fission source = 10E-5.

Machine on which the calculations were performed and (if possible) CPU time

Sun Sparcstation 60 running Solaris 8.

2-D = 182420.50 seconds/51 hours, 3-D = 571364.63 seconds/159 hours.

All times are computational times

Other assumptions and characteristics, comments useful for interpreting correctly the results

Due to cancellation of error it is believed that better results can be achieved with lower angular approximations. It is clear from single pin cell calculations that an angular approximation of around P_{27}-P_{31} is necessary to yield a proper eigenvalue. This is not possible with this method at this time.

The solutions for both the two-dimensional and three-dimensional problems were limited because of the available amount of disk space. Both calculations reported in eight suffered from low memory availability resulting in a significant amount of time being spent transferring data to and from the disk. Finally, the node size in the *z* direction and the source approximation were significantly constrained for the three-dimensional problem because of a sheer lack of available disk space (needs several Gb).

Only the P_N angular solutions were provided because it was found that the SP_N approximation proved to be quite inaccurate for this specific problem. Not necessarily for heterogeneous problems such as this, but a more specific problem was found with the seven-group cross-set used for this benchmark problem. Two-group and Twelve-group solutions have shown that the SP_N method can provide accurate solutions.

ANL-3

Name of participant(s)

Micheal A. Smith,[1,†] Nicholas Tsoulfanidis,[1] Elmer E. Lewis,[2]
Giuseppe Palmiotti,[3] Temitope Taiwo,[3] Roger Blomquist[3]

Establishment(s)

[1]University of Missouri-Rolla
[2]Northwestern University
[3]Argonne National Laboratory

[†]*Now at Argonne National Laboratory*

Name of code system(s) used

ASEVANT: A prototypic version of the VARIANT code.

Computational method used

Response matrix form of the variational nodal method with a spherical harmonics angular approximation.

Type and level of angular approximation

P_{13} in 2-D.

Type and level of spatial discretisation

A variational nodal method utilising finite element sub-elements within each node.

- Two-dimensional:
  - A cubic Lagrange multiplier nodal interface approximation (spatial).
  - A consistent source approximation of the finite element mesh.
  - A triangular finite element mesh with quadratic basis functions: 113 DOF (degrees of freedom.

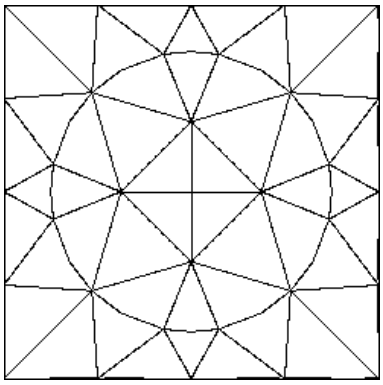

Convergence

- Eigenvalue = 10E-6.
- Pointwise:
  - Pointwise fission source = 10E-5.
  - Average fission source = 10E-5.

Machine on which the calculations were performed and (if possible) CPU time

Sun Sparcstation 60 running Solaris 8.

2-D = very long.

All times are computational times

Other assumptions and characteristics, comments useful for interpreting correctly the results

We basically found that our previous result was too “good” because of cancellation of error. A more rigorous treatment of the source corrected most of the problems and thus we provide a more “accurate” solution. As can be seen the result has become worse with a better approximation. To obtain an accurate solution, a much higher order angular approximation is necessary which is clearly not possible with this method.

9. Los Alamos National Laboratory (LANL), USA

Name of participant(s)

Jon A. Dahl, Raymond E. Alcouffe

Establishment(s)

Transport Methods Group
Los Alamos National Laboratory
Los Alamos, NM 87545

Calculation details

Introduction

In early 2001 the Expert Group on 3-D Radiation Transport Benchmarks of the Nuclear Energy Agency solicited participants for a proposed benchmark [1]. The benchmark, known as C5G7 MOX, is intended to be a basis for measuring current transport code abilities in the treatment of reactor core problems without spatial homogenisation. We participated with the code transport code PARTISN [2]. PARTISN (PARallel TIme Dependent SN) solves the linear Boltzmann transport equation in static and time-dependent forms on one-, two- and three-dimensional orthogonal grids using the deterministic (S_N) method. A variety of spatial discretisation methods are incorporated into PARTISN, however all calculations performed here used the diamond difference approach, coupled with a volume fraction method for non-Cartesian problem geometries. Acceleration of the source iterations is accomplished with diffusion synthetic acceleration (DSA).

Description of work

For the two-dimensional C5G7 MOX problem we used an X-Y Cartesian grid. Rather than creating a "stair stepped" grid to represent each fuel pin, we began with an unstructured quadrilateral grid created using ICEM CFD Engineering grid generation tools. This unstructured grid more closely represents the actual geometry of each water channel/fuel pin combination. We then overlay a Cartesian mesh onto the unstructured grid and calculate to volume fractions of each material where a Cartesian mesh cells is intersected by an unstructured mesh material boundary. This methodology allows the preservation of mass without changing the density in cells which are not intersected by actual material interfaces. We generated three grids for the two-dimensional case, a coarse, medium and fine, corresponding to a 5×5, 10×10 and 15×15 grid in each water channel/fuel pin cell, and 30 mesh cells in each direction of the water reflector. An example of the medium mesh grid in a typical water channel/fuel pin region can be found in Figure 1. The cells containing an X indicate mesh cells where volume fractions of fuel and water have been calculated. The unmarked cells contain just one material, either the appropriate water or fuel.

The grid for the three-dimensional problem was generated in the same way, beginning with a three-dimensional unstructured mesh and calculating the corresponding volume fractions for Cartesian X-Y-Z mesh cells intersecting material interfaces. We performed calculations on two three-dimensional grids, one coarse and one medium, which, as in the two-dimensional case, contained 5×5 and 10×10 mesh cells respectively, in each water channel/fuel pin cell, and 30 mesh cells in each direction of the water reflector. The coarse mesh fuel region contained 20 cells in the Z direction, for a total of $200 \times 200 \times 50$ or six million cells. The fuel region of the

Figure 1. Representation of fuel pin meshing

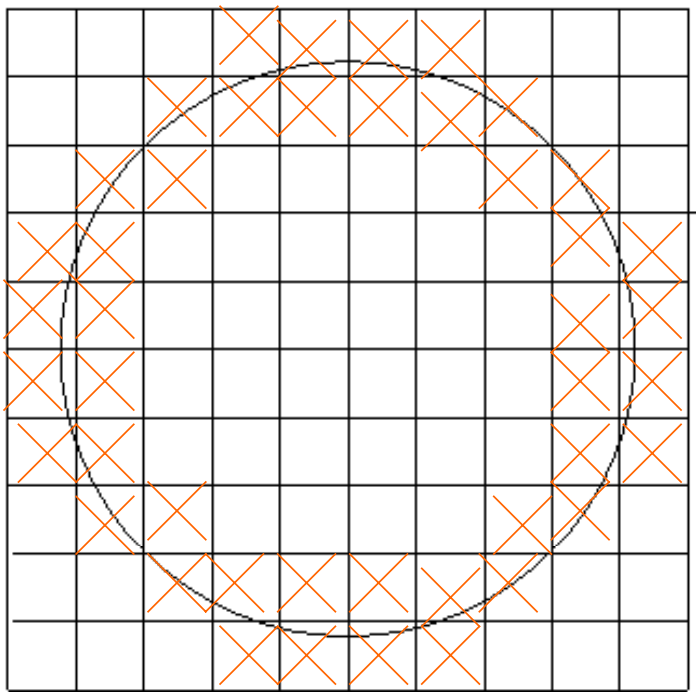

medium mesh was comprised of 50 cells in the Z direction for a total of 370 × 370 × 80, or 10 952 000 cells. We also generated a fine three-dimensional mesh, consisting of 17 496 000 cells, but two-dimensional convergence studies indicated that a mesh this fine is not required.

We ran each problem using the square Tchebechev-Legendre quadrature set [3] and diamond difference spatial differencing. The pointwise fluxes were converged to an error of 1.0E-05. The diffusion equations for the DSA were solved using a parallel multi-grid technique described by Alcouffe [4]. Varying S_N orders for each mesh were run to determine that spatial and angular convergence was achieved.

Both the two- and three-dimensional problems were run on the Bluemountain computer, located at the Los Alamos National Laboratory. Bluemountain consists of 48 SGI Origin 2000 boxes with 128 processors each. The two-dimensional problems were run with 16 processors, while the three-dimensional problems were run with 126 to 768 processors, depending on mesh size and S_N order.

Computational results

For this benchmark, we report the eigenvalues and pin powers for the medium mesh grids run with S_{26} square Legendre-Tchebychev quadrature. Table 1 presents the eigenvalues for both the two- and three-dimensional cases.

Table 1. K eigenvalues for 2-D/3-D C5G7 MOX benchmark problems

Dimension	k eigenvalue
2-D	1.18637
3-D	1.18362

In Table 2, the normalised minimum and maximum pins powers for the two-dimensional coarse and medium mesh and the three-dimensional coarse mesh are shown. These results were also generated with a quadrature order of S_{26}. Complete pin power results can be found in Tables 3-7.

Table 2. Maximum and minimum normalised pin powers for 2-D/3-D C5G7 MOX benchmark problem

Mesh	Maximum	Minimum
2-D medium mesh	2.5025	0.2319
3-D medium mesh	2.5018	0.2318

Acknowledgements

We wish to thank Todd Wareing for generating the unstructured quadrilateral grid with ICEM CFD Engineering software.

This work was performed under the auspices of the Department of Energy.

References

[1] Lewis, E.E., *et al*., *Benchmark Specification for Deterministic 2-D/3-D MOX Fuel Assembly Transport Calculations Without Spatial Homogenisation*, Nuclear Energy Agency, Nuclear Science Committee, Expert Group on 3-D Radiation Transport Benchmarks Report, NEA/NSC/DOC(2001)17, (2001).

[2] Alcouffe, R.E., R.S. Baker, J.A. Dahl and S.A. Turner, *PARTISN Code Abstract*, Physor 2000 International Topical Meeting, Advances in Reactor Physics and Mathematics and Computation into the Next Millennium, Pittsburgh (2000).

[3] O'Dell, R.D., R.E. Alcouffe, *Transport Calculations for Nuclear Analysis: Theory and Guidelines for Effective Use of Transport Codes*, LA-10983-MS, Los Alamos National Laboratory, September 1987.

[4] Alcouffe, R.E., "A Parallel Multigrid Method for Inversion of the Diffusion Operator in Neutronics Applications," *Proceedings ANS International Meeting on Mathematical Methods for Nuclear Applications*, Salt Lake City, UT, September (2001).

Table 3. Two-dimensional UO_2 pin powers near axis of symmetry

	1	2	3	4	5	6	7	8	9	10	11	12	13	14	15	16	17	
1	2.0829	2.1399	2.1888	2.2155	2.2264	2.2307	2.1875	2.1508	2.1230	2.0586	2.0024	1.9518	1.8583	1.7559	1.6341	1.4857	1.2810	1
2		2.1790	2.2238	2.2699	2.3035	2.3746	2.2577	2.2175	2.2540	2.1232	2.0657	2.0773	1.9233	1.7985	1.6561	1.4941	1.2811	2
3			2.3052	2.4417	2.4737		2.3872	2.3398		2.2416	2.1822		2.0657	1.9343	1.7147	1.5134	1.2851	3
4					2.5025	2.4599	2.2994	2.2498	2.2962	2.1542	2.1025	2.1492	2.0844		1.8166	1.5416	1.2926	4
5					2.4069	2.4322	2.2834	2.2363	2.2827	2.1416	2.0885	2.1261	2.0061	1.9780	1.8367	1.5638	1.2971	5
6							2.3524	2.3062		2.2103	2.1519		2.0309	1.9434		1.6153	1.3008	6
7							2.2226	2.1822	2.2300	2.0910	2.0355	2.0605	1.9076	1.8187	1.7716	1.5338	1.2761	7
8								2.1440	2.1906	2.0551	2.0002	2.0223	1.8709	1.7821	1.7392	1.5092	1.2573	8
9										2.1019	2.0445		1.9140	1.8216		1.5412	1.2458	9
10										1.9716	1.9198	1.9431	1.7978	1.7137	1.6748	1.4538	1.2120	10
11											1.8708	1.8948	1.7571	1.6777	1.6369	1.4208	1.1850	11
12													1.7941	1.7207		1.4398	1.1635	12
13													1.6961	1.6773	1.5670	1.3399	1.1166	13
14															1.4794	1.2635	1.0675	14
15															1.3205	1.1768	1.0128	15
16																1.0812	0.9534	16
17																	0.8770	17

Table 4. Two-dimensional UO_2 pin powers near water reflector

UO2-2 Normalised Pin Powers

	18	19	20	21	22	23	24	25	26	27	28	29	30	31	32	33	34	
18	0.7936	0.7896	0.7714	0.7501	0.7253	0.6995	0.6589	0.6212	0.5873	0.5444	0.5052	0.4702	0.4290	0.3941	0.3734	0.3901	0.5025	18
19		0.8271	0.8317	0.8262	0.8117	0.8088	0.7402	0.6977	0.6806	0.6133	0.5693	0.5475	0.4863	0.4425	0.4140	0.4247	0.5293	19
20			0.8653	0.9003	0.8877		0.8018	0.7541		0.6652	0.6172		0.5373	0.4896	0.4403	0.4389	0.5355	20
21					0.8928	0.8521	0.7691	0.7236	0.7100	0.6382	0.5947	0.5815	0.5409		0.4656	0.4443	0.5318	21
22					0.8404	0.8251	0.7496	0.7069	0.6937	0.6246	0.5820	0.5667	0.5139	0.4936	0.4637	0.4425	0.5217	22
23							0.7532	0.7110		0.6303	0.5860		0.5095	0.4736		0.4449	0.5079	23
24							0.6898	0.6533	0.6434	0.5793	0.5395	0.5233	0.4656	0.4318	0.4258	0.4122	0.4852	24
25								0.6198	0.6101	0.5504	0.5127	0.4964	0.4417	0.4092	0.4039	0.3923	0.4624	25
26										0.5433	0.5053		0.4363	0.4029		0.3849	0.4401	26
27										0.4900	0.4567	0.4432	0.3940	0.3651	0.3611	0.3501	0.4124	27
28											0.4262	0.4133	0.3685	0.3420	0.3373	0.3272	0.3853	28
29													0.3602	0.3349		0.3155	0.3595	29
30													0.3266	0.3132	0.2961	0.2817	0.3295	30
31															0.2705	0.2560	0.3014	31
32															0.2417	0.2360	0.2778	32
33																0.2319	0.2667	33
34																	0.2878	34

Table 5. Two-dimensional MOX pin powers

MOX Normalised Pin Powers

	18	19	20	21	22	23	24	25	26	27	28	29	30	31	32	33	34	
1	1.3138	1.0614	0.9356	0.8632	0.8112	0.7672	0.7118	0.6623	0.6194	0.5688	0.5232	0.4831	0.4370	0.3974	0.3762	0.4086	0.6002	1
2	1.2966	1.3434	1.1704	1.0927	1.0478	1.0446	0.9182	0.8499	0.8385	0.7324	0.6718	0.6565	0.5663	0.5032	0.4689	0.5154	0.5922	2
3	1.2902	1.3205	1.1770	1.1744	1.1188		0.9489	0.8686		0.7545	0.6873		0.6061	0.5412	0.4738	0.5066	0.5883	3
4	1.2923	1.3323	1.2621		1.1116	1.1271	0.9566	0.8794	0.8752	0.7583	0.6971	0.7018	0.5878		0.5122	0.5119	0.5876	4
5	1.2951	1.3594	1.2889	1.1810	1.1438	1.0824	0.9272	0.8538	0.8517	0.7367	0.6764	0.6765	0.6097	0.5370	0.5169	0.5225	0.5878	5
6	1.2965	1.4249		1.2792	1.1415		0.9834	0.9005		0.7841	0.7127		0.6192	0.5760		0.5489	0.5877	6
7	1.2741	1.3329	1.2223	1.1462	1.0367	1.0355	0.8988	0.8314	0.8320	0.7187	0.6584	0.6524	0.5601	0.5205	0.4869	0.5135	0.5810	7
8	1.2559	1.3119	1.1981	1.1226	1.0171	1.0164	0.8854	0.8204	0.8204	0.7098	0.6501	0.6426	0.5514	0.5116	0.4789	0.5074	0.5757	8
9	1.2431	1.3619		1.1887	1.0723		0.9424	0.8670		0.7569	0.6873		0.5884	0.5398		0.5307	0.5723	9
10	1.2120	1.2687	1.1624	1.0888	0.9876	0.9898	0.8618	0.7993	0.8013	0.6929	0.6351	0.6290	0.5393	0.5005	0.4694	0.4969	0.5637	10
11	1.1861	1.2434	1.1410	1.0738	0.9742	0.9740	0.8486	0.7870	0.7881	0.6827	0.6267	0.6210	0.5343	0.4972	0.4652	0.4916	0.5570	11
12	1.1643	1.2860		1.1617	1.0417		0.9041	0.8312		0.7276	0.6632		0.5781	0.5385		0.5150	0.5520	12
13	1.1216	1.1873	1.1347	1.0410	1.0143	0.9676	0.8317	0.7695	0.7718	0.6690	0.6163	0.6189	0.5581	0.4921	0.4758	0.4814	0.5416	13
14	1.0777	1.1250	1.0787		0.9621	0.9811	0.8380	0.7752	0.7752	0.6749	0.6234	0.6299	0.5296		0.4640	0.4642	0.5324	14
15	1.0356	1.0829	0.9845	0.9966	0.9579		0.8237	0.7602		0.6677	0.6120		0.5443	0.4881	0.4282	0.4570	0.5278	15
16	1.0062	1.0911	0.9847	0.9406	0.9155	0.9219	0.8191	0.7651	0.7596	0.6689	0.6175	0.6058	0.5261	0.4699	0.4386	0.4774	0.5361	16
17	1.0135	0.9092	0.8546	0.8184	0.7865	0.7555	0.7101	0.6680	0.6305	0.5840	0.5412	0.5030	0.4582	0.4194	0.3968	0.4203	0.5771	17

Table 6. Three-dimensional UO_2 pin powers near axis of symmetry

	1	2	3	4	5	6	7	8	9	10	11	12	13	14	15	16	17	
1	2.0827	2.1396	2.1884	2.2150	2.2258	2.2302	2.1870	2.1503	2.1226	2.0582	2.0020	1.9514	1.8580	1.7556	1.6339	1.4856	1.2811	1
2		2.1786	2.2233	2.2694	2.3028	2.3741	2.2571	2.2170	2.2534	2.1227	2.0651	2.0768	1.9229	1.7982	1.6559	1.4940	1.2812	2
3			2.3046	2.4410	2.4731		2.3866	2.3392		2.2411	2.1817		2.0652	1.9340	1.7145	1.5133	1.2851	3
4					2.5018	2.4592	2.2988	2.2493	2.2956	2.1536	2.1019	2.1487	2.0839		1.8163	1.5415	1.2926	4
5					2.4062	2.4314	2.2827	2.2358	2.2821	2.1410	2.0881	2.1256	2.0057	1.9776	1.8364	1.5637	1.2971	5
6							2.3519	2.3056		2.2097	2.1514		2.0304	1.9430		1.6151	1.3008	6
7							2.2220	2.1817	2.2295	2.0904	2.0350	2.0600	1.9072	1.8183	1.7714	1.5338	1.2761	7
8								2.1434	2.1901	2.0545	1.9996	2.0217	1.8706	1.7819	1.7390	1.5091	1.2573	8
9										2.1013	2.0441		1.9135	1.8212		1.5411	1.2459	9
10										1.9710	1.9193	1.9426	1.7974	1.7134	1.6745	1.4537	1.2120	10
11											1.8704	1.8944	1.7567	1.6774	1.6366	1.4207	1.1850	11
12													1.7937	1.7204		1.4398	1.1636	12
13													1.6957	1.6770	1.5667	1.3398	1.1166	13
14															1.4792	1.2634	1.0675	14
15															1.3205	1.1768	1.0129	15
16																1.0813	0.9536	16
17																	0.8771	17

Table 7. Three-dimensional UO_2 pin powers near water reflector

	18	19	20	21	22	23	24	25	26	27	28	29	30	31	32	33	34	
18	0.7937	0.7898	0.7715	0.7502	0.7254	0.6996	0.6590	0.6213	0.5874	0.5444	0.5053	0.4703	0.4291	0.3942	0.3734	0.3900	0.5022	18
19		0.8272	0.8319	0.8263	0.8118	0.8088	0.7403	0.6977	0.6806	0.6133	0.5693	0.5475	0.4863	0.4425	0.4140	0.4246	0.5290	19
20			0.8653	0.9003	0.8877		0.8017	0.7541		0.6652	0.6172		0.5373	0.4895	0.4403	0.4388	0.5351	20
21					0.8928	0.8520	0.7690	0.7236	0.7100	0.6382	0.5947	0.5814	0.5409		0.4654	0.4441	0.5315	21
22					0.8403	0.8250	0.7495	0.7068	0.6936	0.6245	0.5819	0.5666	0.5138	0.4935	0.4635	0.4422	0.5213	22
23							0.7532	0.7109		0.6302	0.5859		0.5095	0.4735		0.4447	0.5075	23
24							0.6897	0.6532	0.6433	0.5792	0.5394	0.5232	0.4655	0.4316	0.4257	0.4120	0.4849	24
25								0.6197	0.6100	0.5503	0.5127	0.4963	0.4417	0.4092	0.4039	0.3921	0.4620	25
26										0.5433	0.5053		0.4362	0.4028		0.3848	0.4398	26
27										0.4899	0.4567	0.4431	0.3939	0.3650	0.3610	0.3500	0.4120	27
28											0.4261	0.4132	0.3684	0.3419	0.3371	0.3270	0.3850	28
29													0.3601	0.3348		0.3153	0.3592	29
30													0.3265	0.3131	0.2960	0.2815	0.3292	30
31															0.2704	0.2559	0.3011	31
32															0.2416	0.2360	0.2775	32
33																0.2318	0.2665	33
34																	0.2875	34

Table 8. Three-dimensional MOX pin powers

	18	19	20	21	22	23	24	25	26	27	28	29	30	31	32	33	34	
1	1.3139	1.0617	0.9359	0.8634	0.8115	0.7674	0.7121	0.6626	0.6197	0.5691	0.5235	0.4833	0.4372	0.3976	0.3764	0.4087	0.5999	1
2	1.2967	1.3436	1.1707	1.0931	1.0481	1.0449	0.9186	0.8503	0.8389	0.7328	0.6721	0.6568	0.5665	0.5033	0.4691	0.5154	0.5920	2
3	1.2903	1.3207	1.1772	1.1747	1.1191		0.9493	0.8690		0.7548	0.6877		0.6064	0.5414	0.4740	0.5068	0.5880	3
4	1.2924	1.3325	1.2624		1.1120	1.1274	0.9569	0.8798	0.8756	0.7587	0.6975	0.7022	0.5880		0.5124	0.5120	0.5874	4
5	1.2951	1.3595	1.2891	1.1813	1.1441	1.0829	0.9276	0.8542	0.8521	0.7370	0.6768	0.6768	0.6099	0.5372	0.5171	0.5225	0.5876	5
6	1.2966	1.4251		1.2796	1.1419		0.9838	0.9009		0.7845	0.7131		0.6194	0.5763		0.5489	0.5876	6
7	1.2742	1.3331	1.2225	1.1464	1.0372	1.0359	0.8991	0.8317	0.8324	0.7190	0.6587	0.6528	0.5603	0.5208	0.4871	0.5135	0.5808	7
8	1.2560	1.3120	1.1985	1.1230	1.0174	1.0168	0.8858	0.8208	0.8208	0.7101	0.6505	0.6430	0.5517	0.5118	0.4791	0.5074	0.5755	8
9	1.2433	1.3621		1.1891	1.0726		0.9427	0.8674		0.7573	0.6878		0.5887	0.5401		0.5307	0.5721	9
10	1.2121	1.2689	1.1627	1.0892	0.9879	0.9901	0.8622	0.7997	0.8017	0.6932	0.6354	0.6293	0.5396	0.5008	0.4695	0.4969	0.5634	10
11	1.1862	1.2436	1.1412	1.0742	0.9746	0.9743	0.8490	0.7873	0.7884	0.6831	0.6270	0.6214	0.5345	0.4974	0.4653	0.4916	0.5568	11
12	1.1645	1.2863		1.1621	1.0420		0.9044	0.8316		0.7279	0.6636		0.5782	0.5388		0.5150	0.5518	12
13	1.1217	1.1874	1.1350	1.0413	1.0147	0.9679	0.8320	0.7698	0.7721	0.6693	0.6166	0.6191	0.5582	0.4923	0.4759	0.4814	0.5414	13
14	1.0779	1.1252	1.0789		0.9625	0.9814	0.8383	0.7756	0.7755	0.6752	0.6236	0.6301	0.5297		0.4641	0.4643	0.5322	14
15	1.0357	1.0831	0.9848	0.9969	0.9582		0.8240	0.7605		0.6679	0.6122		0.5444	0.4883	0.4282	0.4570	0.5275	15
16	1.0063	1.0913	0.9849	0.9408	0.9158	0.9222	0.8194	0.7653	0.7598	0.6691	0.6178	0.6060	0.5262	0.4700	0.4386	0.4773	0.5359	16
17	1.0136	0.9094	0.8548	0.8185	0.7867	0.7556	0.7102	0.6681	0.6307	0.5841	0.5414	0.5032	0.4583	0.4195	0.3968	0.4202	0.5769	17

10. Los Alamos National Laboratory (LANL), USA

Name of participant(s)

Todd A. Wareing, John M. McGhee

Establishment(s)

Los Alamos National Laboratory

Name of code system(s) used

2-D benchmark: Pericles.

3-D benchmark: Attila.

Computational method used

S_N.

Type and level of angular approximation

We examined several different quadrature sets and level of approximations and have settled on using the Square-Tchebyshev-Double-Legendre quadrature set.

For the 2-D calculations, we provide results for S_{16} and for 3-D we provide results for S_{12}.

Type and level of spatial discretisation

For 2-D, we use bi-linear discontinuous finite element spatial differencing on quadrilateral elements. The grids were created using ICEM CFD Engineering Quad™. We provide results for two different mesh refinements. The coarse 2-D mesh contains 17 465 quads and the fine 2-D mesh contains 62 079 quads. See Figure 1 for a subsection of the coarse 2-D mesh and Figure 2 for a subsection of the fine 2-D mesh.

For 3-D, we use linear discontinuous finite element spatial differencing on tetrahedral elements. The grid was created using a combination of ICEM CFD Engineering's meshing modules. The mesh contains 954 427 tetrahedra. A subsection of the 3-D mesh is given in Figure 3.

Convergence

- Eigenvalue: 1×10^{-5}.
- Flux pointwise: 1×10^{-4}.

Machine on which the calculations were performed and (if possible) CPU time

SGI with 250 MHz R10000 processor. CPU times are difficult to access and are not included.

Figure 1. Subsection of coarse 2-D mesh

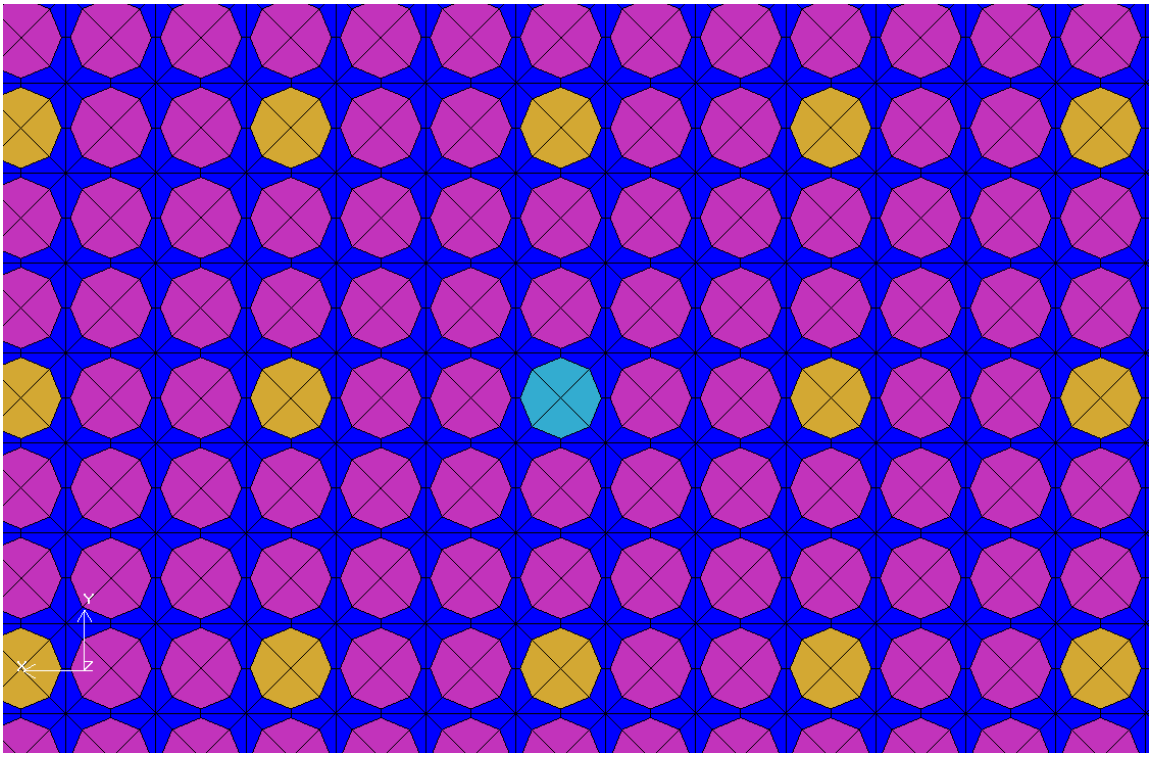

Figure 2. Subsection of fine 2-D mesh

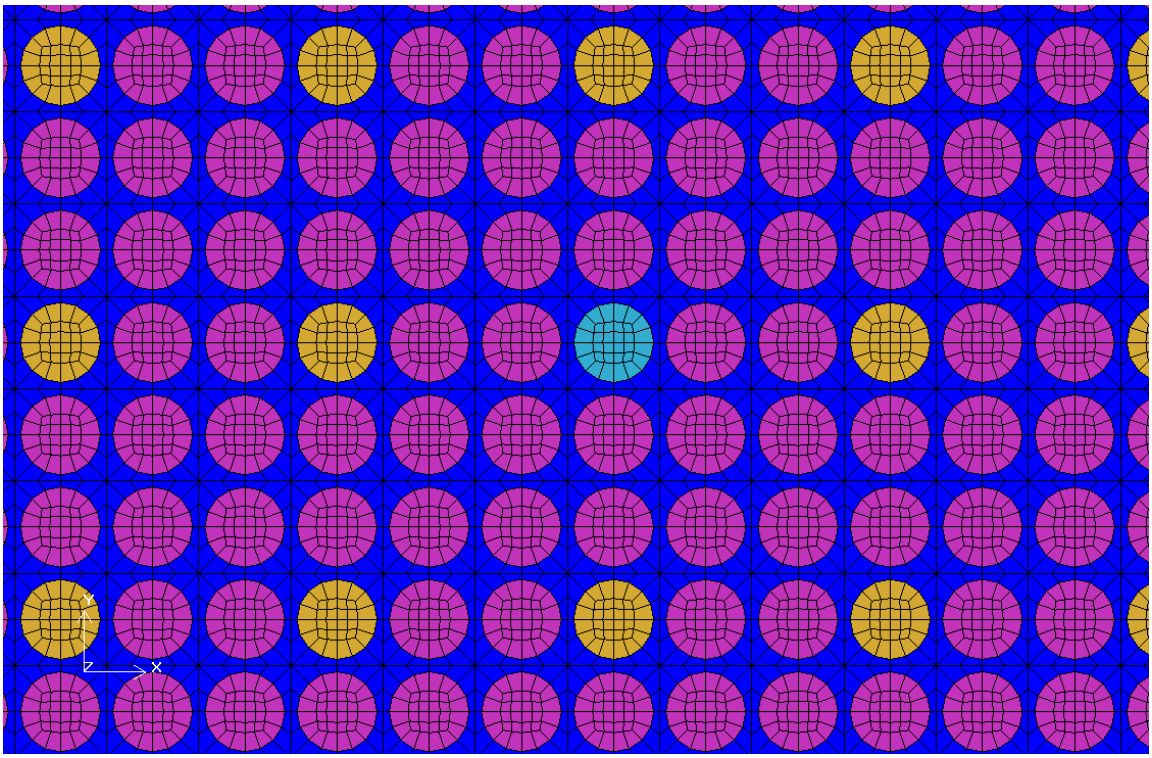

Figure 3. Subsection of 3-D mesh

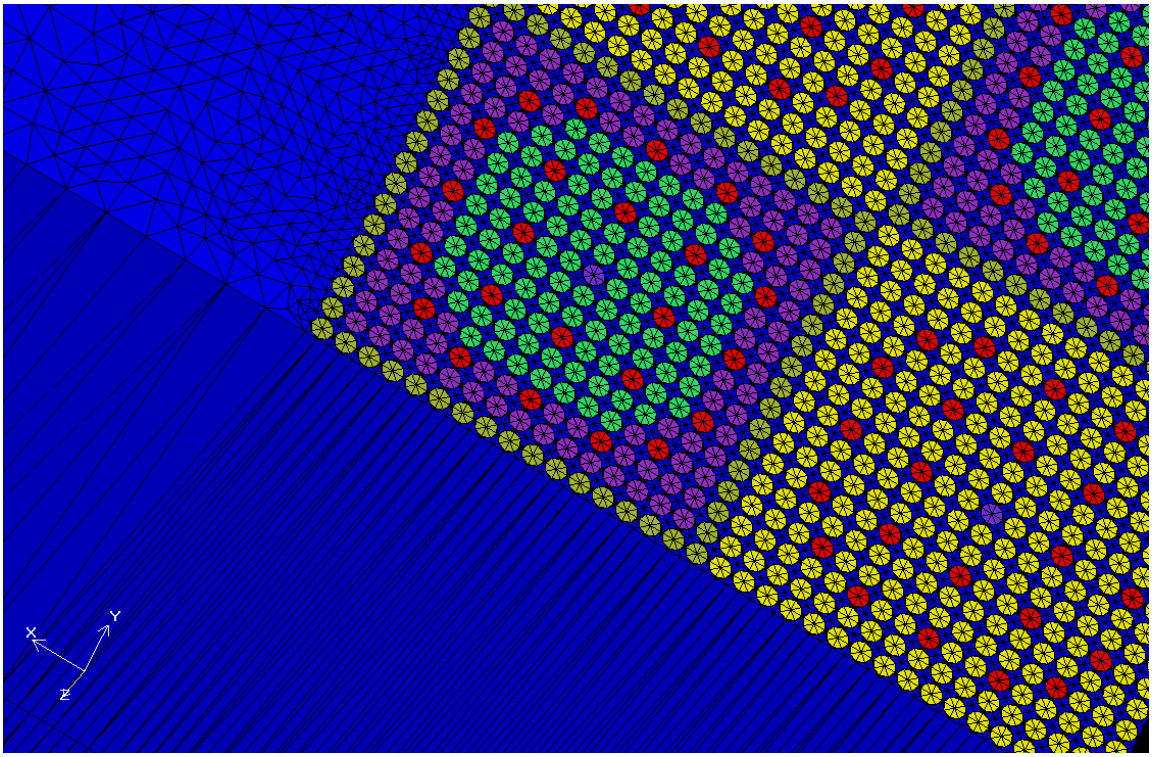

Other assumptions and characteristics, comments useful for interpreting correctly the results

All of the meshes were created to preserve the volume, and hence, the mass of the materials. We performed much of the parameter studies for the 2-D problem. Here we used two different mesh refinements and varying orders of angular quadrature. Table 1 provides our eigenvalue results for the 2-D benchmark problem as a function of both mesh and angular refinement. For the 3-D benchmark, the mesh is similar in refinement to that of the coarse 2-D mesh.

Table 1. Eigenvalue results for 2-D benchmark as a function of mesh refinement and angular refinement

S_N order	Coarse mesh	Fine mesh
4	1.18454	1.18424
8	1.18606	1.18610
12	1.18628	1.18641
16	1.18642	1.18658

11. Oak Ridge National Laboratory (ORNL), USA

Name of participant(s)

Yousry Y. Azmy,[1] Jess C. Gehin,[1] Roberto Orsi[2]

Establishment(s)

[1]Oak Ridge National Laboratory
P.O. Box 2008, MS 6363
Oak Ridge, TN 37831-6363

[2]ENEA Centro Dati Nucleari
Via Martiri di Monte Sole, 4
40129 Bologna, Italy

Name of code system(s) used

- 2-D: DORT.
- 3-D: TORT-MPI.
- Pre- & post-processing: BOT3P.

Computational method used

S_N.

Type and level of angular approximation

S_{16} fully symmetric quadrature (distributed with DOORS package).

Type and level of spatial discretisation

- Two-dimensional (see Figure 1):
  - Theta-weighted with theta = 0.9 (default).
  - Computational cells per lattice cell = 27 × 27.
  - Total computational cells = 930 × 930.
- Three-dimensional (see Figure 2):
  - Linear nodal method.
  - Computational cells per lattice cell = 5 × 5 × 40.
  - Total computational cells = 182 × 182 × 40.

Figure 1

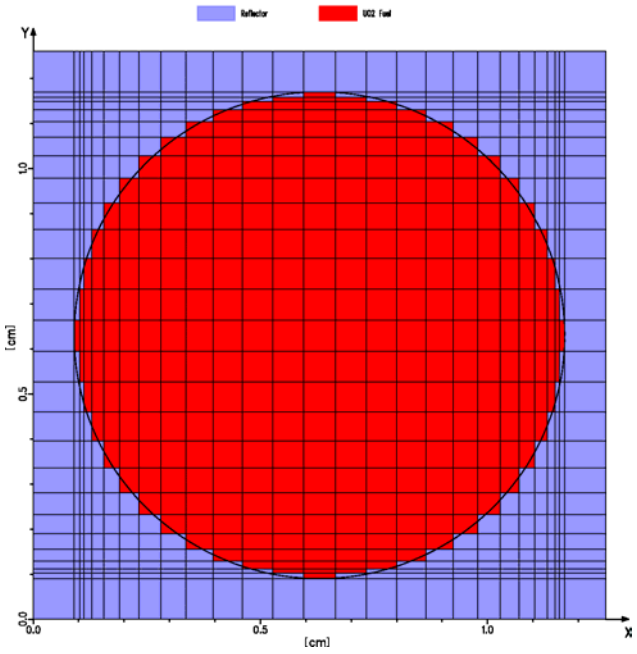

Figure 2

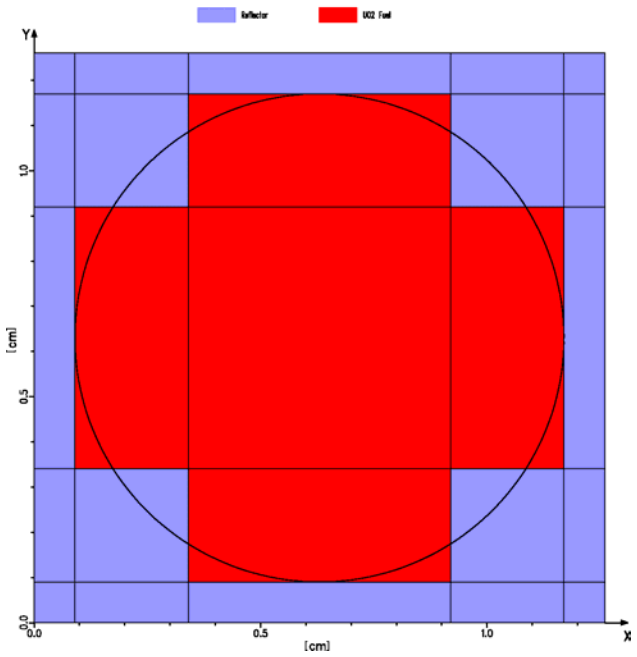

Convergence

	Eigenvalue	Fission	Flux
2-D	7.1 E-8	2.1 E-7	4.0 E-6
3-D	4.3 E-7	2.4 E-4	8.1 E-4

Machine on which the calculations were performed and (if possible) CPU time

Compaq AlphaServer SC, with ES40 nodes.

CPU hours: 2-D – 17.2, 3-D – not available.

Other assumptions and characteristics, comments useful for interpreting correctly the results

All calculations performed in 64-bit arithmetic precision.

DORT: converged in 56 outer iterations with forced four inner iterations per outer.

TORT-MPI executed in parallel on 12 processors; multiple runs necessary due to time limit per run; total number of iterations and CPU time unavailable because output file lost in system crash.

Extensive study of solution convergence with model refinement reveals rapid convergence of eigenvalue with mesh refinement, but slower convergence with rising order of angular quadrature. Hence, coarser models executing much faster than those submitted here were only slightly less accurate.

12. Indira Gandhi Centre for Atomic Research (IGCAR), India

Participant(s)

P. Mohanakrishnan

Establishment(s)

Reactor Physics Division
Indira Gandhi Centre for Atomic Energy
Kalpakkam, T.N., 603102, India

Name of code system(s) used

COHINT (see Ref. [1]).

Computational method used

Interface Current Method with P_N half space expansion of angular fluxes at region interfaces is used to solve the neutron transport equation in X-Y geometry by dividing the problem into small regions. Full details of the method are given in Ref. [2]. The code RICANT which solves X-Y geometry problems has been submitted to the NEA Data Bank [3]. The COHINT computer code includes RICANT as well as another code to solve the neutron transport equation in 2-D cylindrical pin cluster geometry (as for example in PHWR fuel assemblies or FBR control rods).

Type and level of angular approximation

A P_2 half space expansion has been used for angular fluxes at region interfaces. Following is the six-term expansion found suitable for 2-D geometries with severe heterogeneities [2].

$$\Psi(\beta,\phi) = a_0 + a_1\cos\beta\cos\phi + a_2\cos\beta\sin\phi + a_3\cos^2\beta + a_4\cos^2\beta\sin^2\phi + a_5\cos^2\beta\cos\phi\sin\phi$$

Ψ is the neutron angular flux at region interface (half space). The expansion coefficients "*a*" are different in the two half spaces made by the region interface. Angles β and ϕ define the neutron direction with respect to the region surface normal. It had also been found that a four-term expansion consisting of the first four terms above gives practically the same results as the full six-term expansion. Four-term expansion has been used in the present analysis. The outgoing neutron angular flux at a region interface is contributed by incoming fluxes at the surfaces and neutron source inside the region. The matrix equation for iterative solution is set up by making use of the superposition principle of neutron angular fluxes.

Type and level of spatial discretisation

Neutron flux and source is assumed to be flat inside a region. A unit cell of the lattice was divided into 25 regions. A diagram of the unit cell discretisation is shown in Figure 1.

In the moderator/reflector near core, region size of $0.521 \times 0.521 cm^2$ was used. Beyond 11.42 cm from core 1.0×1.0 cm^2 regions were used. Total number of meshes in X and Y directions were 201 each. Half-core symmetry was made use of in COHINT. The resulting number of total regions for solution were 20 301 in half core.

Figure 1. Unit cell discretisation – 1.26 × 1.26 cm^2

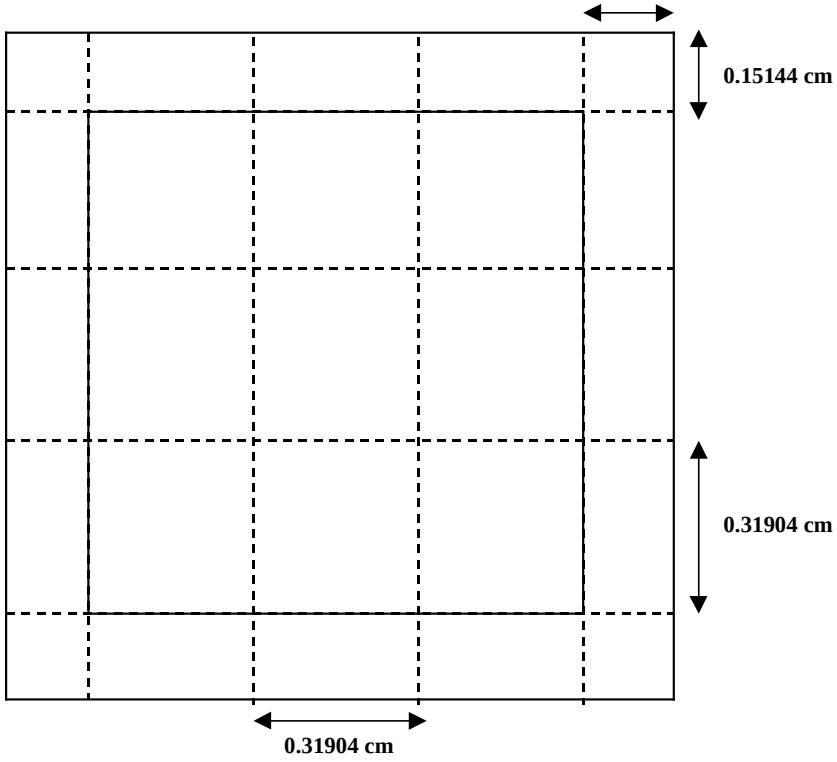

Convergence

- Eigenvalue – less than 3×10^{-6}.
- Flux region wise – less than 4×10^{-4}.

Summary of results

Eigenvalue = 1.17530.

Peak pin relative fission rate = 2.395 in UO_2 assembly.

The above results are with the use of transport cross-section in COHINT. Eigenvalue with the use of total cross-section and corresponding adjustment of self-scattering cross-section in the group is 1.20362.

In the EXCEL tables, only the results using the transport cross-section are presented.

Machine on which the calculations were performed and (if possible) CPU time

SGI, CPU time 190 minutes (half-core symmetry).

Other assumptions and characteristics, comments useful for interpreting correctly the results

The fuel region cross-section has been approximated as square as against the actual circle. Only 2-D results are presented here.

References

[1] Mohanakrishnan P., *COHINT – A Computer Code to Treat Control Rod Heterogeneity and its Application to Fast Reactor Core Analysis*, IGC-130 (1992).

[2] Mohanakrishnan P., *Annals of Nuclear Energy*, Vol. 9, p. 261 (1982).

[3] Mohanakrishnan P., "Program Abstract of Computer Code RICANT", NEA Data Bank of OECD, IAEA0929/01 (1987), *NEA Data Bank News* (June 1990).

13. TEPCO Systems Corporation (TEPSYS), Japan

Name of participant(s)

Shinya Kosaka

Establishment(s)

TEPCO Systems Corporation (since 1/10/2001; previously Toden Software, Inc., which merged with another TEPCO group company on that date.)

Name of code system(s) used

CHAPLET.

Computational method used

Method of characteristics.

Type and level of angular approximation

- Sixteen (16) polar angles/90°.
- One-hundred twenty-eight (128) azimuthal angles/360°.
- Width of path interval: 1 mm.

Type and level of spatial discretisation

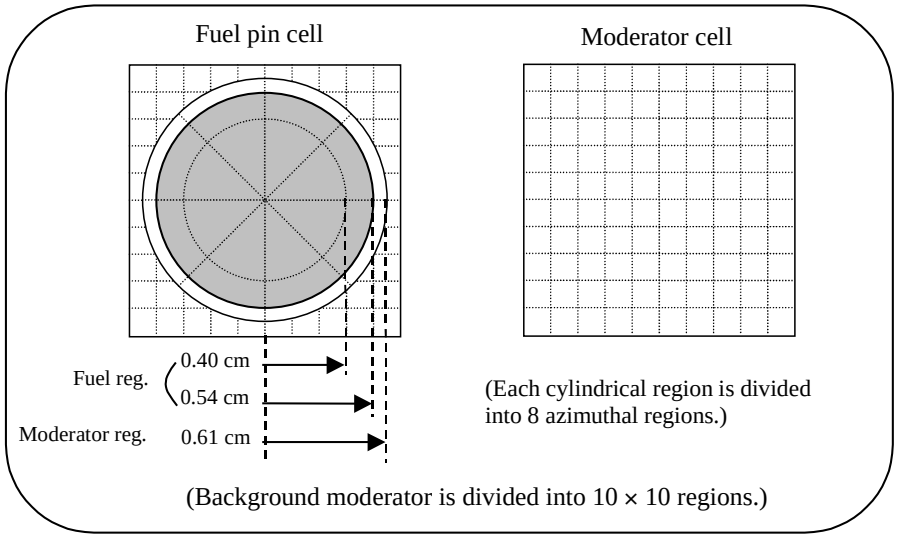

Convergence

- Eigenvalue: 1.0E-6.
- Pointwise: Group-wise scalar flux – 1.0E-5.

Machine on which the calculations were performed and (if possible) CPU time

SUN Ultra-80 450 MHz, 3 CPU parallel calculation. CPU time: 167minutes.

Other assumptions and characteristics, comments useful for interpreting correctly the results

The Direct Neutron Path Linking (DNPL) technique [1] is applied to the CHAPLET code. DNPL is a memory size-saving technique for large-scale characteristics calculations. The idea of this technique came from sharing the neutron path information among assemblies (unit modules) with the same configuration. When cyclic ray tracing, such as that applied to the CACTUS [2] code, is used for preparing neutron paths to each unit module, the whole core characteristics calculation can be performed by linking these module data without holding the core-wide neutron flight path data (see Figures 1 and 2).

As a result, a whole-core characteristics calculation can be made separately among assemblies with small memory size. In addition, the parallelisation of the flux solution was attempted to the CHAPLET code, resulting in significant reduction in the wall-clock time of the calculation.

In this 2-D benchmark analysis, the occupied memory size was about 300 Mbyte.

Figure 1. Ray tracing arrangement in CACTUS and DNPL technique

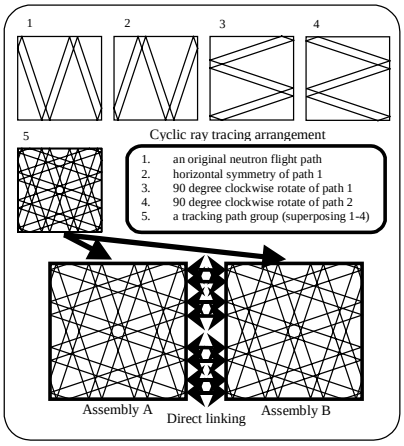

Figure 2. Illustration of DNPL technique in a multi-assembly system

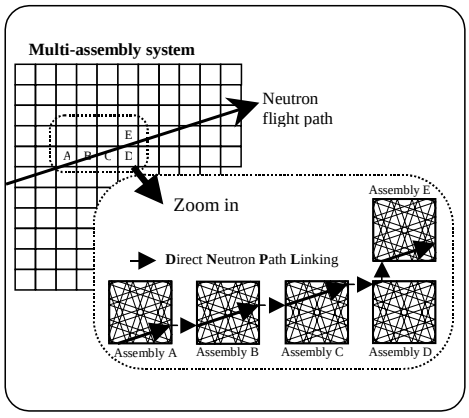

References

[1] Kosaka S., "Transport Theory Calculation for a Heterogeneous Multi-assembly Problem by Characteristics Method with Direct Neutron Path Linking Technique," *Journal of Nuclear Science and Technology,* Vol. 37, No. 12, p. 1015 (2000).

[2] Halsall, M.J., AEEW-R 1291 (1980).

14. Russian Research Centre "Kurchatov Institue" (RRC KI), Russian Federation

Participant(s)

Victor F. Boyarinov

Establishment(s)

Russian Research Centre "Kurchatov Institute"
Nuclear Reactor Institute
Department of Physical & Technical Researches of Advanced Reactors
123182, Moscow, Russia

Names of code system(s) used

For computation this benchmark the following codes were used: options RACCIA and DIC-PN of WIMS-SH [1] system of codes and SUHAM-2D [2] code. The WIMS-SH system of codes was used for computation of the zero*th*, first and second trial matrices for cells $\hat{\varphi}^{(0)}, \hat{\varphi}^{(1)}, \hat{\varphi}^{(2)}$. SUHAM-2D was used both for computation of the third trial matrices for cells with homogeneous cross-sections and for solving the finite-difference equations of Surface Harmonics Method (SHM) with four trial functions.

Computational method used

Surface Harmonics Method with four trial functions was used.

The Surface Harmonics Method [3] is the method for the solving neutron transport equation in a reactor core. A characteristic feature of SHM is that, in general, it does not use the procedure of spatial homogenisation.

In SHM, neutron distribution in a reactor core is presented as a superposition of trial functions:

$$\Phi^N(w) = \sum_{i=1}^{I} \sum_{n=0}^{N} a_{in} \varphi_{in}(w) \tag{1}$$

Here $\varphi_{in}(w)$ are the trial functions describing the neutron field in i-th cell, coefficients a_{in} are the amplitudes of trial functions, n is the trial function number and $(N + 1)$ is the number of trial functions for every cell.

Each trial function is taken as a solution of the neutron transport equation in the internal cell area with certain boundary conditions on the cell surface. Different trial functions differ from one another by the boundary condition.

On Figure 1 schemes for neutron currents incoming through the cell boundary for the first four trial functions in square lattice are shown. These schemes for neutron currents incoming through the cell boundary are given for each energy group g; in so doing, neutron currents incoming through the cell boundary in other groups equal zero. Then, value g is changed. Therefore, the real number of group trial functions equals the number of schemes for incoming neutron currents shown in Figure 1 multiplied by the number of energy groups. Thus, trial matrices appear.

Since the actual number of the trial functions is limited, at substituting the quest solution in the neutron transport equation, a residual appears. The minimisation procedure for this residual gives the finite-difference equations of the SHM.

Finite-difference equations of SHM with four trial functions have the following form.

$$\begin{cases} \hat{\Lambda}_0 \vec{\Phi}_k - \hat{\Sigma} \vec{\Phi}_k + \vec{S}_k^{(0)} = 0 \\ \hat{\Lambda}_0 \vec{X}_k^{(1)} + \hat{\Sigma}_k^{(1)} \vec{X}_k^{(1)} + \vec{S}_k^{(1)} = 0 \end{cases} \tag{2}$$

where:

$$\begin{cases} \vec{S}_k^{(0)} = -\hat{\Lambda}_1' \vec{X}_k^{(1)} \\ \vec{S}_k^{(1)} = -\hat{\Lambda}_1' \vec{\Phi}_k \end{cases} \tag{3}$$

$$\begin{cases} \hat{\Sigma}_k = \dfrac{MS_k}{V_k} \left(\hat{\varphi}_k^{(0)} - \hat{\varphi}_k^{(1)} \right)^{-1} \\ \hat{\Sigma}_k^{(1)} = \dfrac{MS_k}{V_k} \left(\hat{\varphi}_k^{(1)} - \hat{\varphi}_k^{(3)} \right)^{-1} \end{cases} \tag{4}$$

$$\begin{cases} \hat{\Lambda}_0 \vec{A}_k = \dfrac{4}{Mh^2} \sum\limits_{i=1}^{M} \hat{H}_{ik} \left(\vec{A}_{j_i} - \vec{A}_k \right) \\ \hat{\Lambda}_1' \vec{A}_k = \dfrac{4}{Mh^2} \sum\limits_{i=1}^{M} \hat{H}_{ik} \left(\vec{A}_{j_i} - \vec{A}_k \right) \cos(2\alpha_i) \end{cases} \tag{5}$$

$$\begin{cases} \hat{H}_{ik} = 2\hat{D}_{j_i} \left(\hat{D}_{j_i} + \hat{D}_k \right)^{-1} \hat{D}_k \\ \hat{D}_k = \dfrac{h}{2} \left(\hat{\varphi}_k^{(1)} \right)^{-1} \end{cases} \tag{6}$$

Here k is the number of central cells, i is the lateral side number of central cells, j_i is the cell number which has a common side "i" with the central cell, M is the number of lateral sides of the cell, S_k is the square of one lateral side, V_k is the volume of the cell and h is the mesh of the cell. Vectors $\vec{\Phi}_k, \vec{X}_k^{(1)}$ are unknown.

Figure 1. Schemes for neutron currents incoming through the cell boundary for the first four trial functions in square lattice

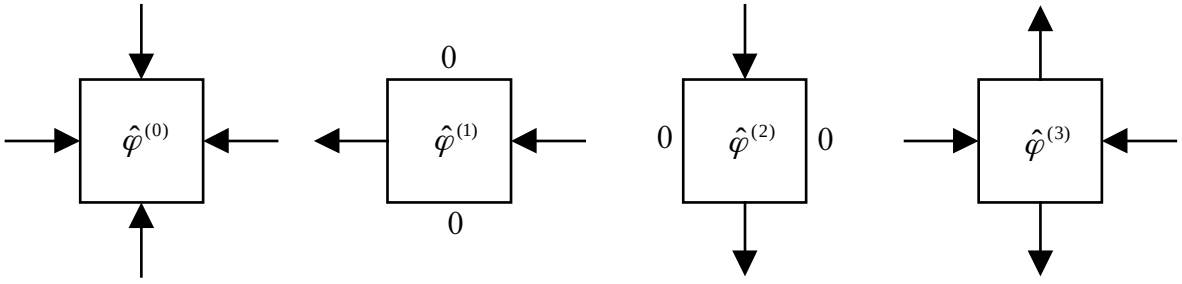

While deriving the finite-difference equations, certain recipes for the calculation of coefficients of these equations (effective cell characteristics) are obtained. These coefficients $\hat{\Sigma}_k^{(i)}, \hat{D}_k$ are functionals of trial functions.

It should be noted that all SHM characteristics depend on the unknown value k_{eff} and, thus, an additional iteration layer must be organised.

Effective cell characteristics are the characteristics of heterogeneous cells, and the obtained finite-difference equations must be solved with only one point per each cell. Reducing calculational mesh size is inadmissible and may give incorrect results. All additional information, which could be obtained in the homogenisation method by decreasing the mesh size to zero, is already contained in effective cell characteristics (and not only this information).

Type and level of angular approximation

For calculation of elements of the zero*th* trial matrix $\hat{\varphi}^{(0)}$ for cells the RACCIA option of the WIMS-SH system of codes was used. In RACCIA, G_3 approximations of Surface Pseudo Sources Method (SPSM) are used for solving the neutron transport equation; the angular variable G_3 approximation corresponds to the P_3 approximation.

P_2 approximation of Spherical Harmonics method (option DIC-PN in WIMS-SH) was used for the calculation of elements of the first and second trial matrices for cells $\hat{\varphi}^{(1)}$, $\hat{\varphi}^{(2)}$.

A procedure of spatial homogenisation and group diffusion approximation was used for calculation of elements of the third trial matrix for cells $\hat{\varphi}^{(2)}$.

SUHAM-2D was used for solving the finite-difference equations of SHM with four trial functions, an in doing so P_2 approximation was used for cell boundaries.

Type and level of spatial discretisation

For calculation of elements of the zero*th* trial matrix $\hat{\varphi}^{(0)}$ for cells the RACCIA option of the WIMS-SH system of codes was used. In RACCIA, G_3 approximations of Surface Pseudo Sources Method are used for solving the neutron transport equation. In this method, surface Green functions are used in every homogeneous zone of the cell.

For calculation of elements of the first and second trial matrices for cells $\hat{\varphi}^{(1)}$, $\hat{\varphi}^{(2)}$ a P_2 approximation of the Spherical Harmonics method (option DIC-PN of WIMS-SH system of codes) was used. Angular moments of neutron distribution function are presented as superposition of Bessel functions in each energy group and each homogeneous zone of the cell. The source of neutrons in each energy group, which appears in this group due to scattering of neutrons in other groups and fission of nuclei, is presented in the following form:

$$Q(\rho) = A_Q \rho + B_Q \frac{1}{\rho} \tag{7}$$

The procedure of spatial homogenisation was used for the calculation of elements of the third trial matrix for cells $\hat{\varphi}^{(3)}$; WIMS-SH was used for the preparation of homogeneous group cross-sections for cells and SUHAM-2D was used for solving group diffusion equation in cells with corresponding boundary conditions. In this case the cell was divided into 100 square meshes (10 × 10).

SUHAM-2D was used for solving the finite-difference equations of SHM with four trial functions and with one point per each cell in a whole volume. It should be noted that reducing calculational mesh size in this stage is inadmissible and may provide incorrect results.

Convergence

The following relative accuracies of convergence were used for solving the finite-difference equations of SHM: 10^{-6} for eigenvalue and 10^{-5} for group local fluxes. For k_{eff} in the additional iteration layer a relative accuracy of 10^{-5} was used.

Machine on which the calculations were performed and CPU time

Pentium-4 1500 Mhz was used for calculation of this benchmark. Total CPU time is 8 minutes and 20 seconds.

References

[1] Laletin, N.I., N.V. Sultanov, V.F. Boyarinov, *et al*., "WIMS-SU Complex Codes and SPEKTR Code", *Proc. of PHYSOR-90*, Marseilles, France, 23-27 April 1990, v. 4, p. PV-148, ANS/ENS (1990).

[2] Boyarinov, V.F., *SUHAM-2.5 Code for Solving 2-D Finite-difference Equations of the Surface Harmonics Method in Square and Triangular Lattices*, Nuclear Technology'99, Karlsruhe, Germany, 18-20 May 1999, pp. 23-26.

[3] Laletin, N.I., "On the Equations of Heterogeneous Reactor", *Voprosi Atomnoi Nauki i Tehniki. Ser. Fisika Yadernih Reactorov*, 5, 18, 31 (1981).

15. Russian Research Centre “Kurchatov Institue” (RRC KI), Russian Federation

Participant(s)

A.A. Polismakov, A.V. Tchibiniaev

Establishment(s)

Russian Research Centre “Kurchatov Institute”
E-mail: achib@dhtp.kiae.ru, polismakov@dhtp.kiae.ru
Tel: ++7-095-196-7016, ++7-095-196-7377

Name of code system(s) used

Structure.

Computational method used

The PS_n method is a specific synthesis of the discrete ordinates and collision probability methods. By analogy with the discrete ordinates method, flux angular distribution at the cell boundary is presented in discrete form (*N* angular directions). The flux is assumed to be constant in each *n*-th angular direction. The coefficients responsible for the neutron transport from one cell boundary to others, and from the inner volume of a cell to its boundaries in each angular direction are derived by balance equations of collision probability method.

Neutrons from an external source and neutrons from inner-group scattering are considered to be a source of neutrons. After calculation of one-side neutron currents throw, all cell boundaries of an average neutron flux in the elementary cells are computed. The average neutron flux is used to calculate a source of inner-group scattering in the following iterations.

Let computational volume consists of a set of elementary cells. Using the approach of isotropic scattering, the average flux in an elementary cell for every energy group is derived from the set of Eqs. (1)-(2):

$$\sum_j \sum_n \left(J^-_{jn} - J^+_{jn}\right)S + \Sigma_t \Phi V = \Sigma_s \Phi V + QV \tag{1}$$

$$J^-_{jn} = \sum_i \sum_m \alpha^{m\to n}_{i\to j} J^+_{im} + \beta^n_j \left(\Sigma_s \Phi + Q\right) + \sum_i \Sigma_s \nabla_{ij} \Phi \lambda^n_{i\to j} \tag{2}$$

$$J^+_{jn} = \int_{\ddot{\Omega}_n}^{\ddot{\Omega}_{n+1}} d\vec{\Omega} \left|\vec{\Omega}, \vec{n}\right| \varphi_j\left(\vec{\Omega}\right) \qquad \left(\vec{\Omega}, \vec{n}_j\right) < 0$$

$$J^-_{jn} = \int_{\ddot{\Omega}_n}^{\ddot{\Omega}_{n+1}} d\vec{\Omega} \left(\vec{\Omega}, \vec{n}\right) \varphi_j\left(\vec{\Omega}\right) \qquad \left(\vec{\Omega}, \vec{n}_j\right) > 0$$

$$\overline{\Phi} = \frac{1}{V} \int_V d\vec{r} \int_{4\pi} \varphi\left(\vec{r}, \vec{\Omega}\right) d\vec{\Omega} \qquad Q = \frac{1}{V} \int_V d\vec{r} \int_{4\pi} q\left(\vec{r}, \vec{\Omega}\right) d\vec{\Omega}$$

where S is the area of the cell boundary, V is the cell volume, i, j are indices of the cell boundary, J_{jn}^{-}, J_{jn}^{+} are the outlet and inlet neutron cell currents in n-th angular direction $\left(\vec{\Omega}_n, \vec{\Omega}_{n+1}\right)$, $n = 1,...,$ N, N is the number of directions dividing angular space on the cell boundary, $\overline{\Phi}$ is an average neutron flux in the cell, and Q is an average neutron source in the cell.

Coefficient $\alpha_{i\to j}^{m\to n}$ is the probability for a neutron entering through i-th boundary in m-th angular direction to escape through j-th boundary in n-th angular direction without any collision.

Coefficient β_j^n is the probability for a neutron born in a cell to reach the j-th boundary without any collision and escape in n-th angular direction.

The third term in Eq. (2) takes into account the influence of the flux linear change $\nabla_{ij}\Phi$ between I-th and j-th boundaries. It is essential, if the size of cell is greater than 0.5-1 neutron free paths.

The set of Eqs. (1)-(2) is supplemented by conditions of the current continuity at cell boundaries and boundary conditions of the computational volume.

Obtained inlet and outlet currents are used for calculation of an average neutron flux and flux linear change between different boundaries of the elementary cell:

$$\overline{\Phi} = \frac{Q(V - \sum_j \sum_n \beta_j^n S_j) + \sum_j \sum_n J_{jn}^{+}(S_j - \sum_i \sum_l \alpha_{j\to i}^{n\to l} S_i)}{\Sigma_t V - \Sigma_S (V - \sum_j \sum_n \beta_j^n S_j)} \tag{3}$$

$$\nabla_{ij}\Phi = \sum_{l=1}^{N} \frac{(J_{il}^{-} + J_{il}^{+}) \cdot \int_{\Omega_l}^{\ddot{\Omega}_{l+1}} d\vec{\Omega}}{\int_{\Omega_l}^{\ddot{\Omega}_{l+1}} d\vec{\Omega} \left|\vec{\Omega} \cdot \vec{n}_i\right|} - \sum_{l=1}^{N} \frac{(J_{jl}^{-} + J_{jl}^{+}) \cdot \int_{\Omega_l}^{\ddot{\Omega}_{l+1}} d\vec{\Omega}}{\int_{\Omega_l}^{\ddot{\Omega}_{l+1}} d\vec{\Omega} \left|\vec{\Omega} \cdot \vec{n}_j\right|} \tag{4}$$

The set of Eqs. (1)-(4) is solved by a method of consequent approaches at simultaneous correction of inner part of neutron source Q.

The level of angular approximation has been derived from serial calculations with different angular nodalisation: PS_{12}, PS_{24}, PS_{36}, PS_{72} (index presents a number of angular directions of one-side neutron currents on a boundary of the elementary cell). Eigenvalues resulting from last two calculations are not practically different from each from other (less than 0.0001). Figure 1 presents the type of angular approximation.

Figure 2 presents the spatial mesh for one lattice zone. So, every regular lattice zone consists of 16 elementary calculate cells.

The accuracy of both eigenvalue and pointwise (e.g. flux) is equal to 10E-6.

Machine on which the calculations were performed and CPU time

The calculations were performed using a Pentium III 800 MHz, 256 MB RAM. The calculation time is about 23 hours for a two-dimensional problem of PS_{36} angular approximation.

Figure 1. Type of angular approximation of one-side neutron currents on a boundary of the elementary cell

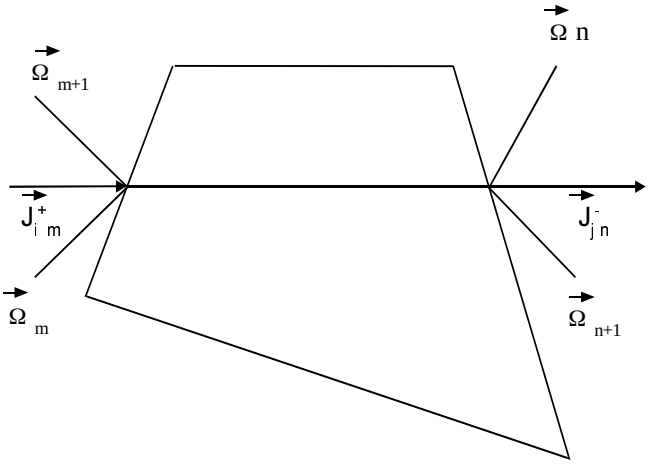

Figure 2. Fuel pin layout (1 – fuel-clad mix, 2 – moderator)

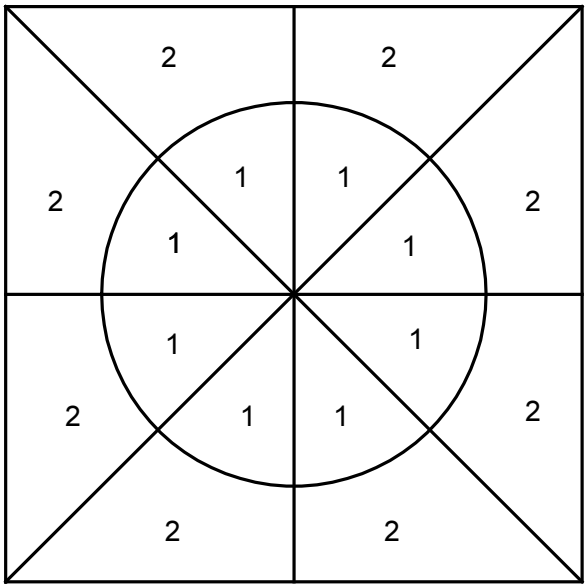

16. Russian Research Centre "Kurchatov Institue" (RRC KI), Russian Federation

Participant(s)

Tamara S. Poveschenko

Establishment(s)

RRC KI, Kurchatov Sq.1, Moscow Russia, 123182
Tel: (095) 196-7377
Fax: (095) 196-3708
E-mail: povesch@dhtp.kiae.ru

Name of code system(s) used

GEFCOP.

Computational method used

General First Collision Probabilities [1].

In this method the neutron flux is approximated with a set of the orthogonal polynomials in every calculation zone. Thus the set of algebraic equations are a result of kinetic equation approximation. This algebraic system contains both the average zone neutron fluxes and the higher spatial moments of neutron flux as well. The coefficients of this algebraic equation system are "general first collision probabilities".

This method is demonstrated when a one-group problem with isotropic internal sources and isotropic surface source is considered:

$$\phi^0(\vec{r}\,') = \int_V d\vec{r}\,' \left[\phi^0(\vec{r}\,')\sigma_s^0(\vec{r}\,') + q(\vec{r}\,')\right] P(\vec{r}\,' \to \vec{r}) + 4\pi \int_S d\vec{r}\,' I(\vec{r}\,')(\vec{\Omega}\vec{n}) P(\vec{r}\,' \to \vec{r}) \qquad (1)$$

Here the following designations are used:

$\tau(\vec{r}\,' \to \vec{r}) = \int_0^1 \sigma(\vec{r}\,' + s(\vec{r} - \vec{r}\,'))\left|\vec{r} - \vec{r}\,' ds\right|$ – "optical distance" between r $\vec{r}$ and $\vec{r}\,'$.

$u(\vec{r} \to \vec{r}) = \exp(-\tau(\vec{r}\,' \to \vec{r}))$ – probability for the neutron free path from $\vec{r}\,'$ to $\vec{r}$.

$P(\vec{r}\,' \to r) = -\dfrac{u(\vec{r} - \vec{r}\,')}{4\pi\left|\vec{r} - \vec{r}\,'\right|^2}$ – usual kernel of the FCPM integral equation.

GFCPM can be applied to the set of integral equations. The main assumption of this method is that the flux is approximated by polynomials of the Cartesian co-ordinates in every uniform mesh:

$$\phi^0(\vec{r}) = \sum_t \sum_{\eta=1}^{N} g_t(\vec{r}) \varphi_{\eta t}^0 f_{\eta t}(\vec{r}) \qquad (2)$$

and the orthogonal relation is valid:

$$\int_{V_t} f_{t\eta}(\vec{r})\, f_{t\eta}(\vec{r})d\vec{r} = \delta_{\eta\eta'} \tag{3}$$

The expansion (2) is substituted in the system (1); every equation is multiplied by function $f_{t\eta}$ consequently; and the integration over "*t*" mesh is carried out. So, if Eq. (3) is taken into account, the set of linear algebraic equations arises:

$$\varphi^0_{\eta t} V_t = \sum_t \sigma_\eta \sum_\eta \varphi_{\eta t} \int_{V_t} d\vec{r} \int_{V_{t'}} d\vec{r}\,' f_{\eta t}(\vec{r})\, f_{t'\eta'}(\vec{r}\,')P(\vec{r}\,' \to \vec{r}) + 4\pi \int_{V_t} d\vec{r} \int_S d\vec{r}\,'(\vec{\Omega}\vec{n})P(\vec{r}\,' \to \vec{r}) \tag{4}$$

The coefficients of the set of linear equations are so-called generalised first collision probabilities. It was shown that if $f_{\eta t}(\vec{r})$ are the polynomials of Cartesian co-ordinates in the cell plane then calculation of the probabilities expressed in the co-ordinates φ, y_φ, x_φ, x'_φ, λ connected with the flight direct neutron is reduced to the 2-D numerical integration. Here, φ is the angle between neutron flight direct projection on the (x,y) plane and x-axis; x_φ, y_φ, z are co-ordinates of point *r* in the Cartesian system turned around z-axis by φ angle; $x'_\varphi, y'_\varphi, z$ are the same for point *r*′, so:

$$y'_\varphi = y_\varphi; x'_\varphi \le x_\varphi$$

After some analytical rearrangement, equations for the general probabilities are reduced to the 2-D numerical integration:

$$P^{\eta\eta'}_{tt'} = \iint \vec{P}^{\eta\leftarrow\eta'}_{t\leftarrow t'}(\varphi, y_\varphi)d\varphi dy_\varphi \tag{5}$$

The subintegral function is reduced to the combinations of trigonometric function φ with Bickley functions of different orders from the next arguments: "optical" distances along neutron fly direction projection on the (x,y) plane from intersection of this projection with neutron birth zone boundary to the intersection of this projection with the neutron first collision zone boundary subintegral function. If there is a complex geometry cell (for example, cluster), then nothing can be predicated about behaviour of functions $P^{\eta\leftarrow\eta'}_{t\leftarrow t'}(\varphi, y_\varphi)$. Thus there are no reasons for their approximation by higher-order polynomial rather then linear polynomial or constant.

Algorithm of numerical integration of the "general first collision probabilities" is based on the interpretation of the Monte Carlo method as a realisation of the standard quadrature formula for multi-dimensional integral calculations. The co-ordinates of the mesh points are defined with the use of "uniform" distributed sequences [2]. The universal combinatorial geometry module SCG-5 [3] is used for geometry description in this code.

Type and level of angular approximation

The algorithm is based on the MMC interpretation as a realisation of the standard quadrature formula for multi-dimensional integral calculations. Let us make the change of variables in Eq. (5):

$$\varphi = \varphi(\gamma_1, \gamma_2) \text{ and } y_\varphi = y_\varphi(\gamma_1, \gamma_2)$$

These variables are co-ordinates of the points in the unite cube and the following relation is valid:

$$\frac{dy_{\varphi}d\varphi}{2\pi S_j} = d\gamma_1 d\gamma_2 \tag{6}$$

After this change of variables all integrals are calculated over the unit cube with the use of the standard quadrature formula: if $\chi(n)$ is the significance of the subintegral function in the mesh point number n, then the integral meaning is the average arithmetical value $\chi(n)$ over all mesh points. The co-ordinates of the mesh points are defined with the use of "uniform" distributed sequences. There are codes used for the integral calculations on the mesh of Hemmersly-Holton, Korobov, Sobol (LP_τ-sequences) [2]. It was shown in some works that the use of these sequences yields a high integration convergence order $\left(\approx 1/N^{1-\varepsilon}\right)$ convergence to zero. Thus this algorithm and MMC algorithm differ only in the choice of mesh points; it is therefore possible to use the universal combinatorial geometry module SCG-5 [3] for geometry description in the calculation of probability codes without any essential change (this module is used in the MMC codes).

Type and level of spatial discretisation

Every fuel-pin cell has been divided into two calculation zones: the fuel zone and the moderator zone. The flat neutron flux approximation is used in these zones. The ability of geometrical module SCG to take into account the symmetrical properties of the system is used. There are therefore 2 346 unknown values in the fuel-pin area.

Linear flux approximation is used in the moderator. It has been divided into ten layers and two linear functions are used in every layer. The unknown values are neutron average fluxes over every layer and two spatial moments of the neutron flux. There are thus 30 unknown values in the moderator and the common number of unknown values is 2 376.

Convergence

The algorithm of the calculation integration uses Korobov generator of the "uniform distributed sequences". It is necessary to use ~100 000 trajectories to reach the convergence of eigenvalue 10 E-5.

Machine on which the calculations were performed and (if possible) CPU time

Pentium-4 1500.

References

[1] Shevelev, Ya.V., T.S. Poveschenko, "Polynomial Approximation of the Neutron Flux in the Collision Probabilities Method", *Atomnaia energiya*, 48, 2, 80, (1986).

[2] Sobol I.M., R.B. Statnikov, *Vybor optimalnyh parametrov v zadachah so mnogimi kriteriiami*, Nauka, M. (1981).

[3] Alekseev, N.I., M.I. Gurevich, *Geometrical Module SCG-5*, pre-print IAE-5616/4,M (1993).

17. Pennsylvania State University (PSU), USA

Participant(s)

Boyan Ivanov,[1] Kostadin Ivanov,[1] Rudi J.J. Stamm'ler[2]

Establishment(s)

[1]Department of Mechanical and Nuclear Engineering
Pennsylvania State University
University Park, PA, USA
bivanov@psu.edu; kni1@psu.edu

[2]Studsvik Scandpower, Norway
rudi.stamm'ler@studsvik.no

Name of the code system(s) used

HELIOS has been used to obtain benchmark solutions. The version of HELIOS used in this project is a special version developed by Studsvik Scandpower to analyse this problem – it skips the resonance and depletion calculations. HELIOS typically is used for lattice burn-up calculations using 45 or 112 energy group nuclear data library based on ENDF-B/VI. In this particular study HELIOS uses a special cross-section library where the isotopes and their cross-sections are the materials cross-sections provided in the benchmark specification.

HELIOS is a two-dimensional (2-D) current-coupling collision-probability code. Current coupling order "4" has been used for these calculations.

Since the problem appeared to be too large for our computational capabilities, it was decided to examine only the diagonal half of it (1/8 of the core). HELIOS allows the user to model fuel assemblies in different ways. Varying degrees of complexity can be used to define the fuel assembly. Usually, the components in a HELIOS assembly will be the pin cell consisting of fuel, gap, clad and surrounding moderator. The fuel, clad and moderator can be subdivided in numerous ways into meshes (called "regions" in HELIOS jargon). In the problem described here, two regions were used – fuel-clad mixture and moderator – as given in the benchmark specifications. The fuel-clad region is divided into three annular meshes. Three cases with different geometry of the moderator region were studied. A coarse mesh was considered for the first case, as shown in Figure 1. In this case the moderator region is divided into four meshes. For the second case (fine mesh) the moderator region was divided into eight meshes (Figure 2). In the last case the moderator was again divided into eight meshes but in different way – "sun mesh" (Figure 3). For all the three cases HELIOS used two different coupling orders – "2" and "4". The best results could be obtained using coupling order "0" (CPs without current coupling), however, because of memory limitations only coupling orders "2" and "4" were examined in detail. The results presented in the attached Excel file are obtained with coupling order "4". Other coupling orders were also used and calculations with them were performed for sensitivity studies.

Machine on which the calculations were performed and (if possible) CPU time

The machine on which the calculations were performed is IBM RS6000. CPU time is 4.74 min.

Figure 1. Case 1 geometry of the fuel pin layout – coarse mesh

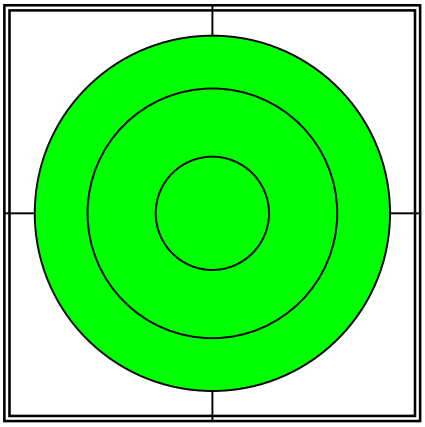

Figure 2. Case 2 geometry of the fuel pin layout – fine mesh

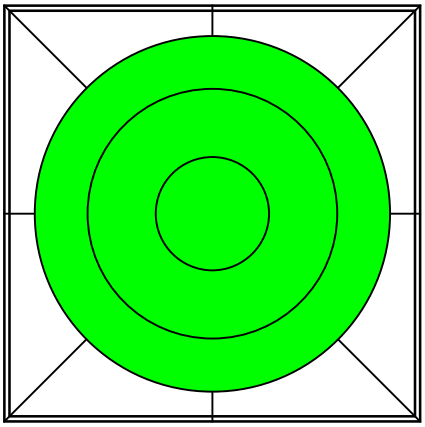

Figure 3. Case 3 geometry of the fuel pin layout – sun mesh

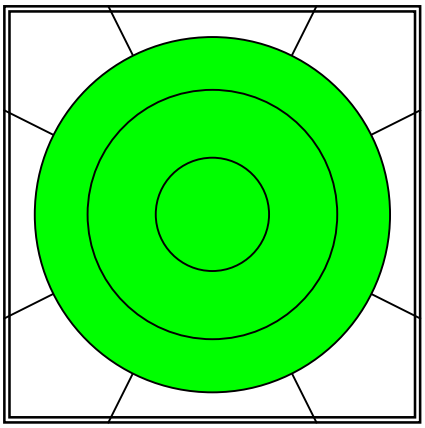

APPENDIX C

Clarification of the AVG, RMS and MRE Error Measures

To clarify the three distribution error measures we provide the following brief instructional example. Consider a problem in which there are ten pin powers to be calculated and an "exact" reference solution is available. As a hypothetical, consider the three solutions in Tables 1, 2, and 3 meant to represent solutions contributed by three participants.

As can be seen in Table 1, the participant obtained a solution for which most of the pin powers were calculated correctly (power distribution is the reference solution). The participants lowest pin power had the greatest amount of error: 0.3%. The RMS error is significantly larger than the AVG error measure, indicating that there are a few pins that have substantial error (if all of the percent errors are roughly the same, then the RMS error will equal the AVG error). The MRE error measure is much smaller than the AVG error measure since a majority of the error resides in the low pin powers.

In Table 2 the participant's largest error is now on the maximum pin power while the smallest error is on the lowest pin power. As can be seen, the AVG and RMS error do not change from Table 1 to Table 2, but the MRE error changes almost by a factor of two. In terms of the accuracy, this participant's solution has significantly more error in the pin power distribution, which can only be captured by the MRE error measure.

In Table 3, the participant exactly calculates several of the fuel pins, but four fuel pins have much significantly larger amounts of error compared to Table 1 and Table 2. Overall, the magnitude of the error has not changed as indicated by both the AVG and MRE error measures. The distribution of those errors has changed quite significantly though, which is only captured by the RMS error measure.

In conclusion, the AVG error provides a point of reference for the RMS and MRE error measures. The RMS error measure gives an estimate of the severity of the percent error distribution and the MRE error measure gives an estimate of the severity of the magnitude of error on the pin power distribution.

Table 1. Hypothetical result #1

Reference power	User per cent error
1.82	0.01
1.64	0.02
1.45	0.03
1.27	0.04
1.09	0.05
0.91	0.06
0.73	0.07
0.55	0.08
0.36	0.09
0.18	0.30
AVG: 0.075 **RMS: 0.109** **MRE: 0.044**	

Table 2. Hypothetical result #2

Reference power	User per cent error
1.82	0.030
1.64	0.02
1.45	0.03
1.27	0.04
1.09	0.05
0.91	0.06
0.73	0.07
0.55	0.08
0.36	0.09
0.18	0.01
AVG: 0.075 **RMS: 0.109** **MRE: 0.091**	

Table 3. Hypothetical result #3

Reference power	User per cent error
1.82	0.13
1.64	0.00
1.45	0.00
1.27	0.00
1.09	0.00
0.91	0.00
0.73	0.00
0.55	0.12
0.36	0.25
0.18	0.25
AVG: 0.075 **RMS: 0.125** **MRE: 0.044**	

LIST OF CONTRIBUTORS

Authors	
M.A. Smith	ANL, USA
E.E. Lewis	Northwestern University, USA
B-C. Na	OECD/NEA

Problem specification	
E.E. Lewis	Northwestern University, USA
M.A. Smith	ANL, USA
N. Tsoulfanidis	University of Missouri, Rolla, USA
G. Palmiotti	ANL, USA
T.A. Taiwo	ANL, USA
R.N. Blomquist	ANL, USA

	Reference solutions	
MCNP and VIM	M.A. Smith	ANL, USA
	N. Tsoulfanidis	University of Missouri, Rolla, USA
	R.N. Blomquist	ANL, USA
	E.E. Lewis	Northwestern University, USA
MCNP	K. Parsons	LANL, USA
KENO	Y. Azmy	ORNL, USA
	J. Gehin	ORNL, USA
	R. Orsi	ENEA, Italy

Benchmark participants	
S. Santandrea	CEA, France
R. Sanchez	CEA, France
F. Moreau	CEA, France
A. Pautz	GRS, Germany
S. Langenbuch	GRS, Germany
W. Zwermann	GRS, Germany
K. Velkov	GRS, Germany
P. Mohanakrishnan	IGCAR, India
S. Kosaka	TEPSYS, Japan
J.K. Kim	Hanyang University, Korea
C.Y. Han	Hanyang University, Korea
H.G. Joo	KAERI, Korea
J.Y. Cho	KAERI, Korea
K.S. Kim	KAERI, Korea
S.Q. Zee	KAERI, Korea
N.Z. Cho	KAIST, Korea
G.S. Lee	KAIST, Korea
C.J. Park	KAIST, Korea
I.R. Suslov	IPPE, Russian Federation
V.F. Boyarinov	RRC KI, Russian Federation
V.D. Davidenko	RRC KI, Russian Federation
V.F. Tsibulsky	RRC KI, Russian Federation
A.A. Polismakov	RRC KI, Russian Federation
A.V. Tchibiniaev	RRC KI, Russian Federation
T.S. Poveschenko	RRC KI, Russian Federation
M.A. Smith	ANL, USA
N. Tsoulfanidis	University of Missouri, Rolla, USA
E.E. Lewis	Northwestern University, USA
G. Palmiotti	ANL, USA
T.A. Taiwo	ANL, USA
R.N. Blomquist	ANL, USA
J.A. Dahl	LANL, USA
R.E. Alcouffe	LANL, USA
R.S. Baker	LANL, USA
T. Wareing	LANL, USA
J. McGhee	LANL, USA
Y. Azmy	ORNL, USA
J. Gehin	ORNL, USA
R. Orsi	ENEA, Italy
B. Ivanov	Penn State University, USA
K. Ivanov	Penn State University, USA
R.J.J. Stamm'ler	Studsvik Scandpower, Norway

OECD PUBLICATIONS, 2 rue André-Pascal, 75775 PARIS CEDEX 16
Printed in France.